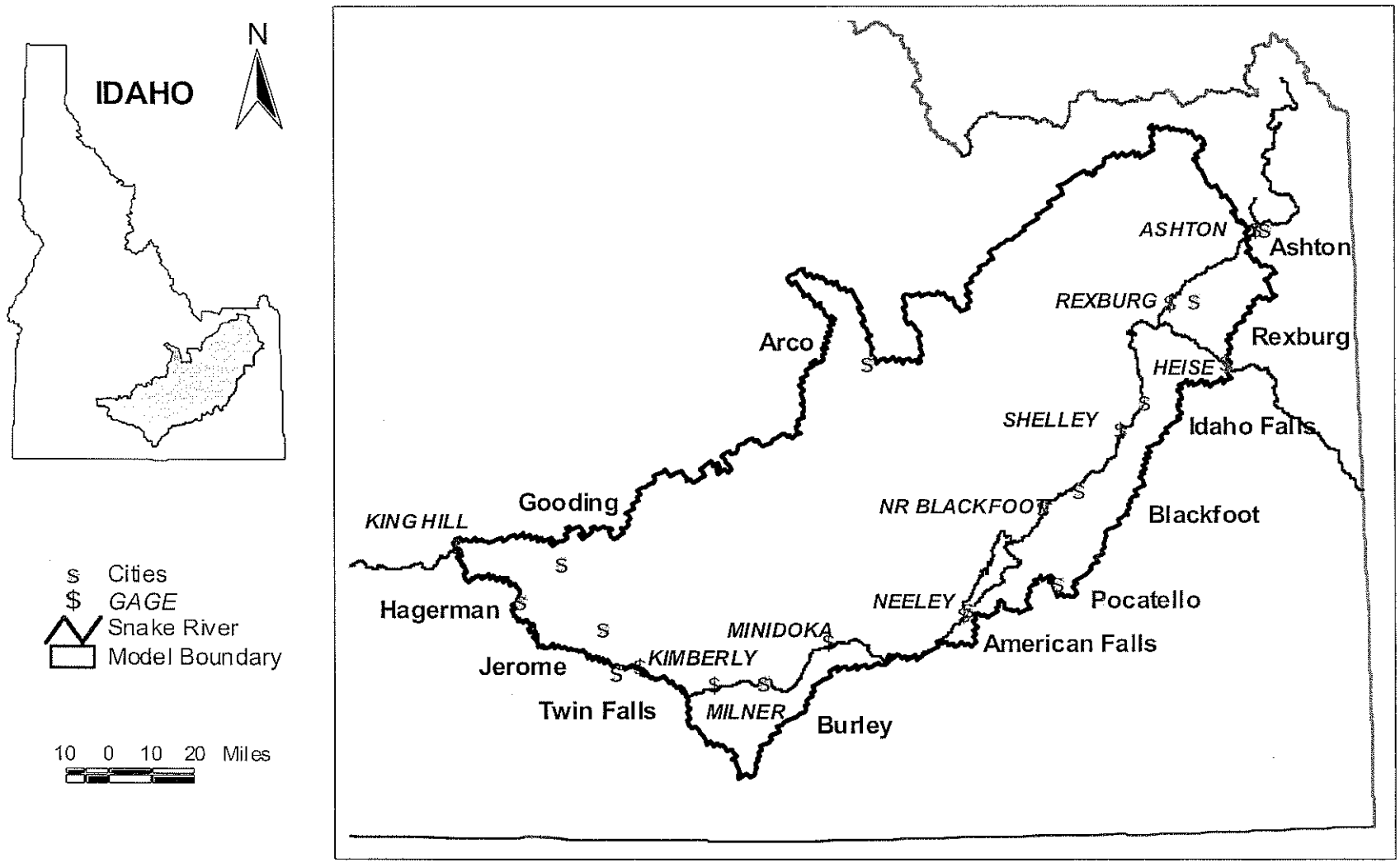

Figure 1. Study area and RASA aquifer boundaries.

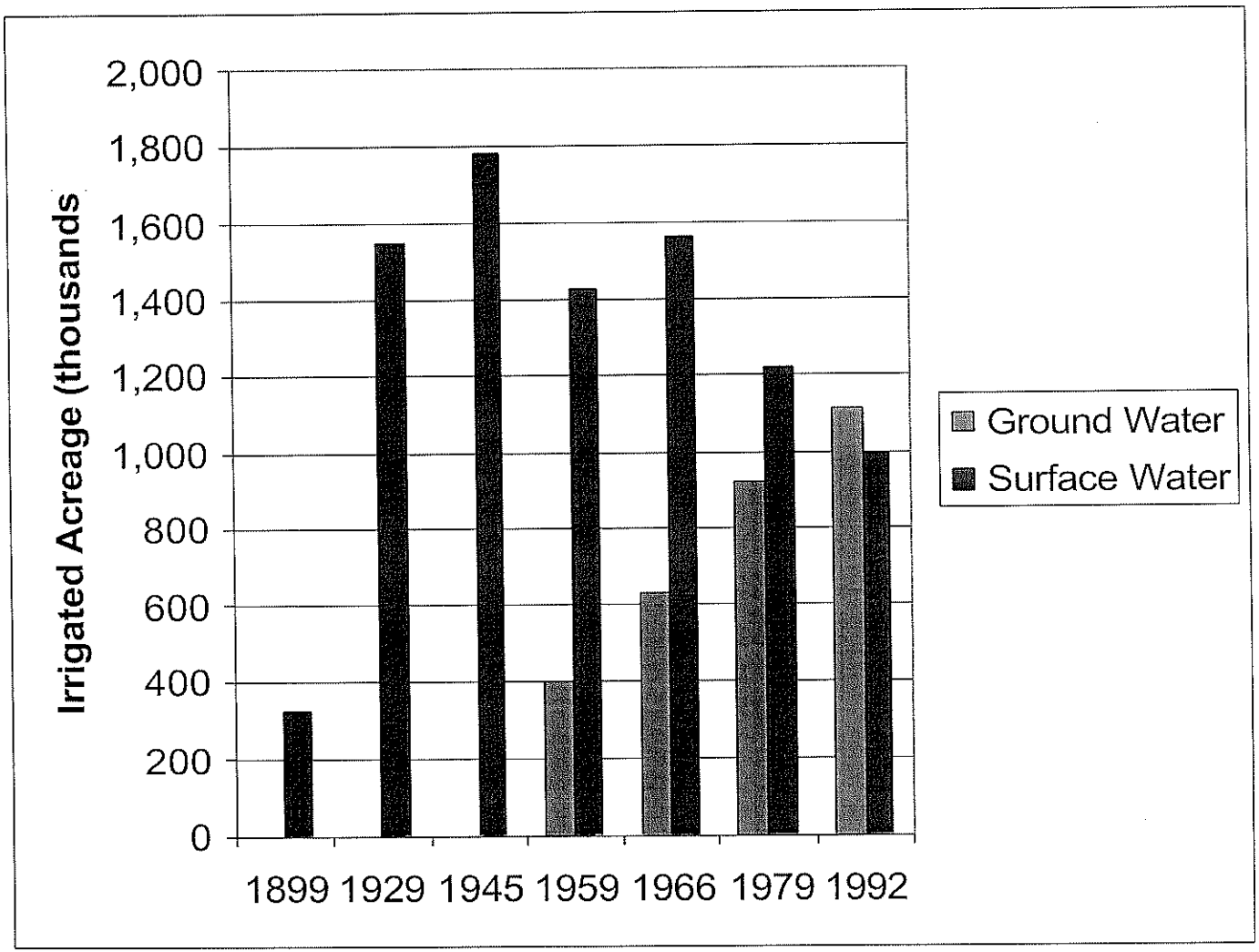

Figure 2. Changes in surface and ground water irrigated acres on the eastern Snake River Plain (after Garabedian, 1992).

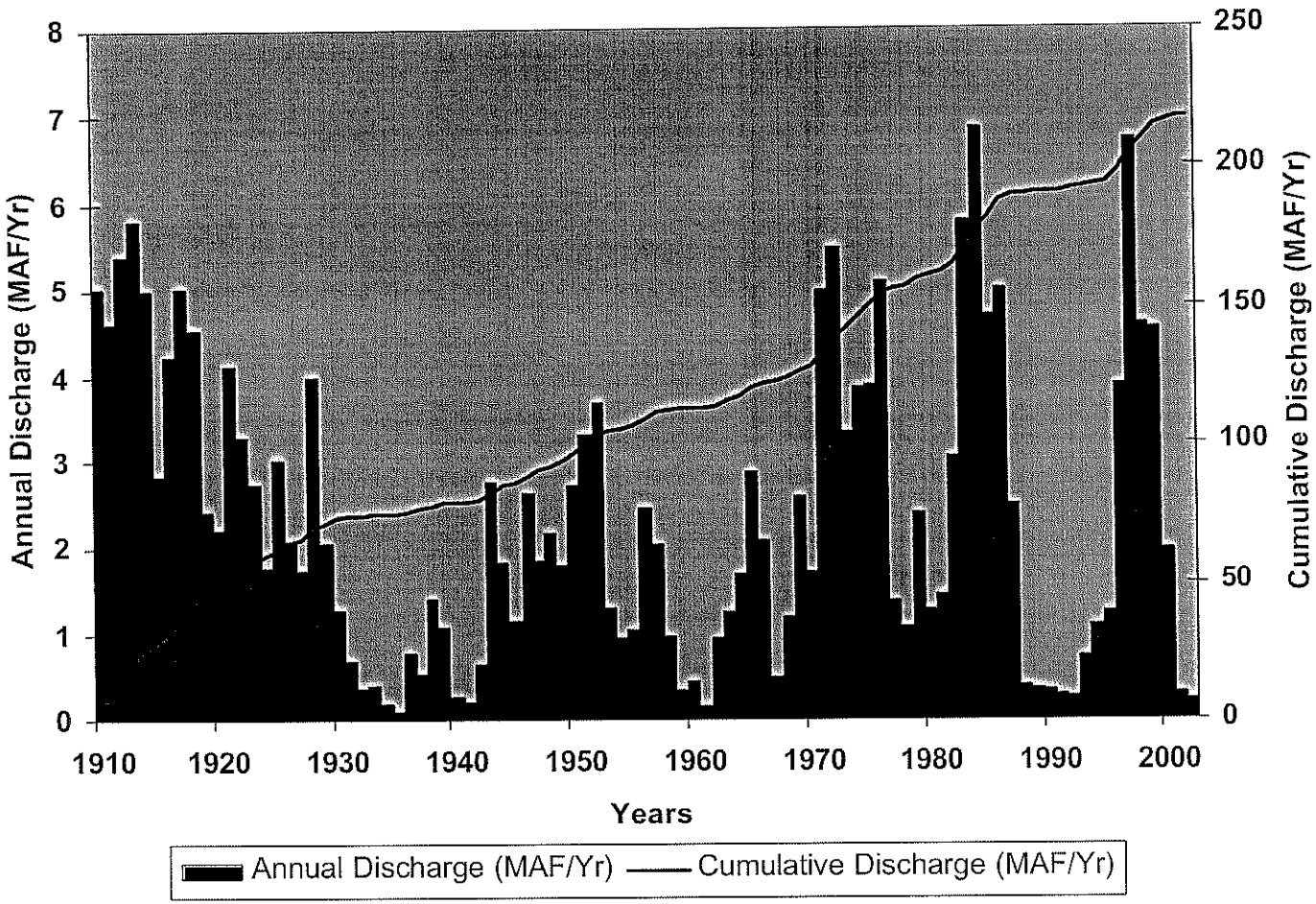

Figure 3. Annual and cumulative discharge of the Snake River near King Hill (U.S. Geological Survey data).

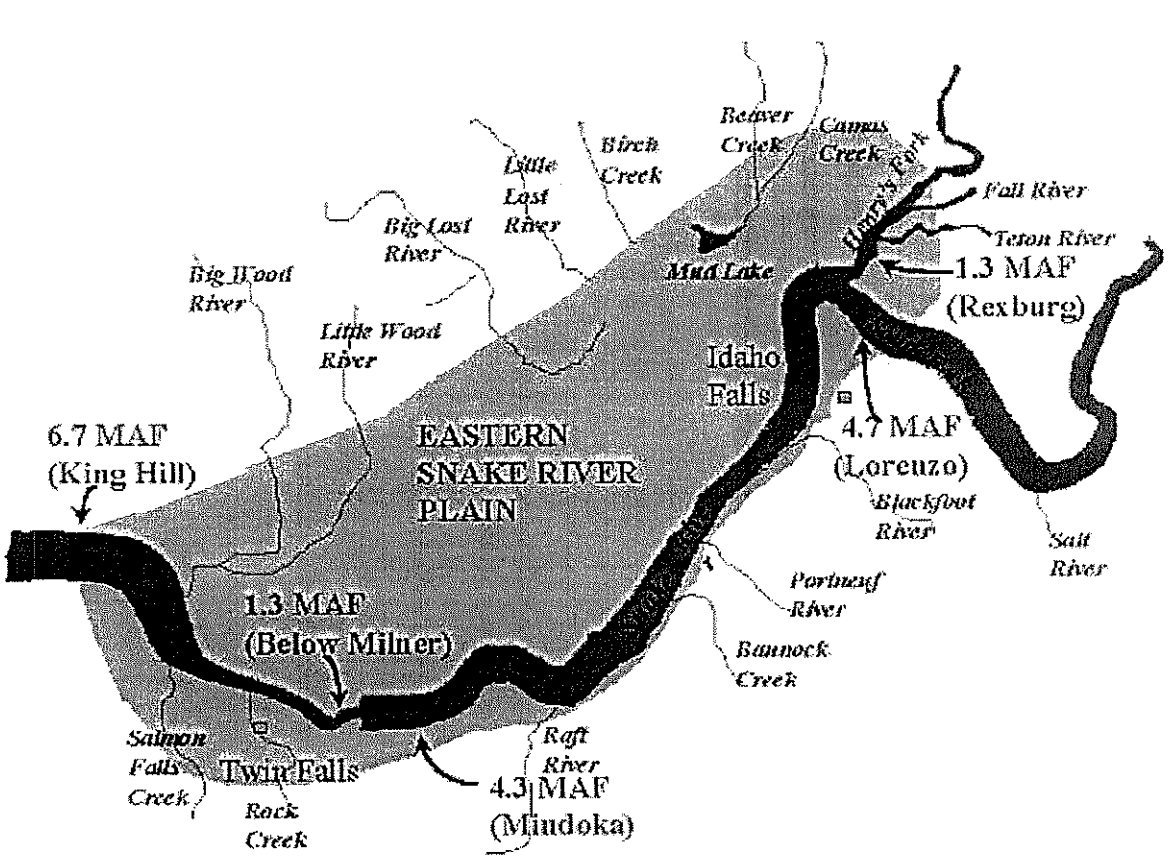

Figure 4. Conceptual illustration of variation in average annual flow of the Snake River (after the U.S. Bureau of Reclamation, 1996).

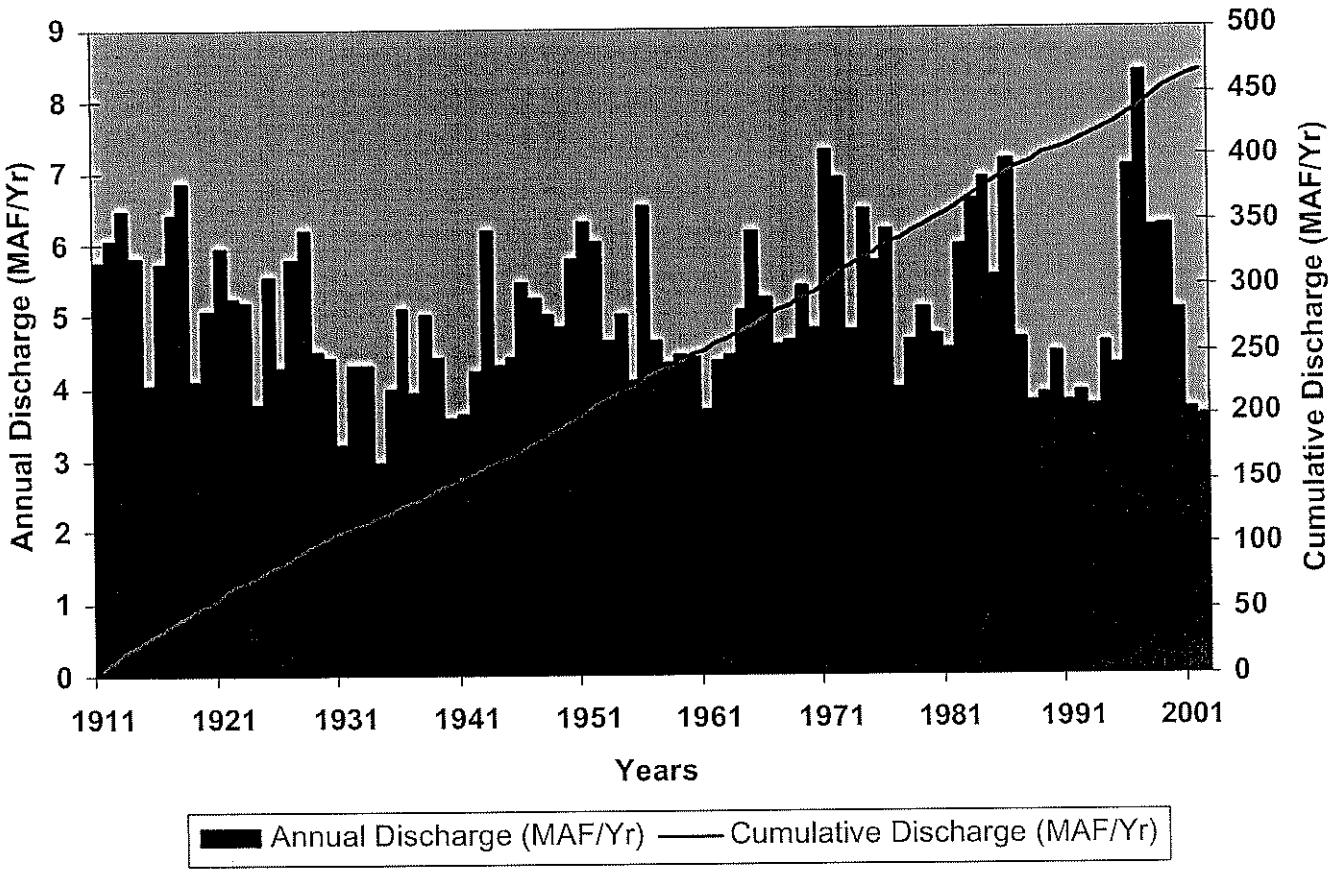

Figure 5. Historic discharge of the Snake River at Milner Dam (U.S. Geological Survey Data).

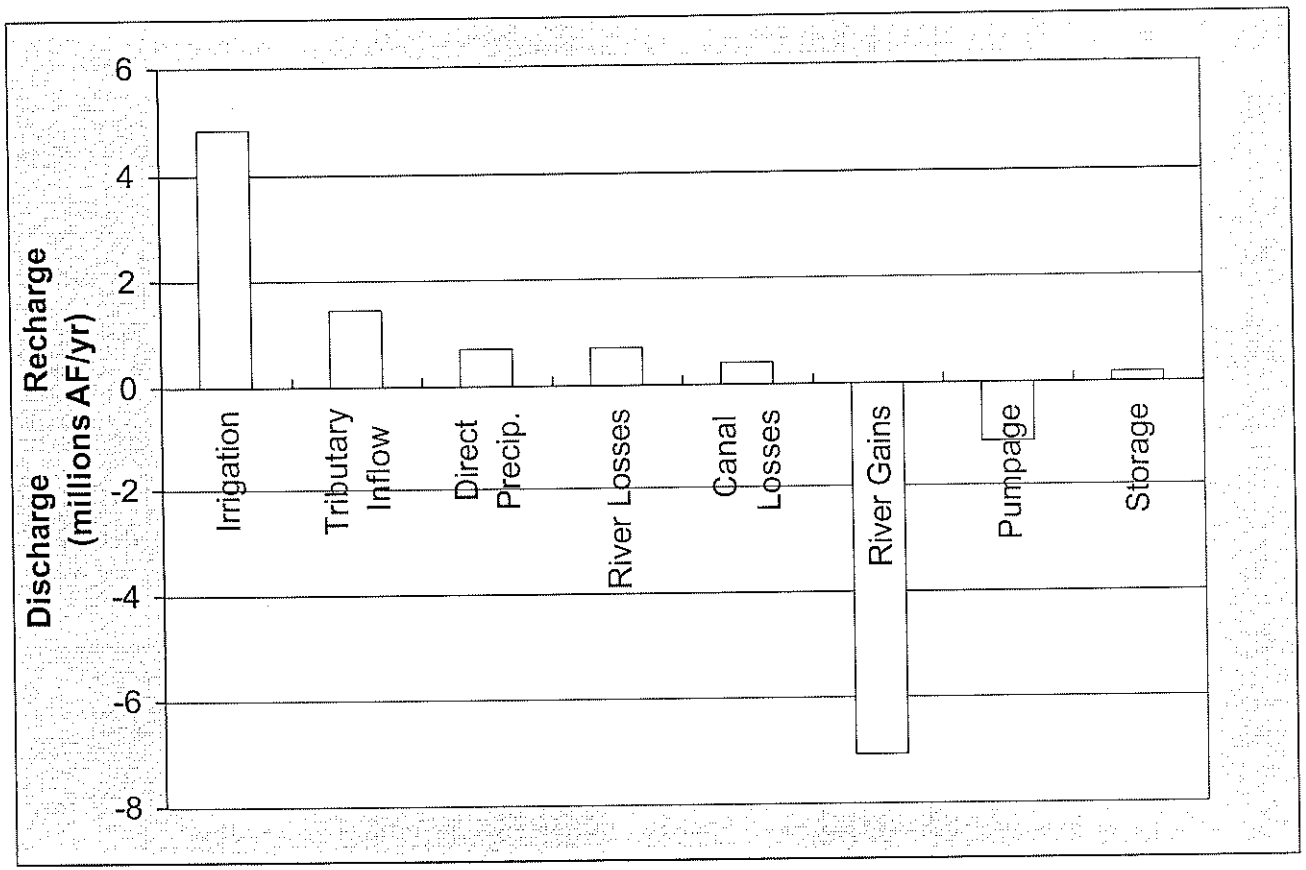

Figure 6. Snake River Plain Aquifer estimated annual recharge and discharge from April 1980 through March 1981 (after Garabedian, 1992).

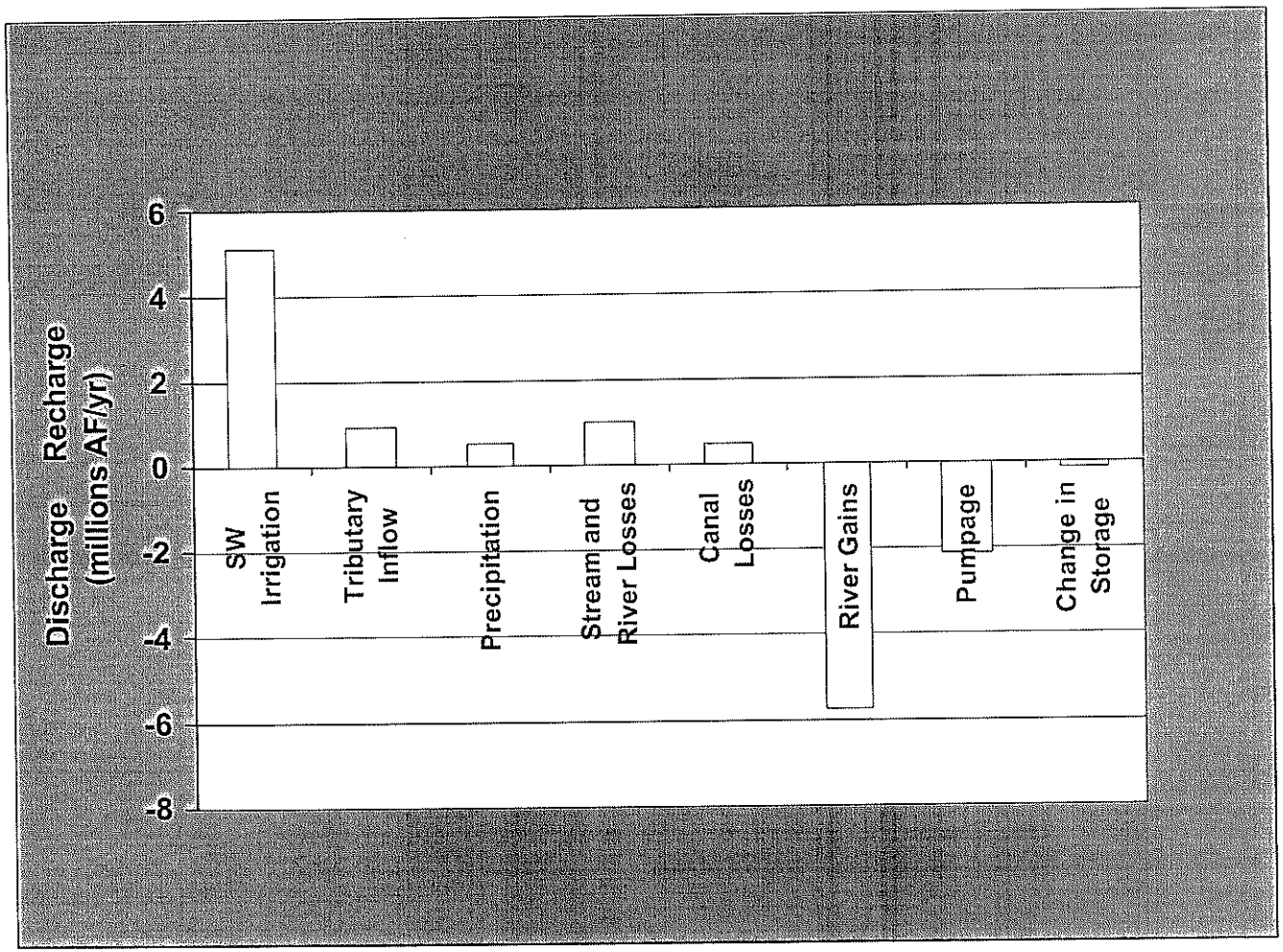

Figure 7. Snake River Plain Aquifer estimated annual recharge and discharge assuming the average irrigation development level of 1980 through 2001 (after IDWR, 1997).

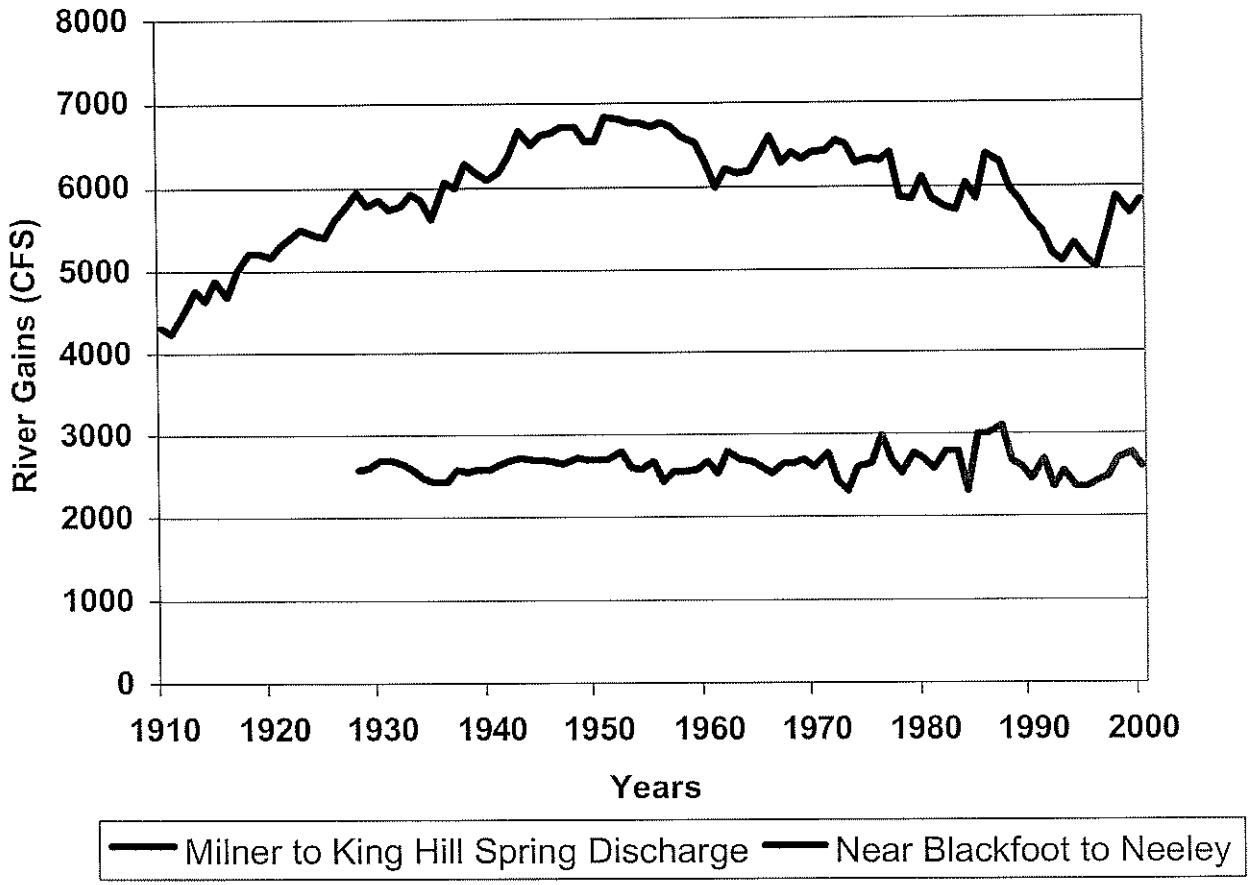

Figure 8. Average annual Snake River gains in the Milner to King Hill and Blackfoot to Neeley reaches. (From IDWR data.)

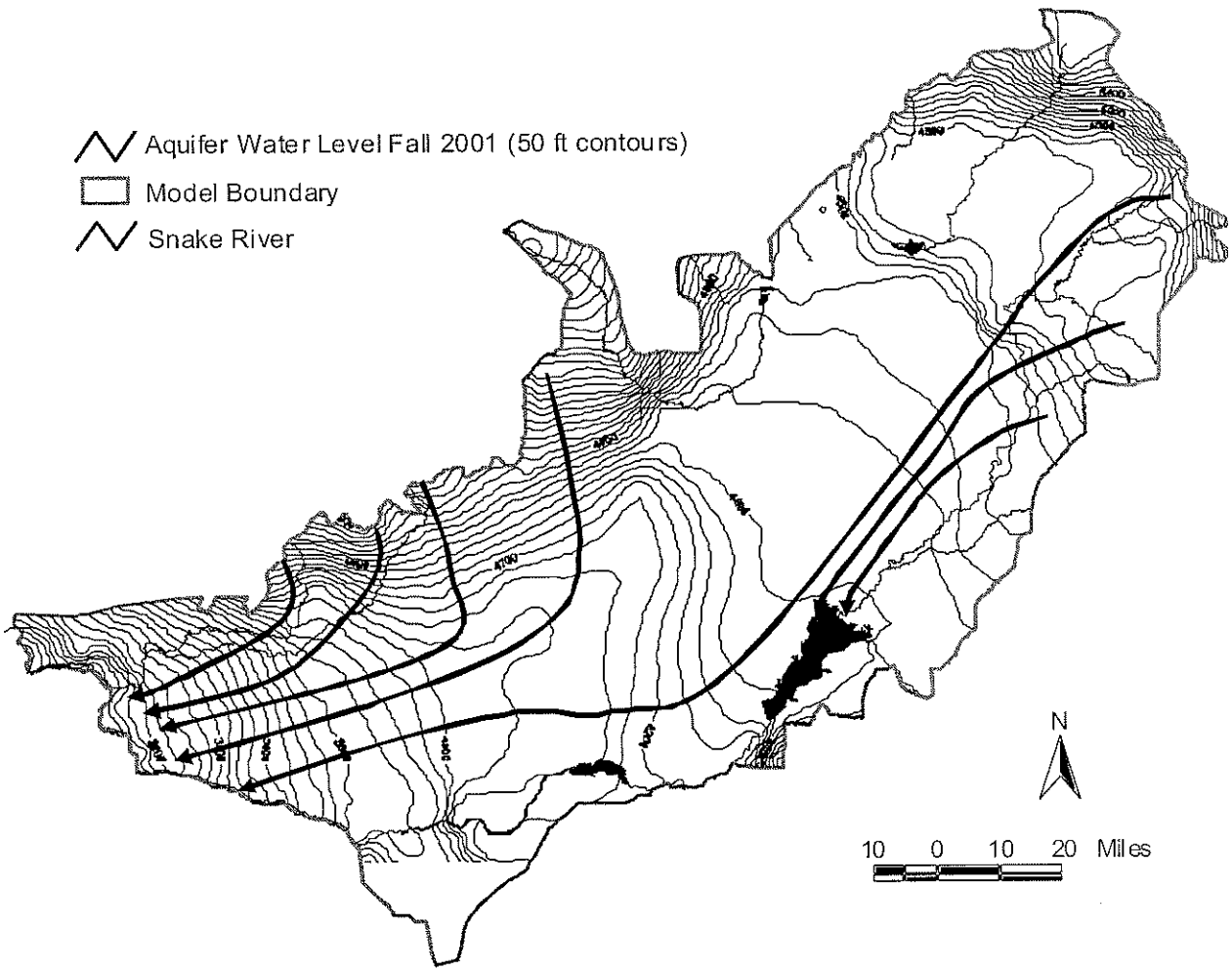

Figure 9. Contours of the potentiometric surface of the Snake River Plain Aquifer and estimated aquifer flow lines.

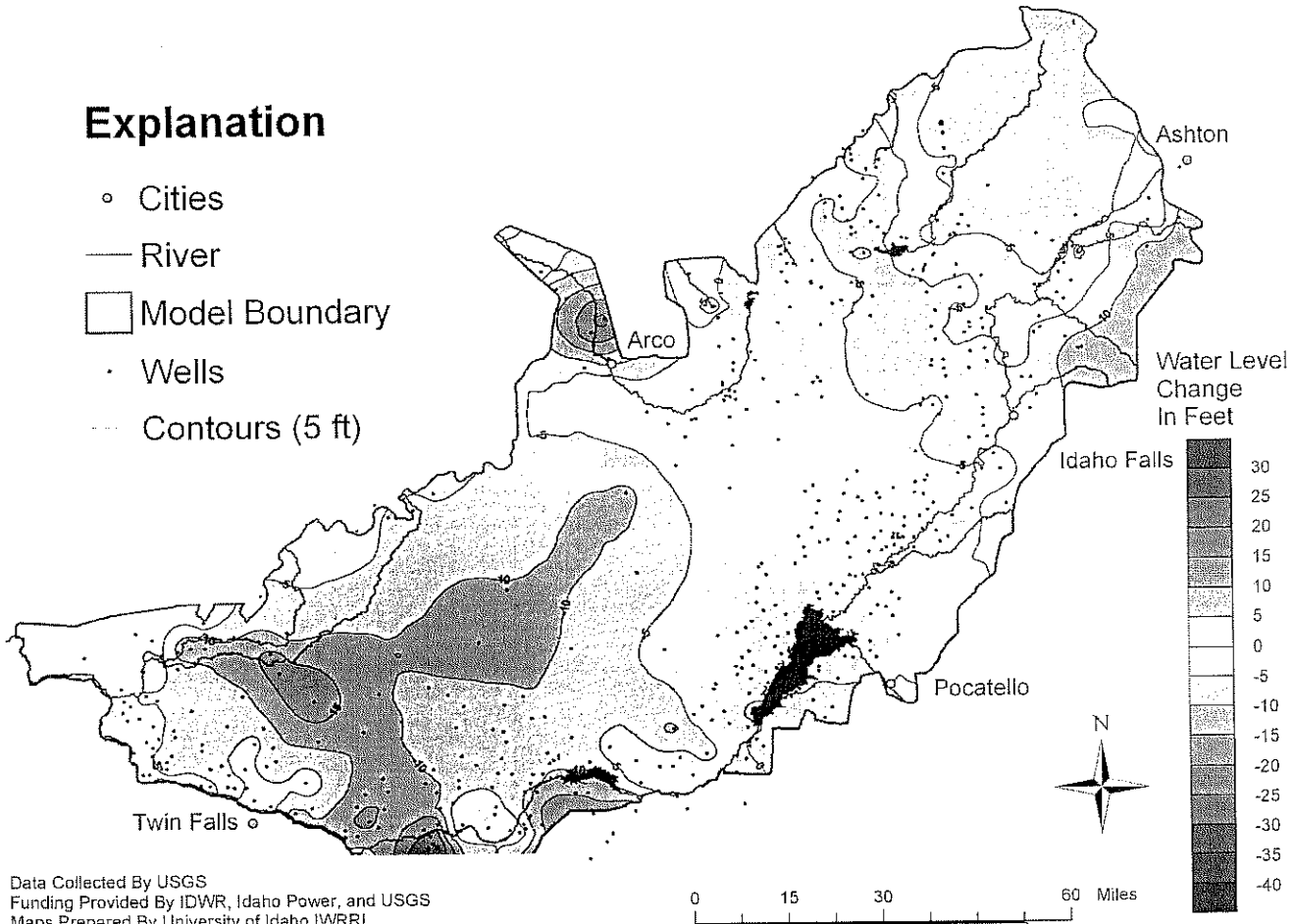

Figure 10. Water level change map spring, 1980 to spring, 2002.

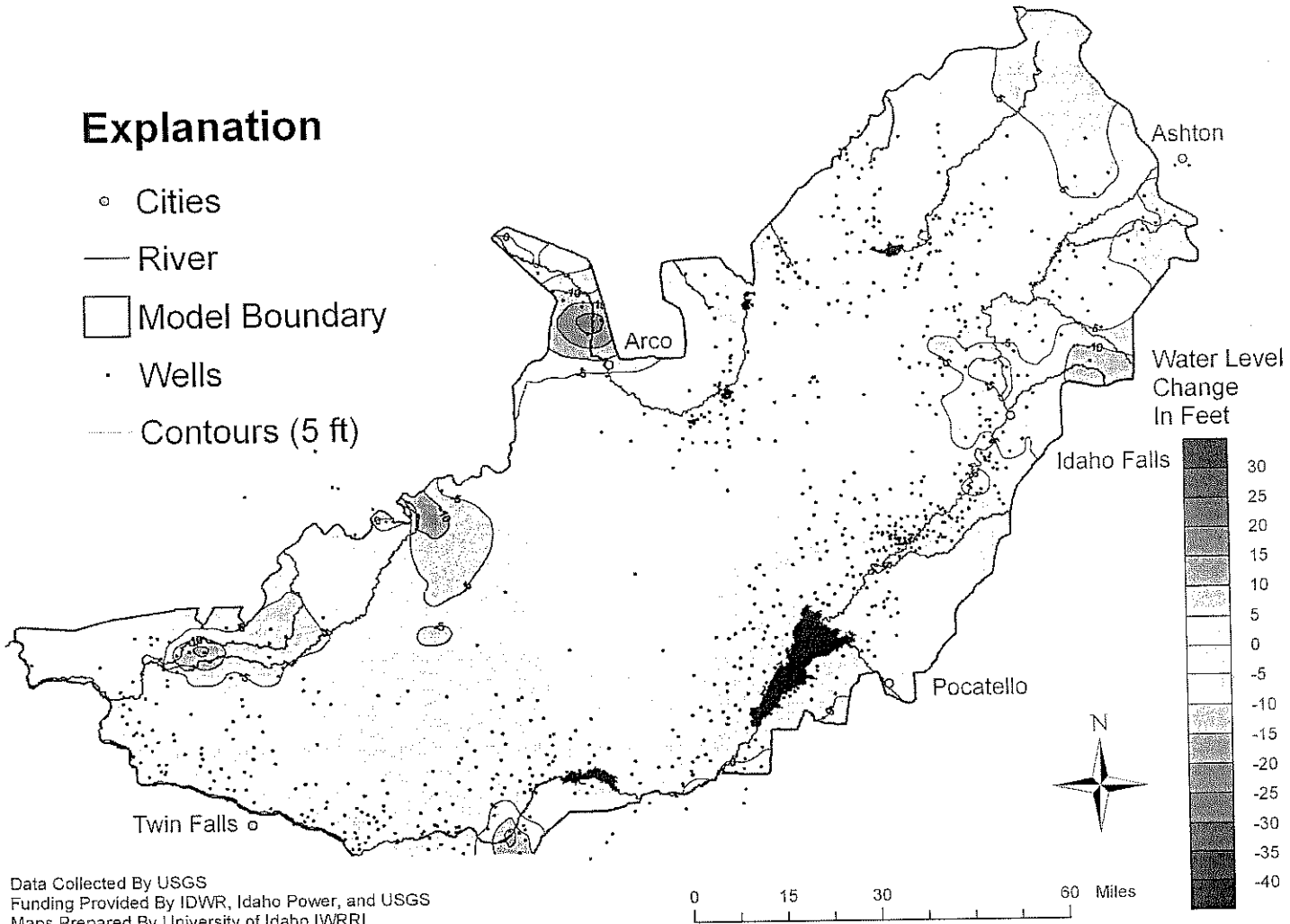

Figure 11. Water level change map spring, 2001 to spring, 2002.

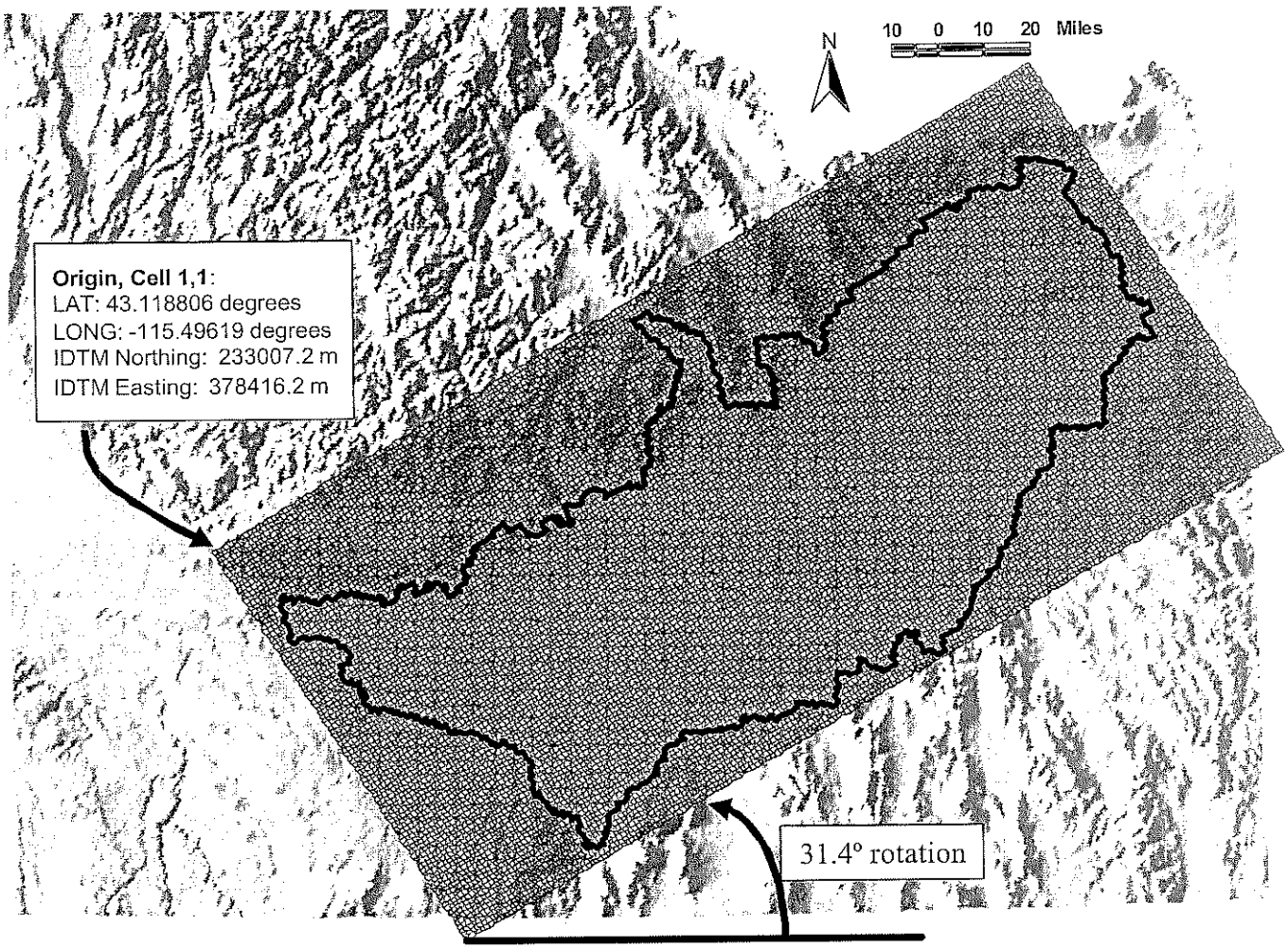

Figure 12. Model grid and origin.

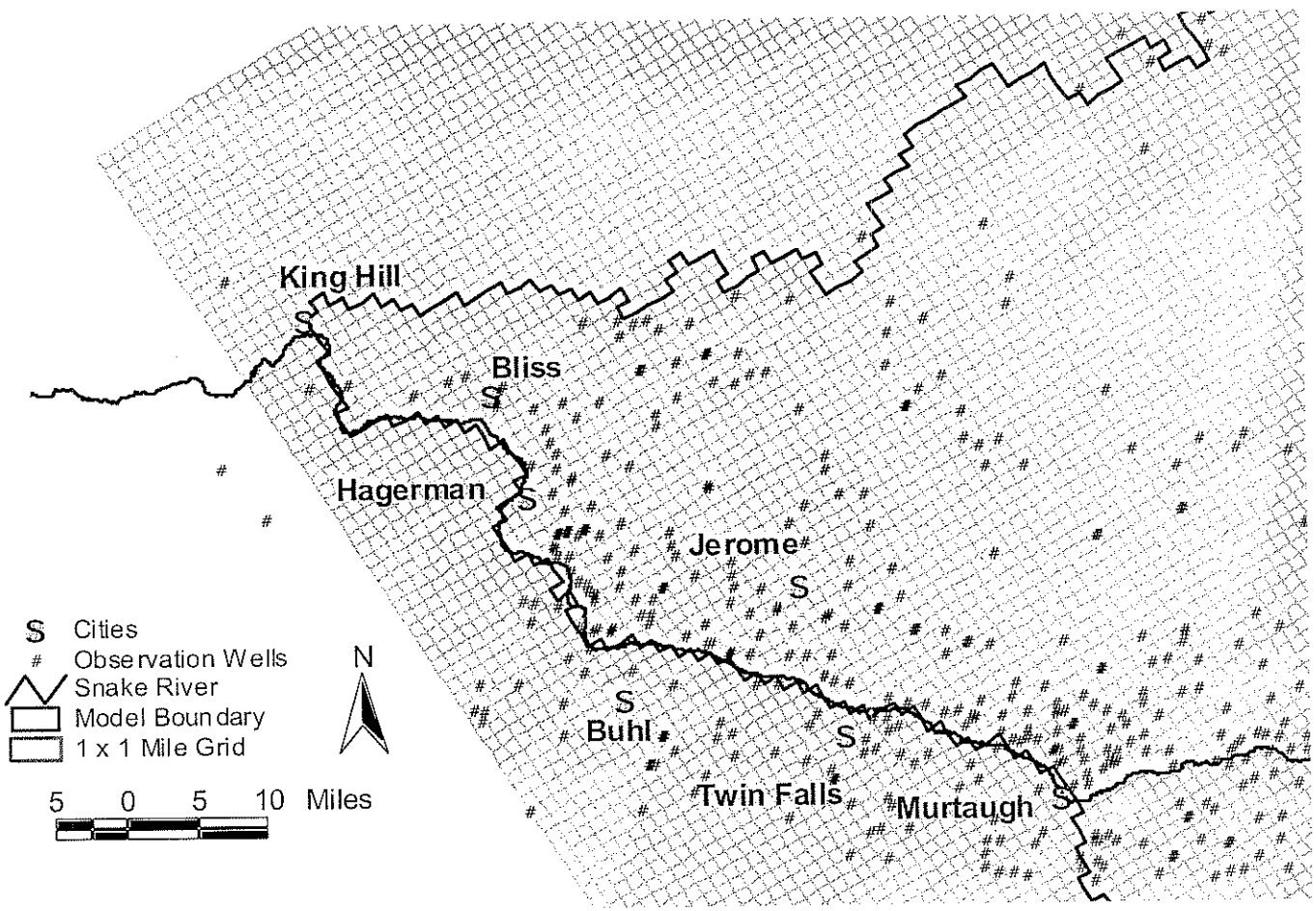

Figure 13. Close-up of model grid in the Thousand Springs area.

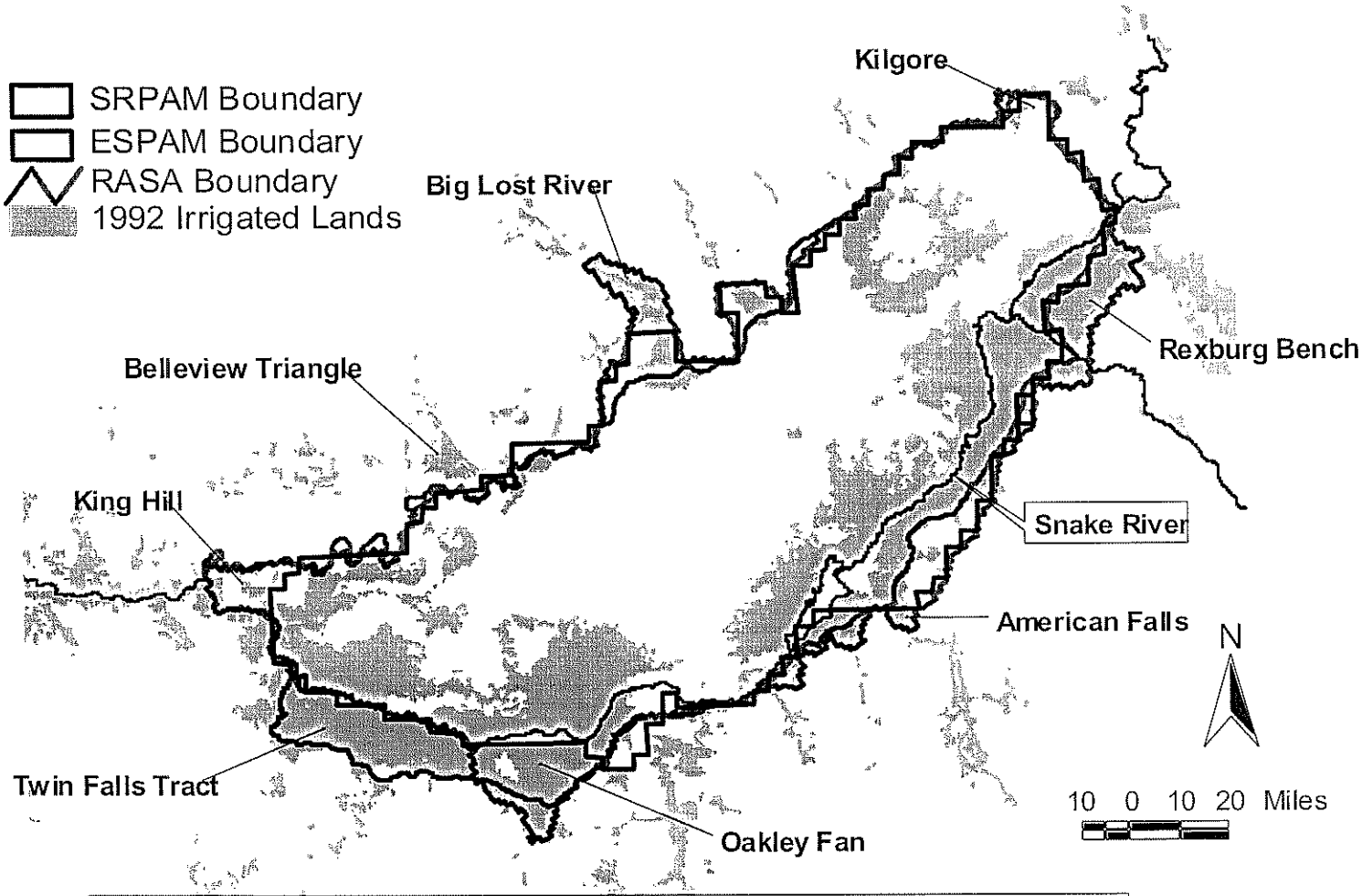

Figure 14. ESPAM model boundary compared with SRPAM and RASA boundaries.

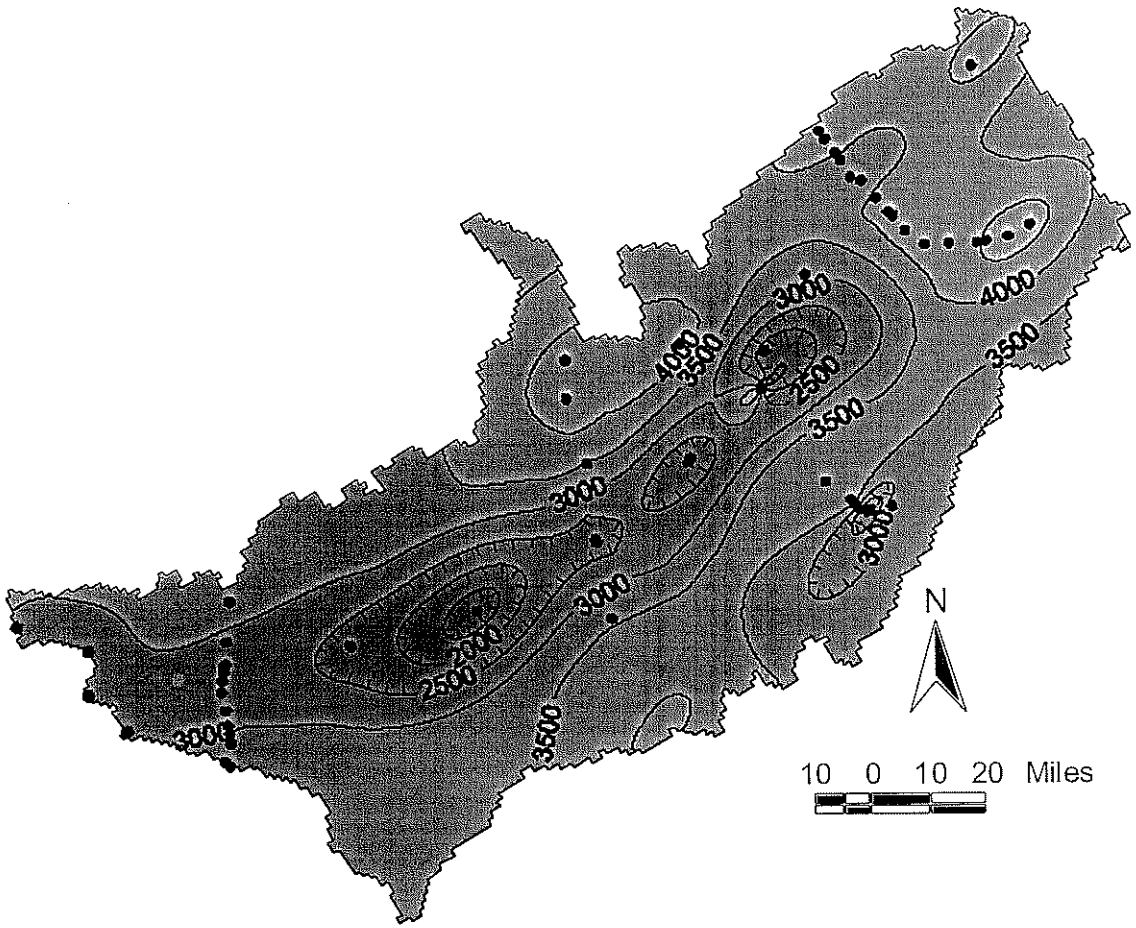

Figure 15. Aquifer bottom elevations with estimated elevation points. Based on modified Whitehead (1986) data. Black dots represent locations used by Whitehead, green dots represent modified Whitehead data points, red dots represent points added to anchor kriged surface.

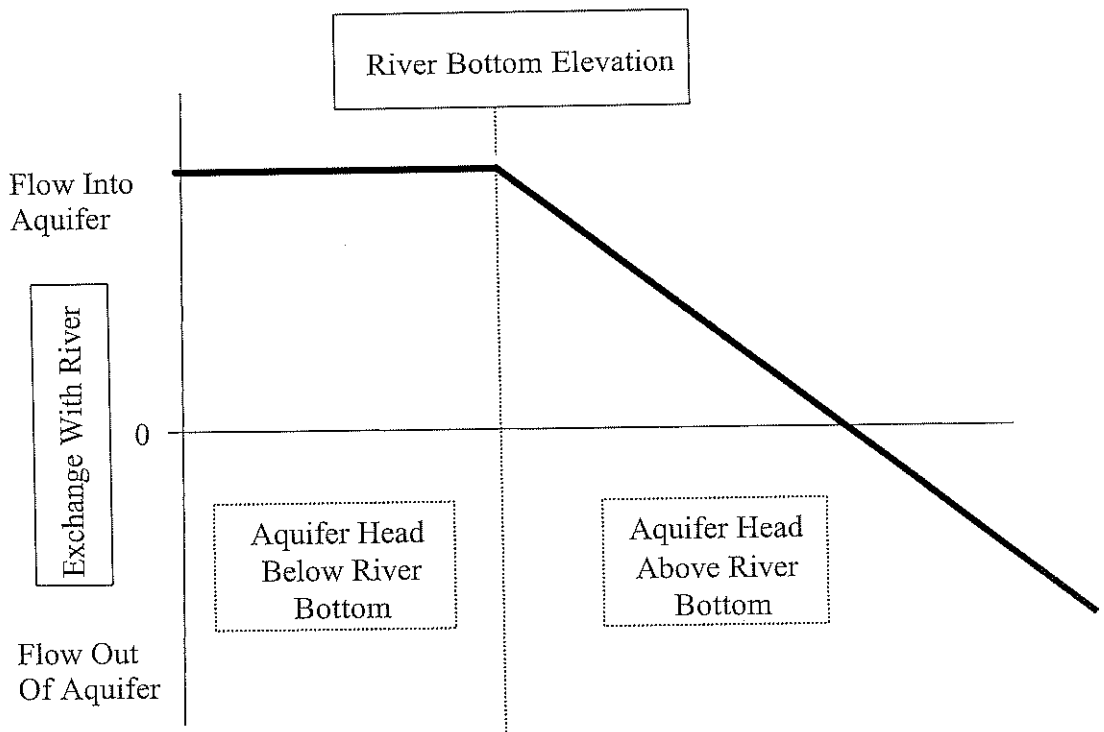

Figure 16. Conceptual illustration of river leakage computation (after McDonald and Harbaugh 1988).

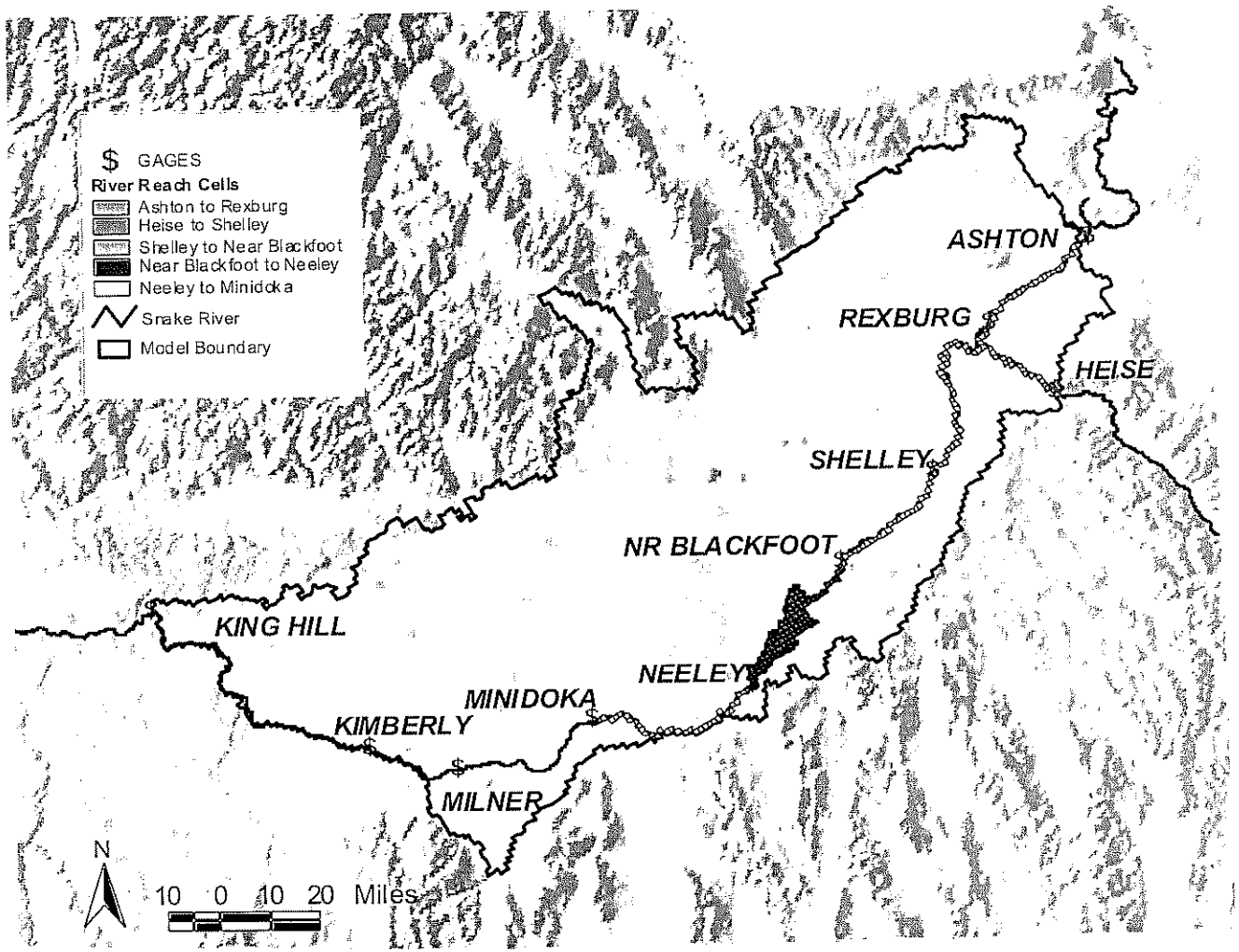

Figure 17. Head-dependent river reaches.

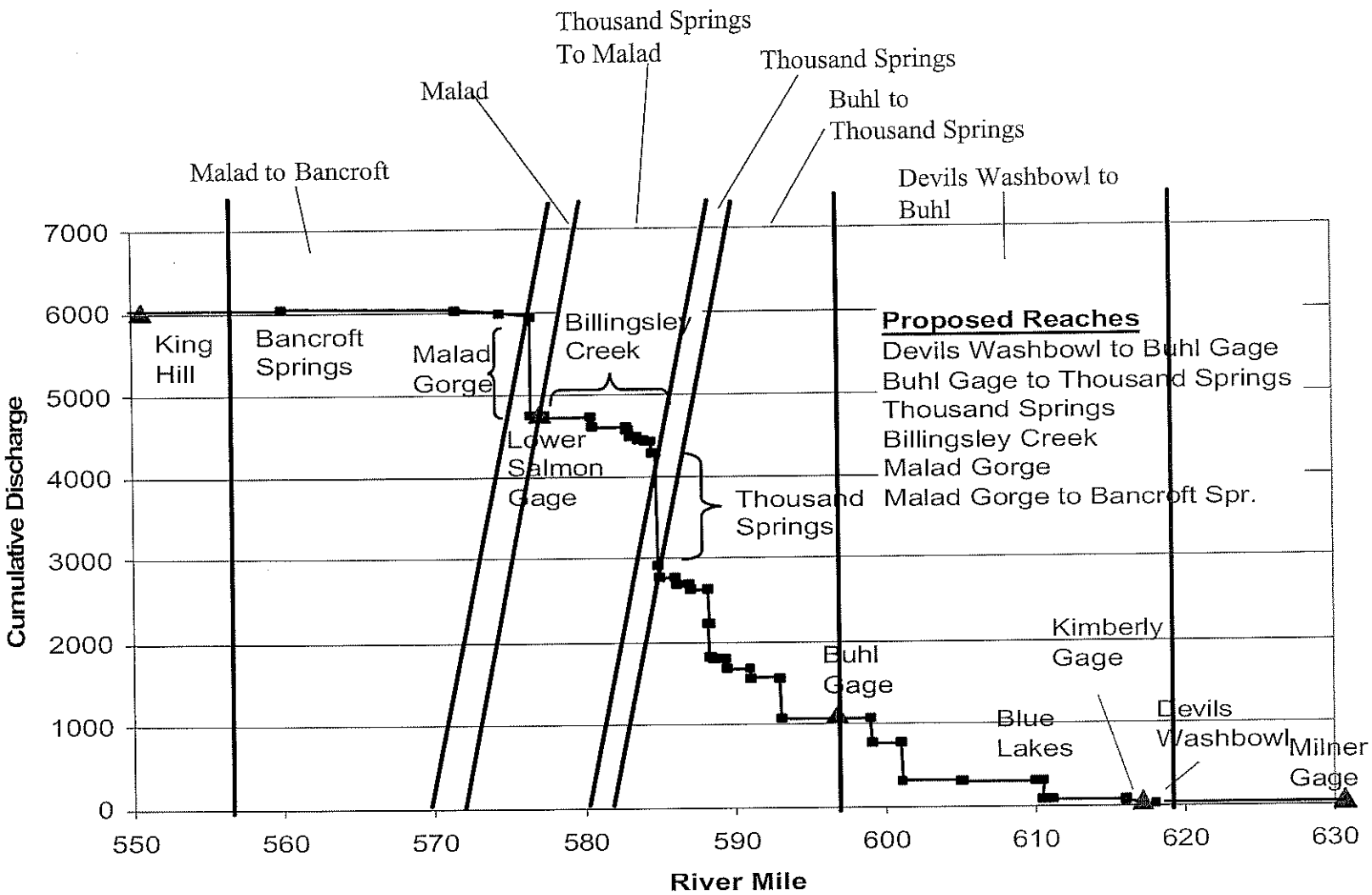

Figure 18. Approximate accumulative spring discharge progressively from Milner Dam to King Hill.

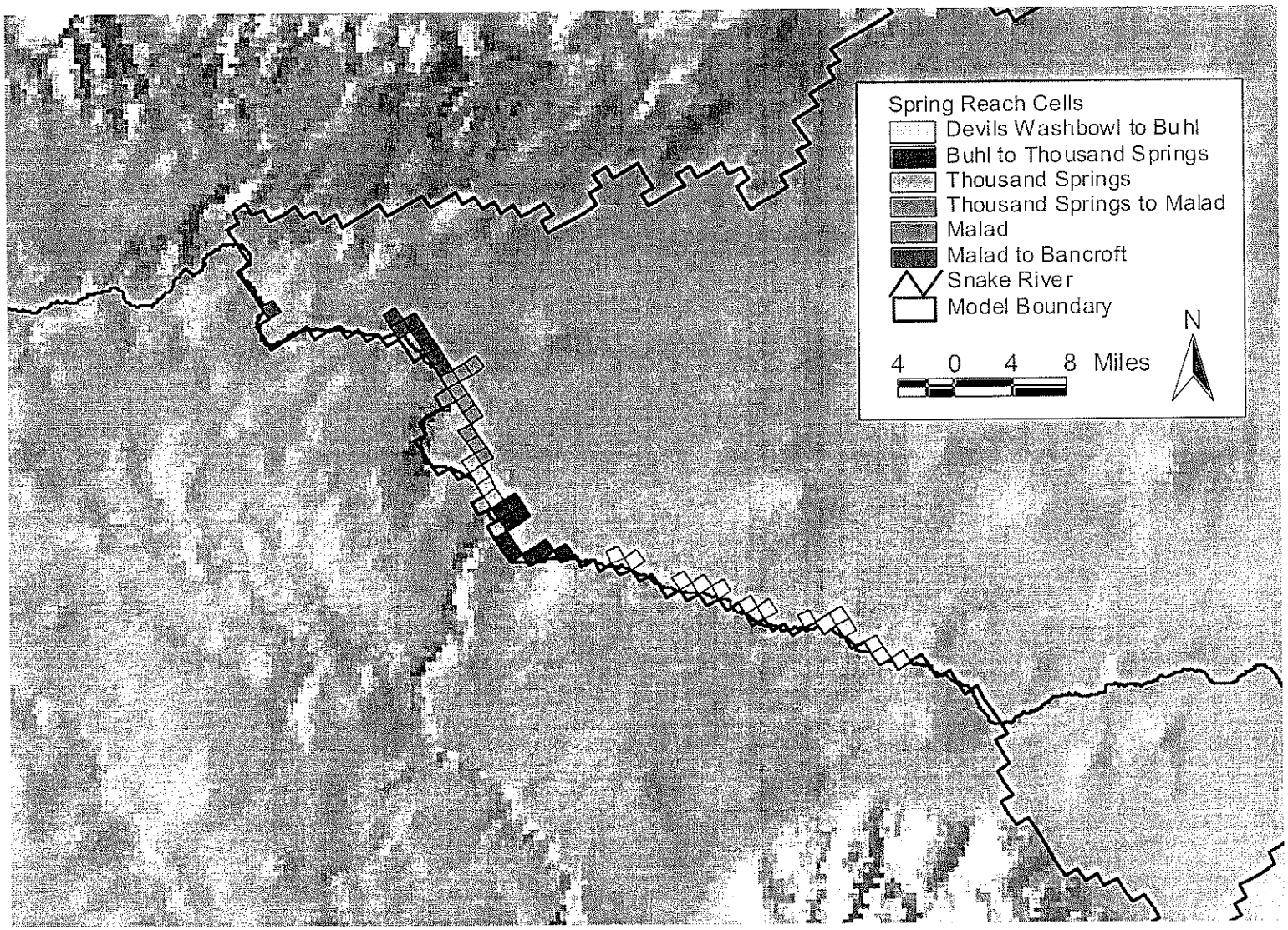

Figure 19. Head-dependent spring reaches.

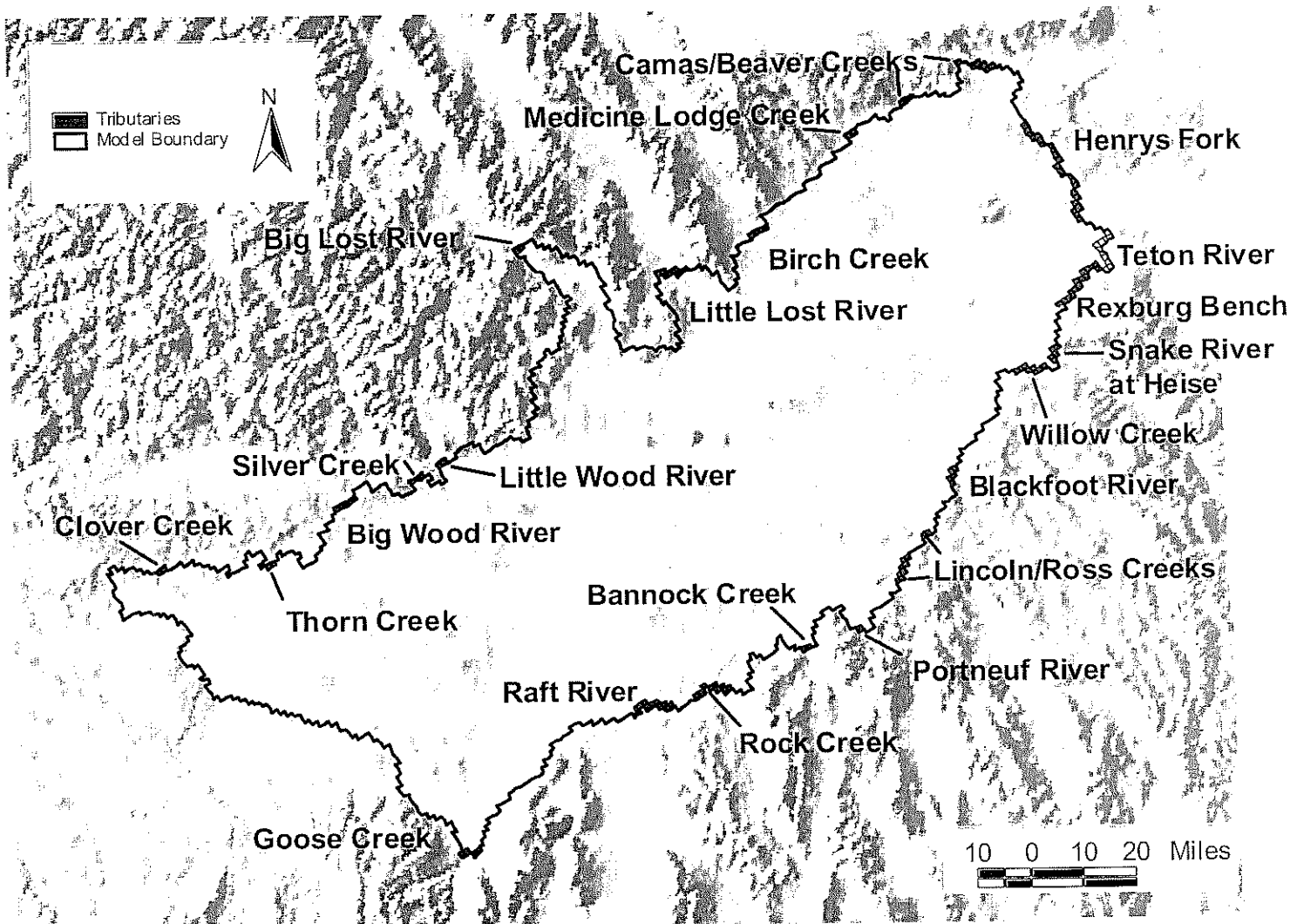

Figure 20. Specified flux tributary underflow locations.

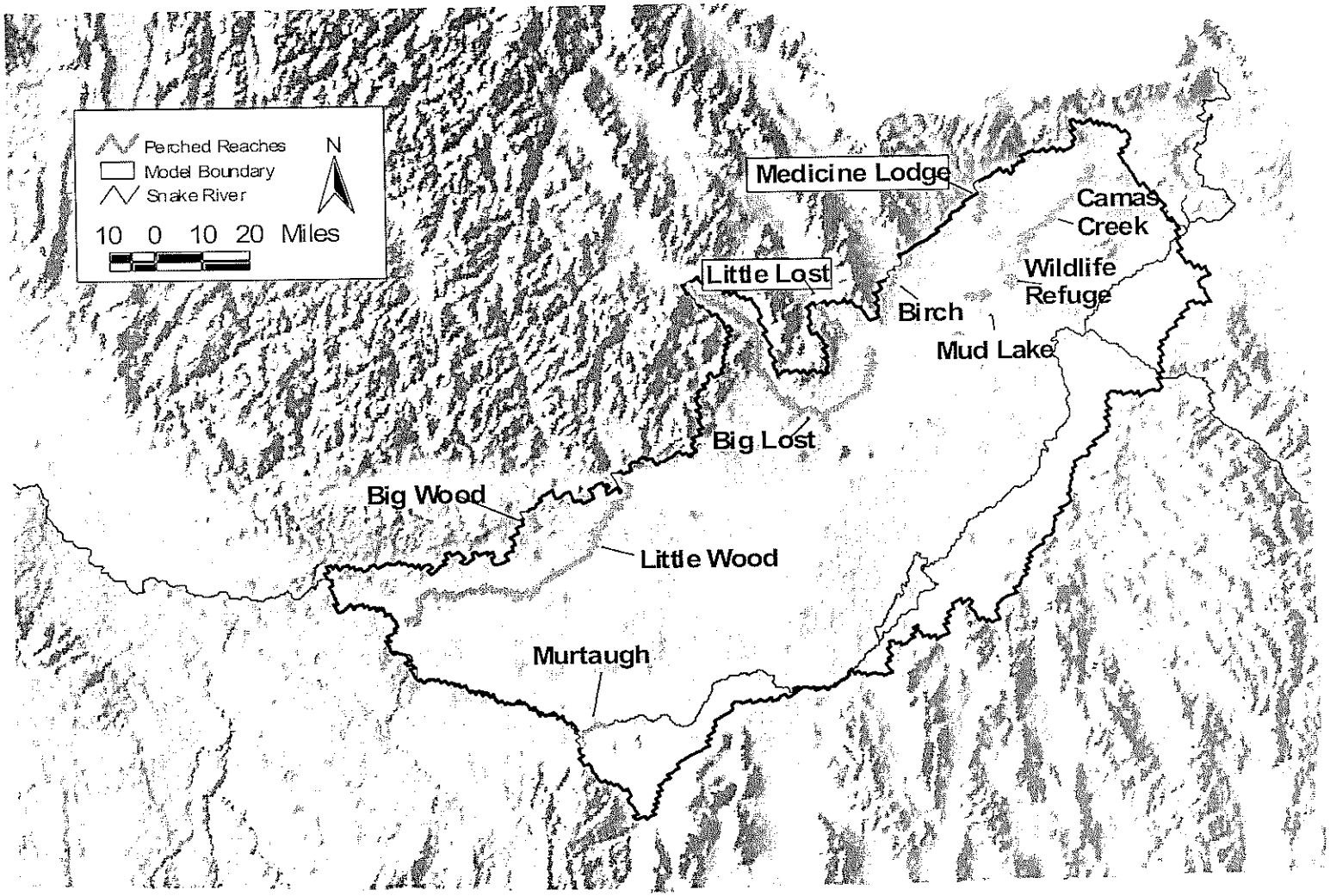

Figure 21. Non-Snake River perched reaches.

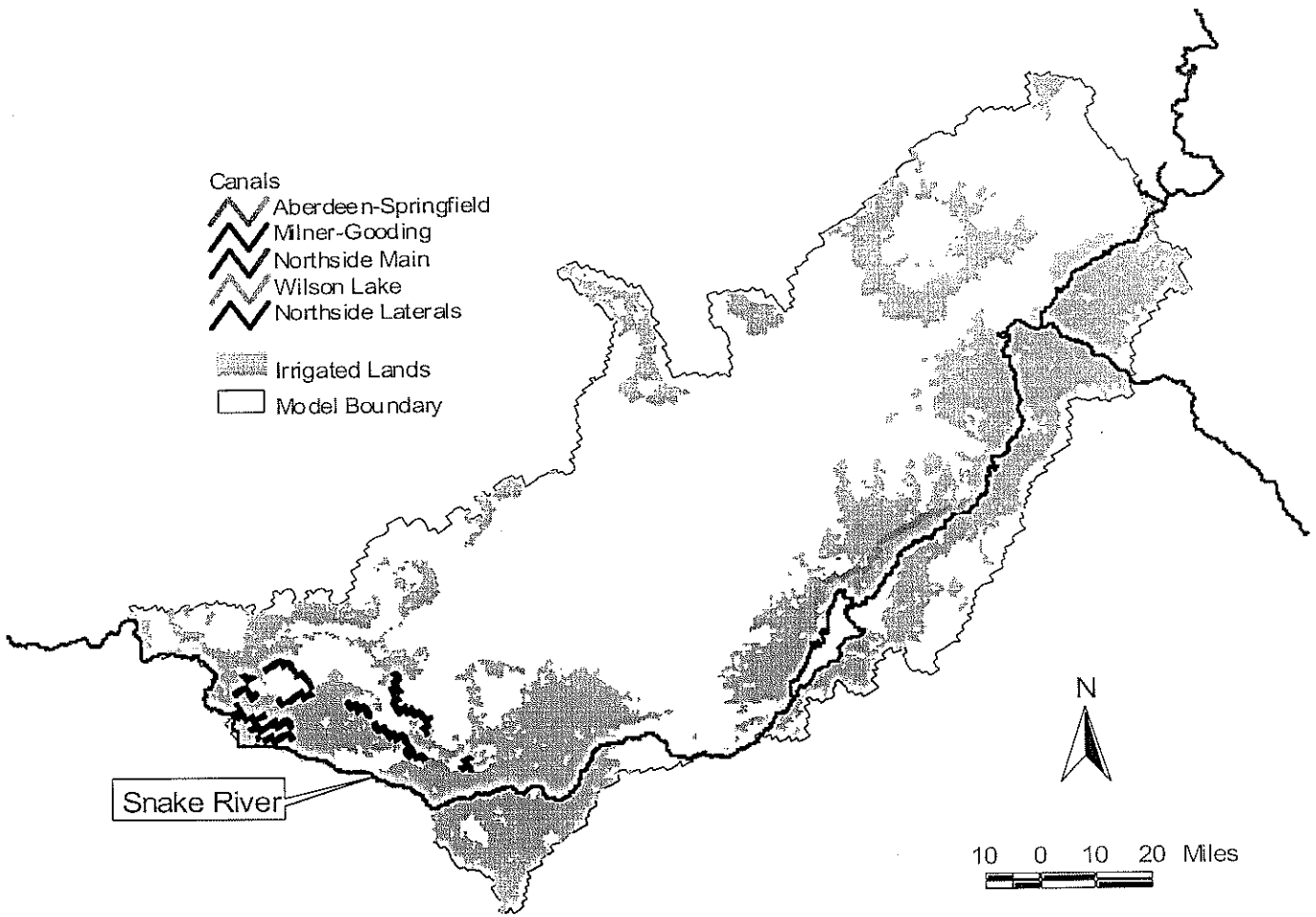

Figure 22. Locations of canals where leakage is explicitly represented.

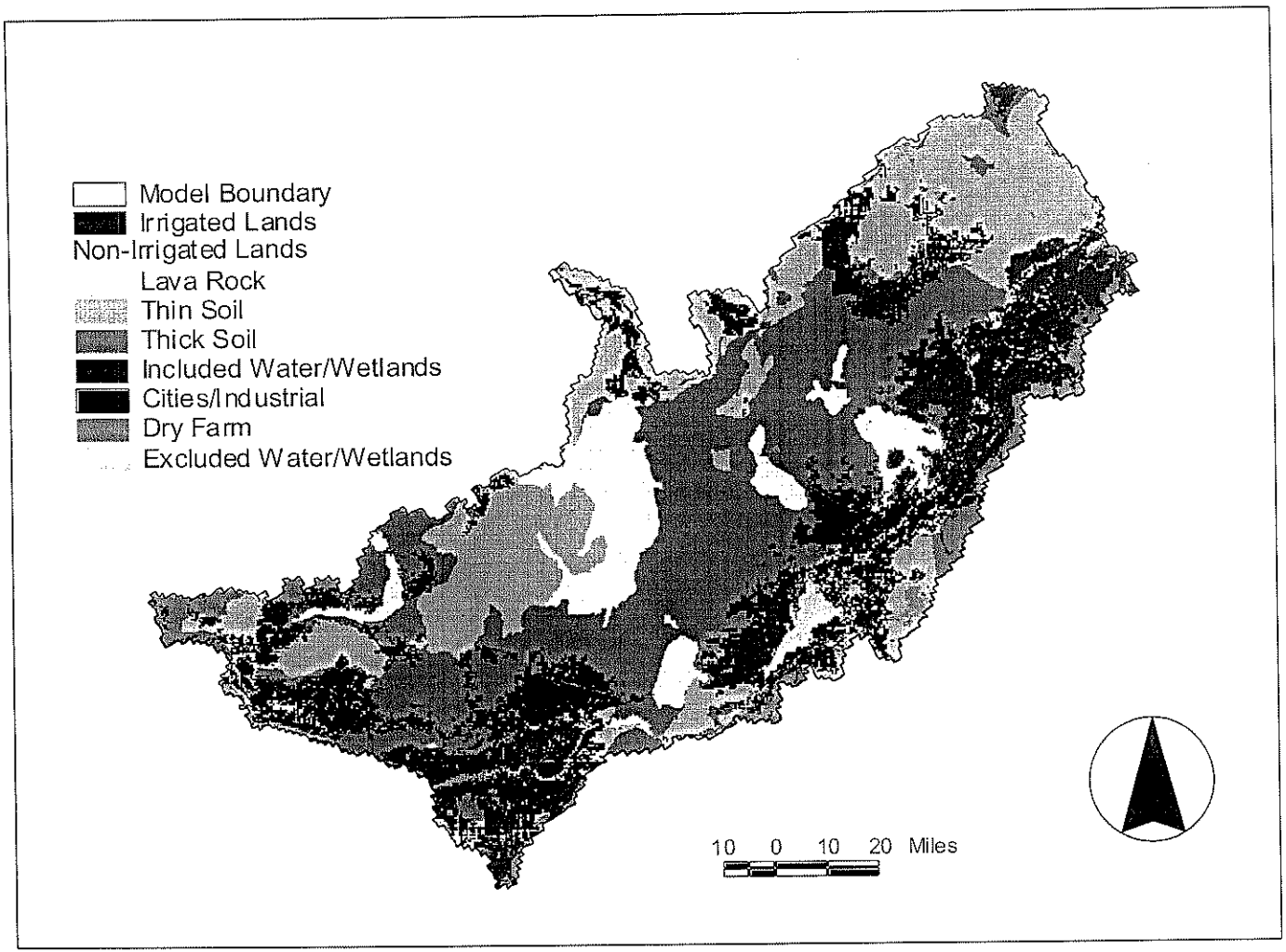

Figure 23. Land use analysis based on 1992 aerial photographs with ground-truthing.

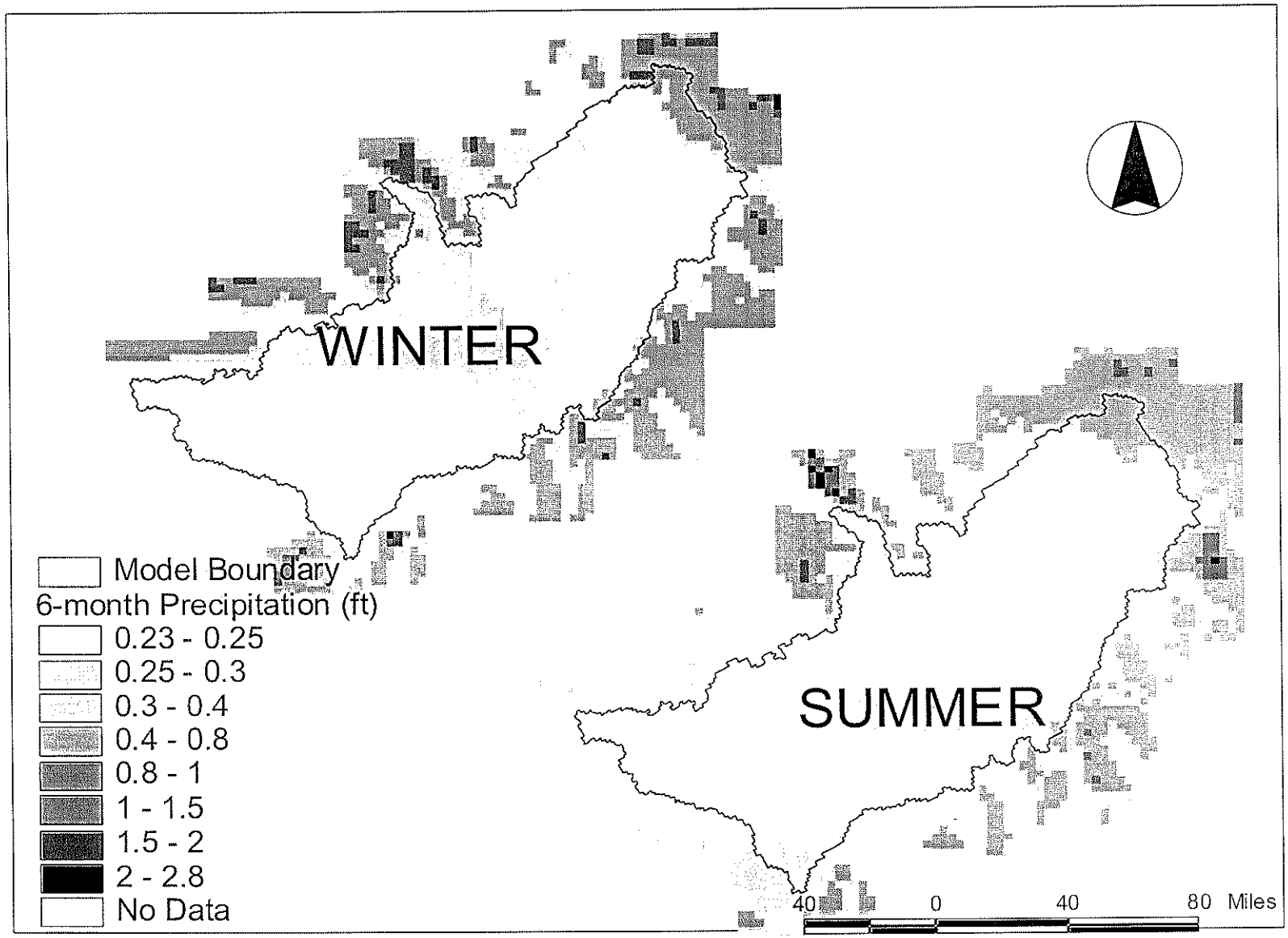

Figure 24. PRISM precipitation maps for the irrigation season and non-irrigation season, based on average precipitation for model period.

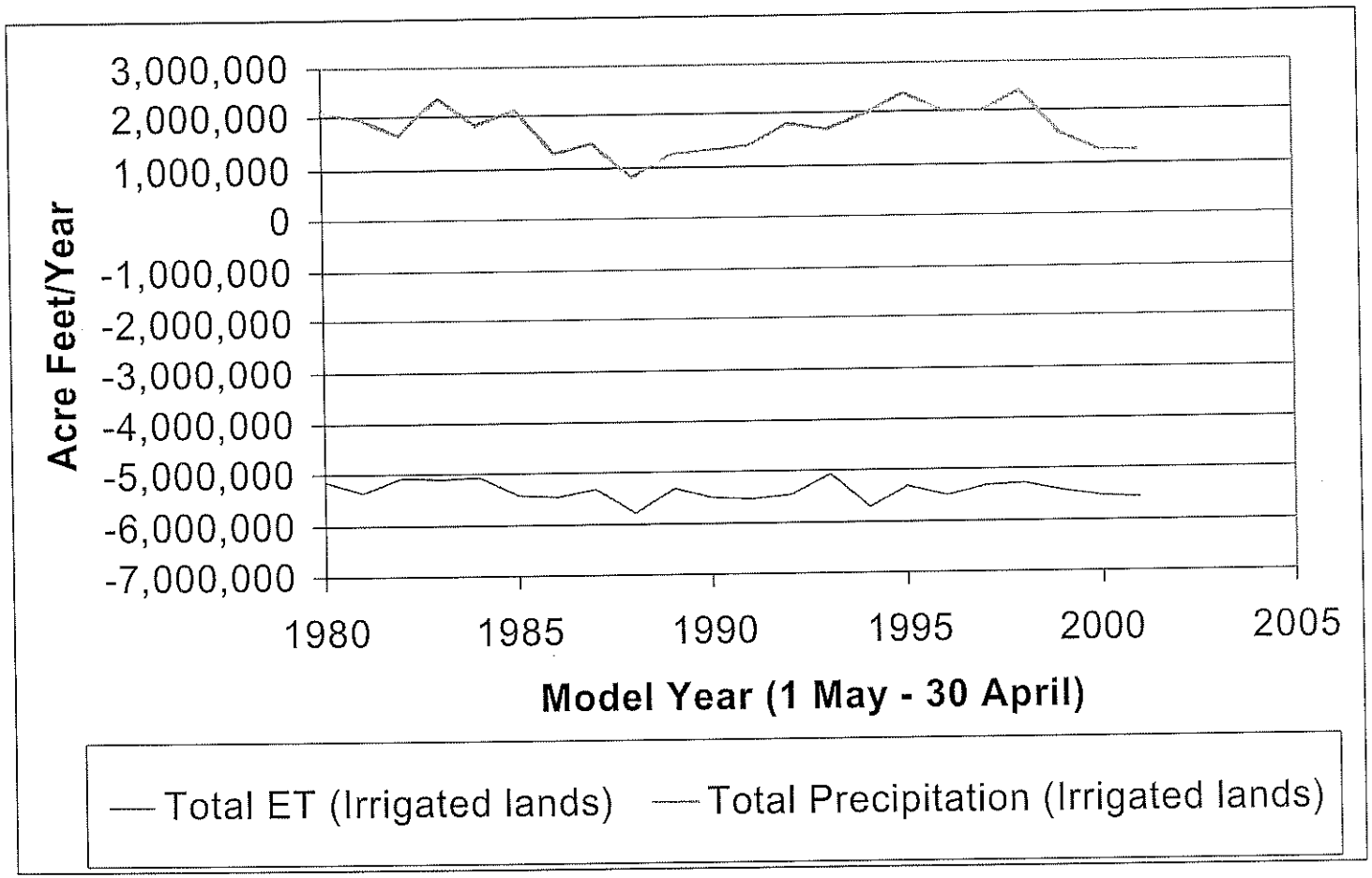

Figure 25. Annual precipitation and evapotranspiration for irrigated lands for the model study period.

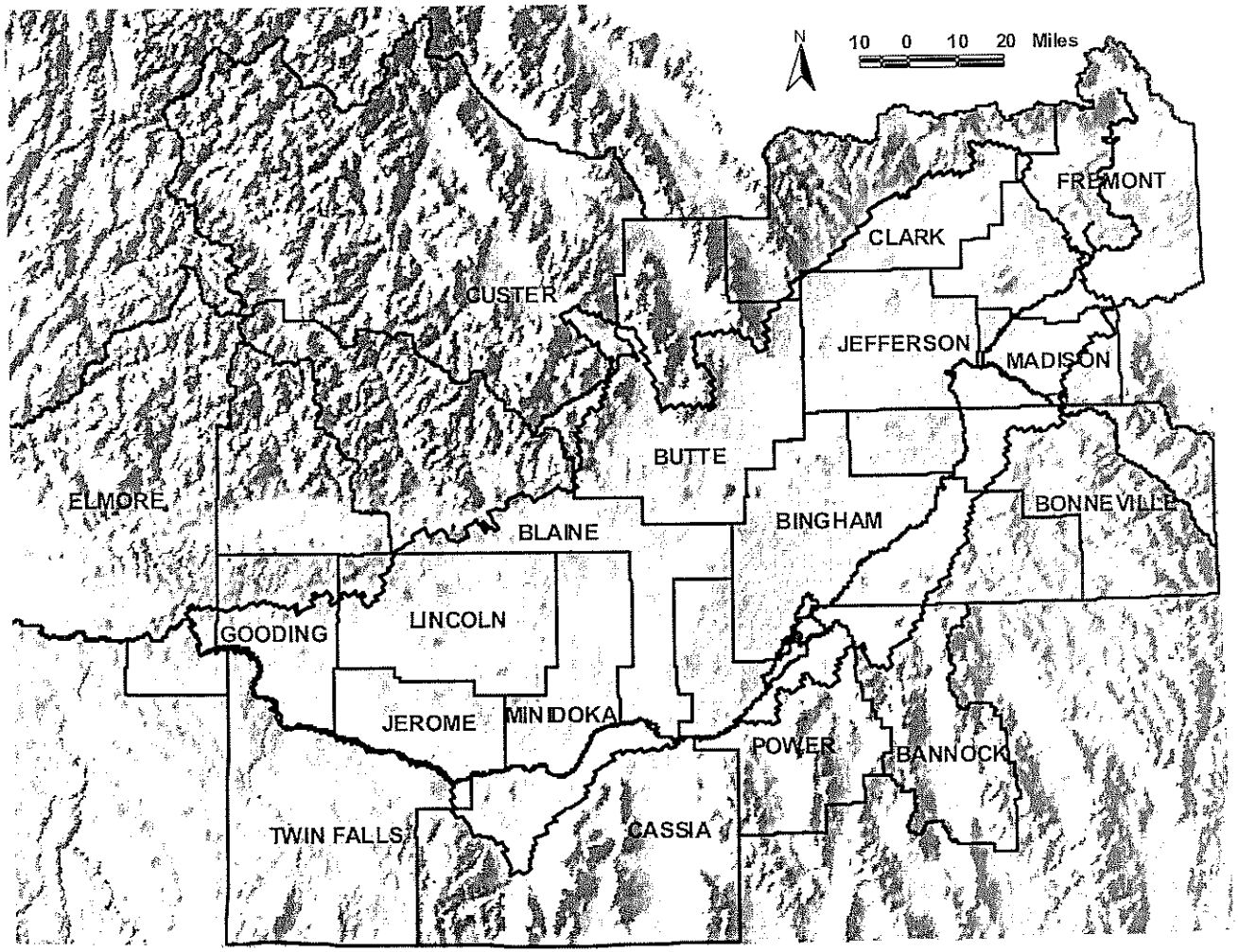

Figure 26. Idaho counties involved in the study area.

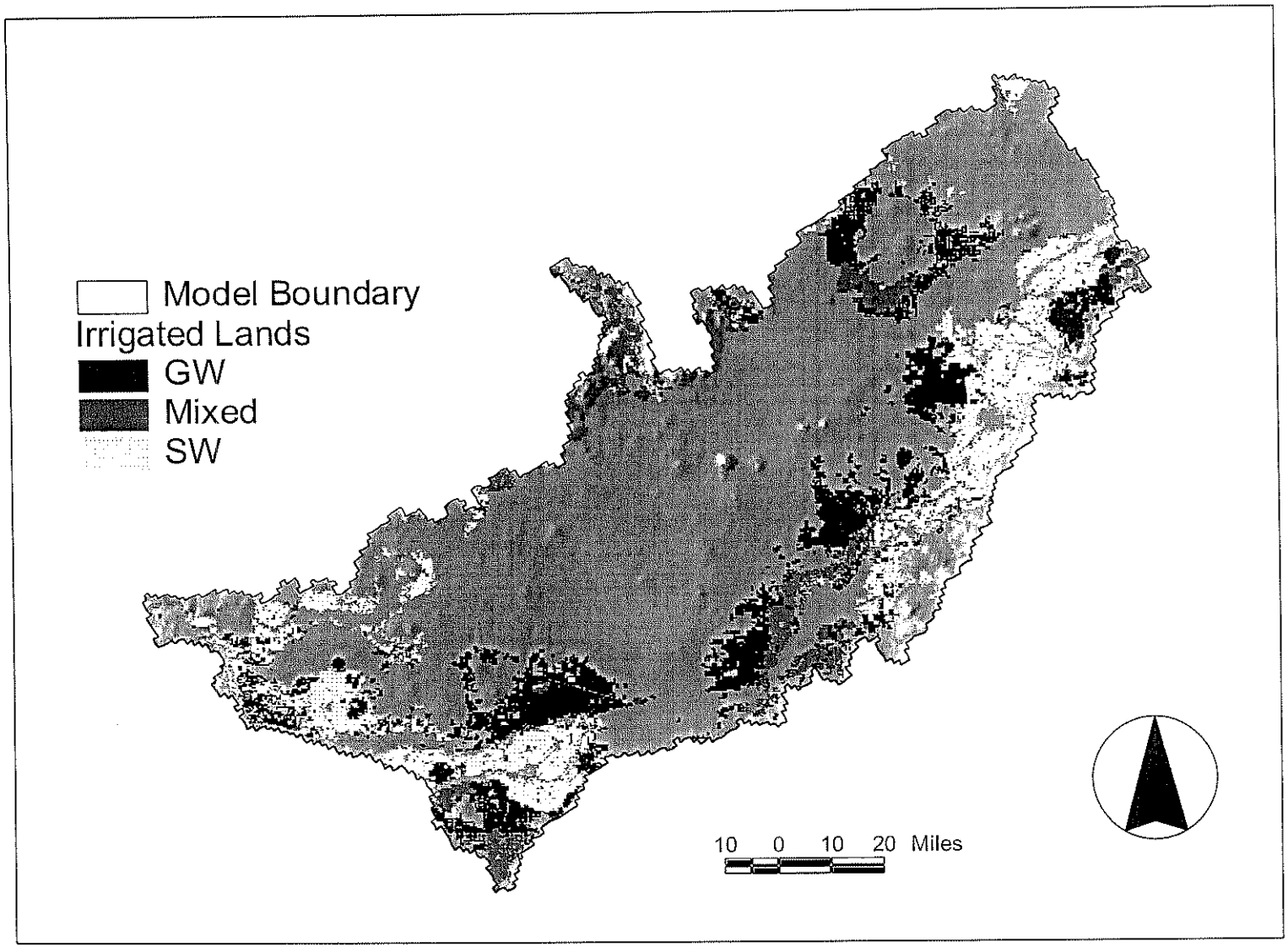

Figure 27. Irrigation water source determined from adjudication data.

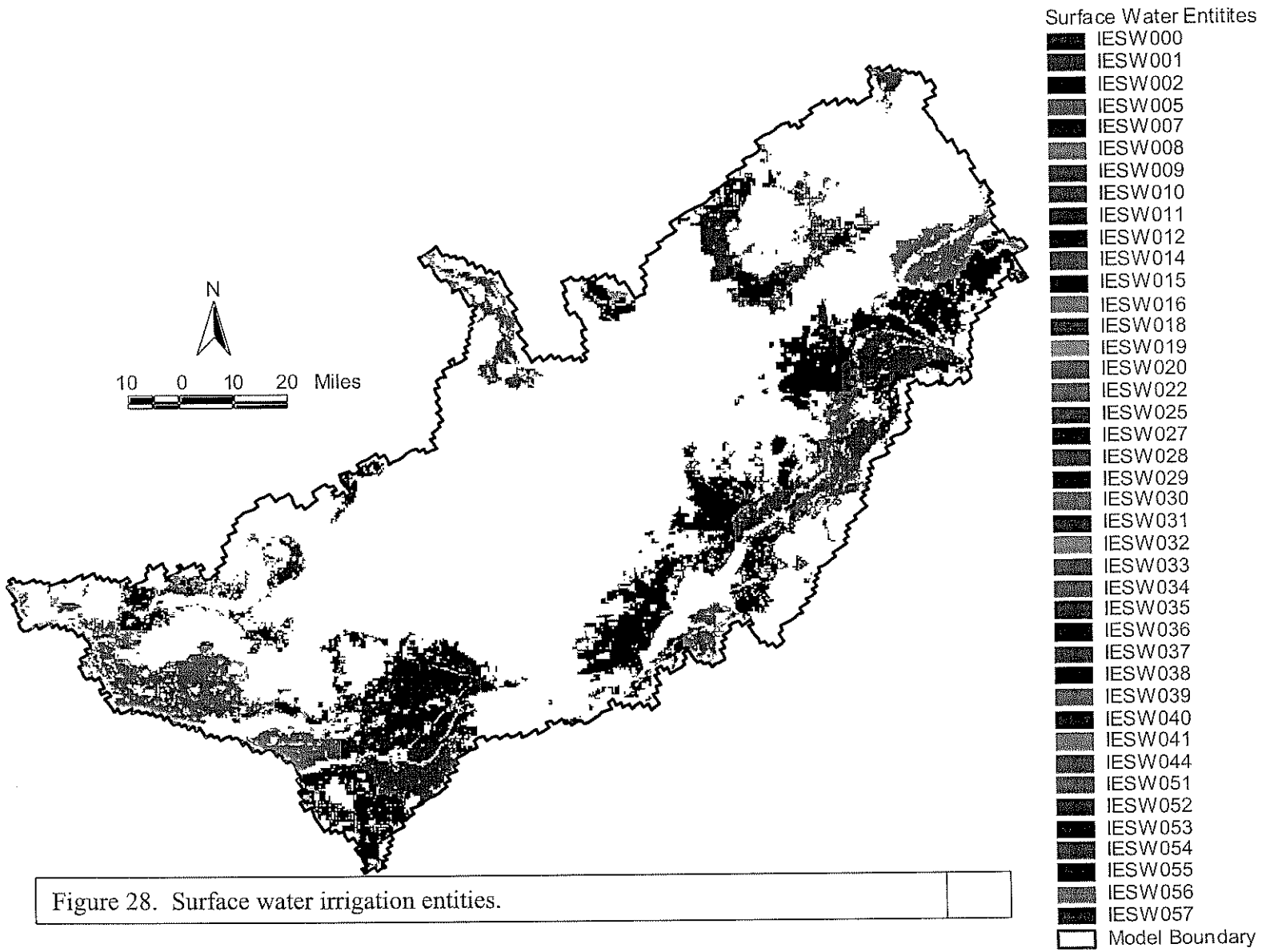

Figure 28. Surface water irrigation entities.

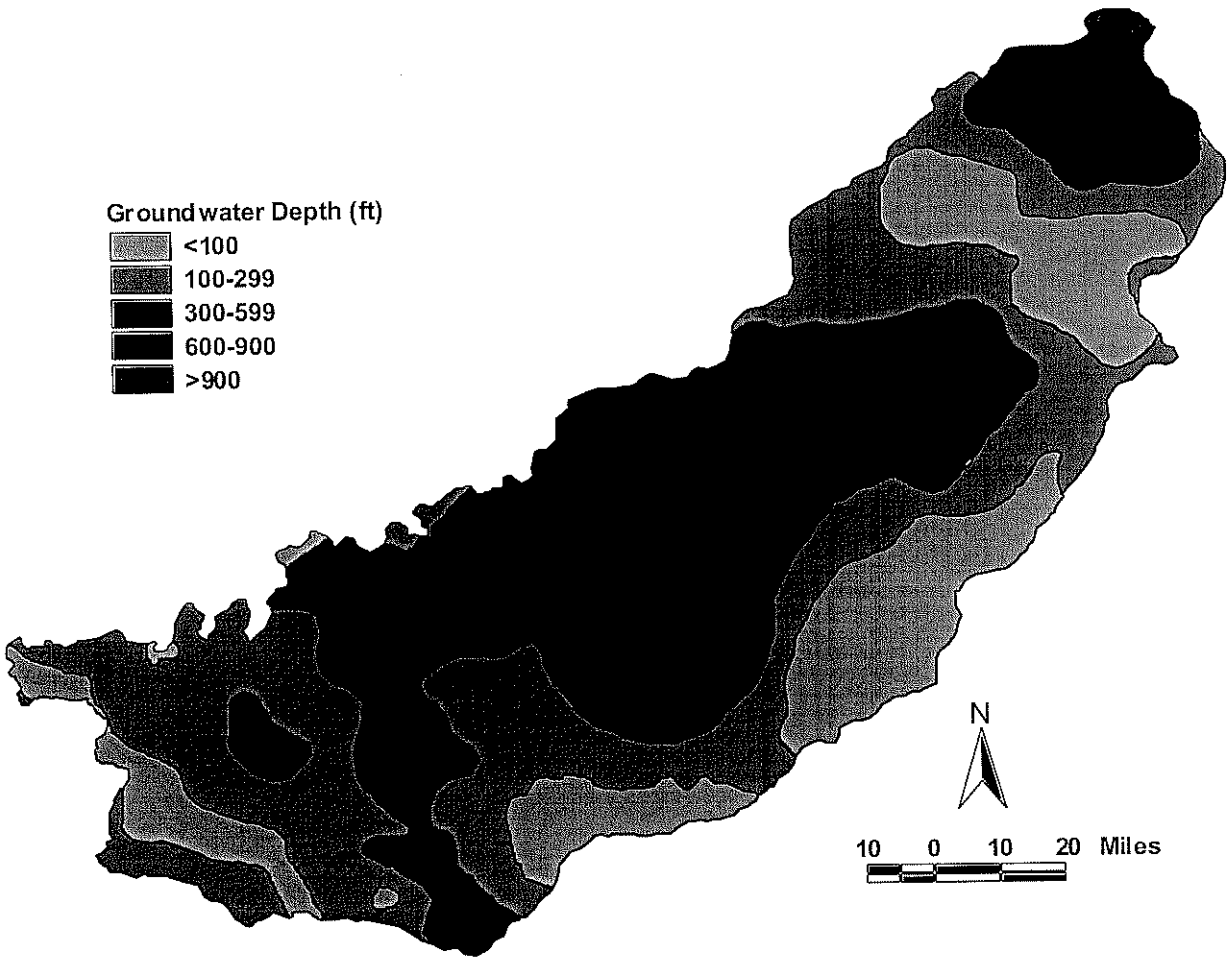

Figure 29. Depth to water (after Lindholm and others, 1988).

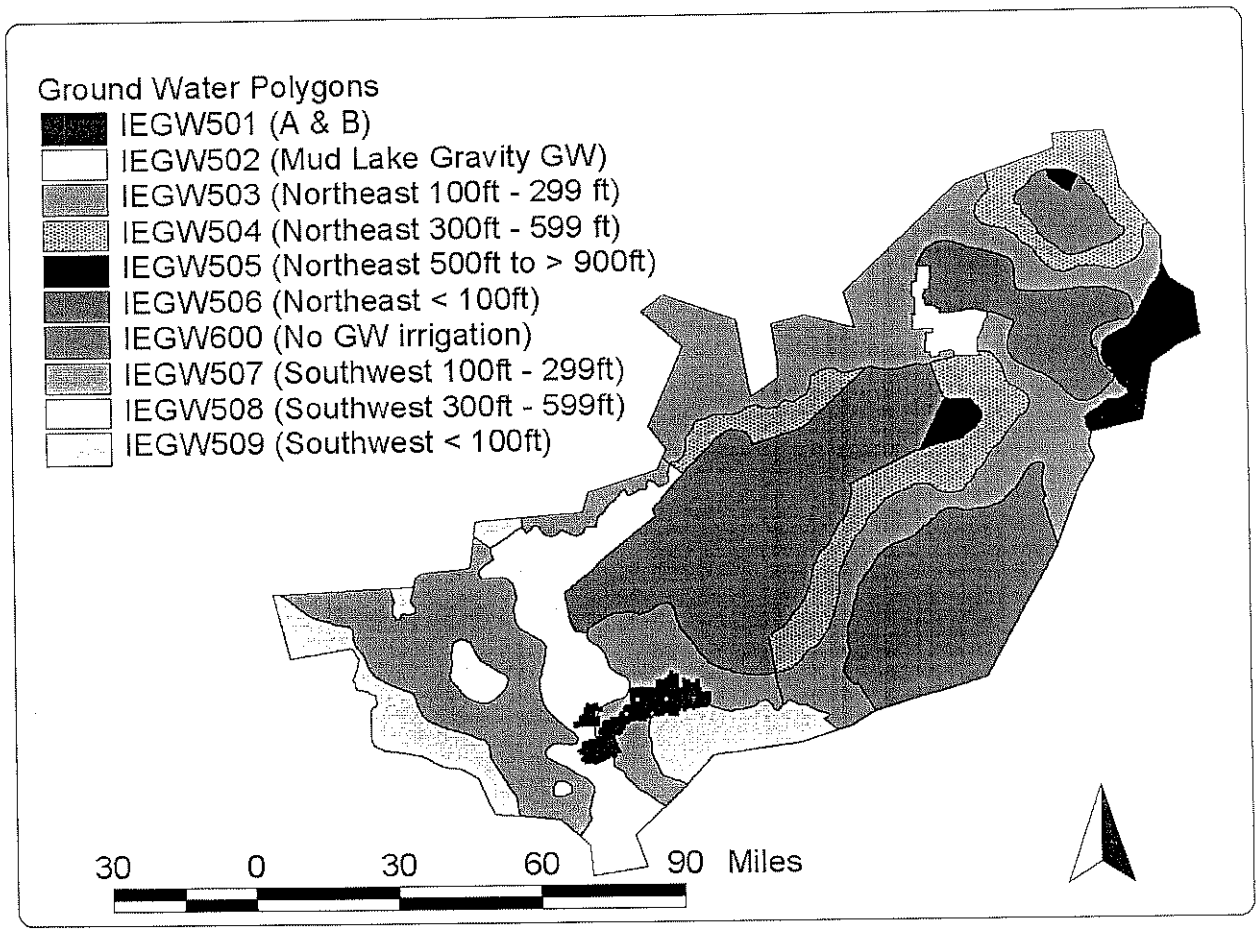

Figure 30. Ground-water polygons.

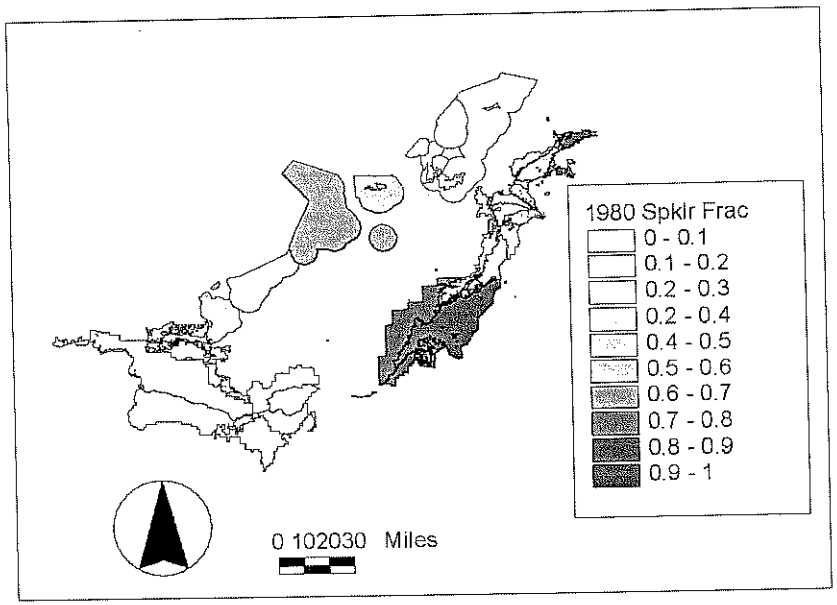

1980

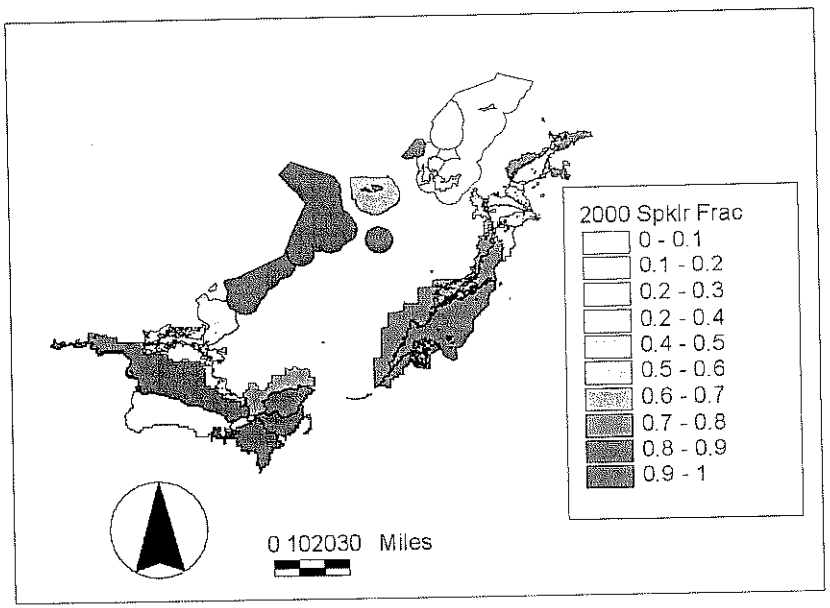

2000

Figure 31. Sprinkler fraction by surface-water entity, 1980 and 2000.

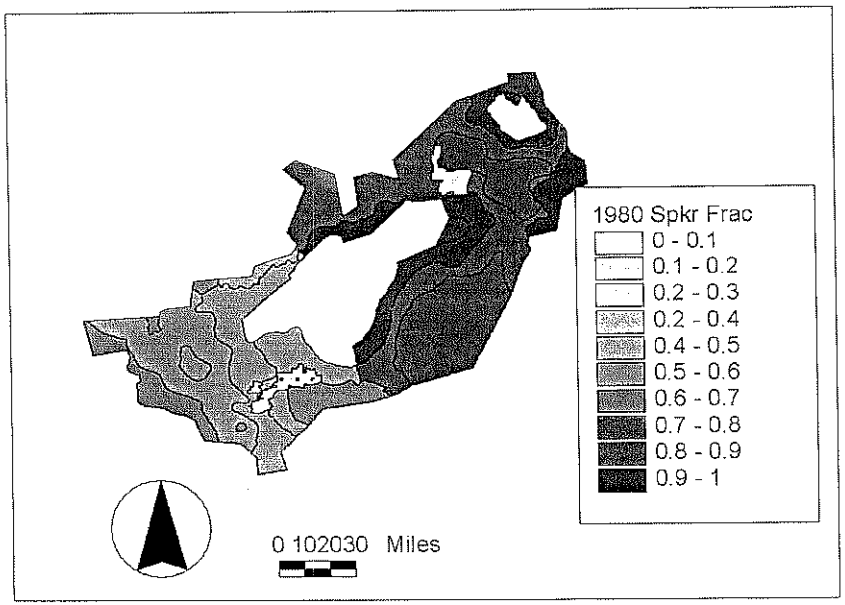

1980

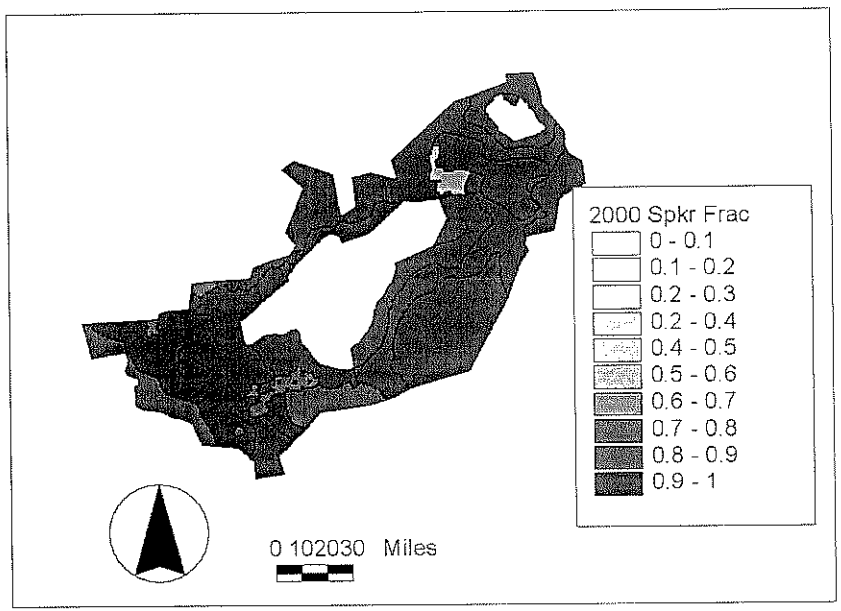

2000

Figure 32. Sprinkler fraction by ground-water polygon, 1980 and 2000.

Figure 33. Upper Snake River return flow measurement sites.

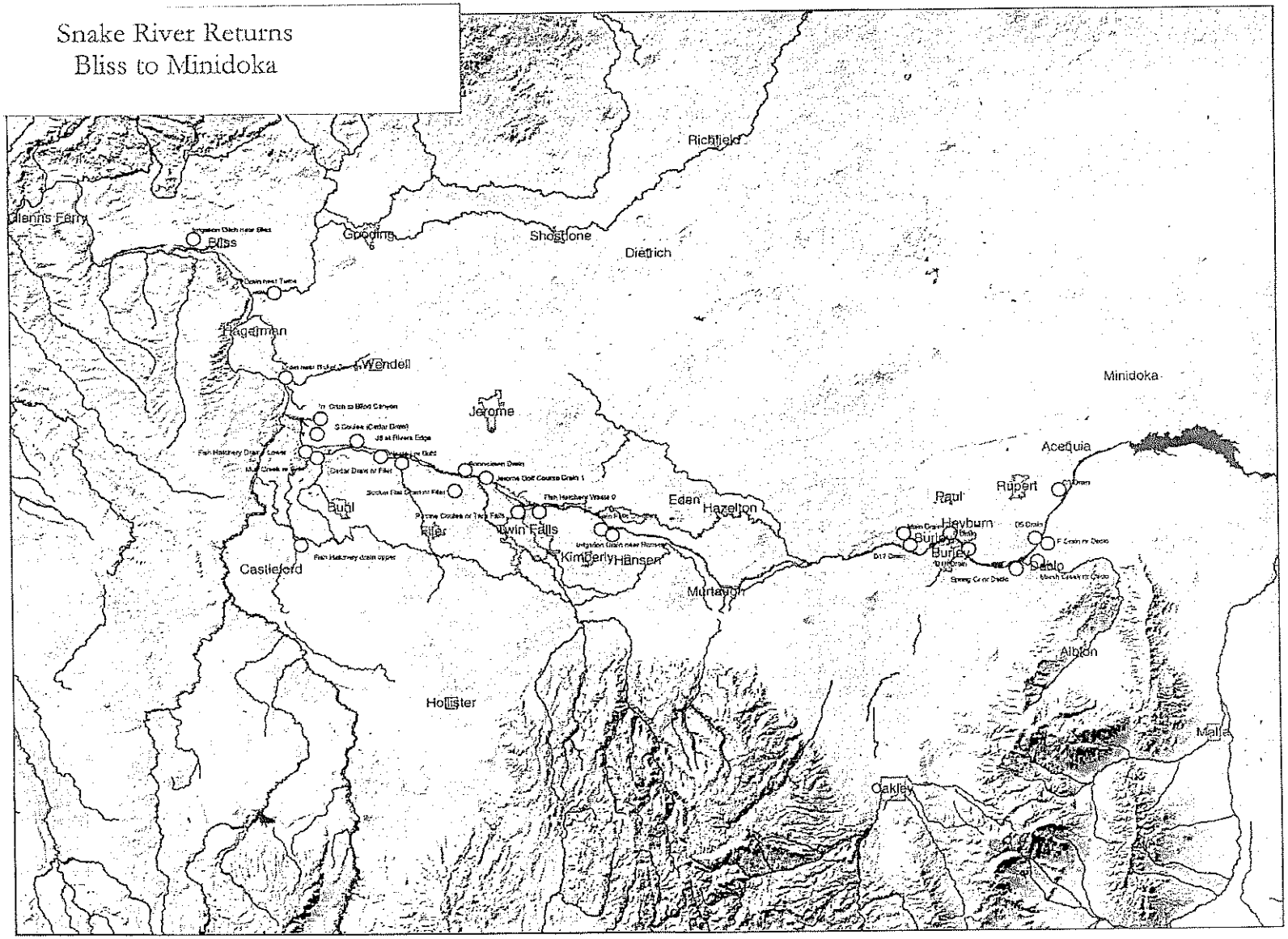

Figure 34. Upper Snake River return flow measurement sites.

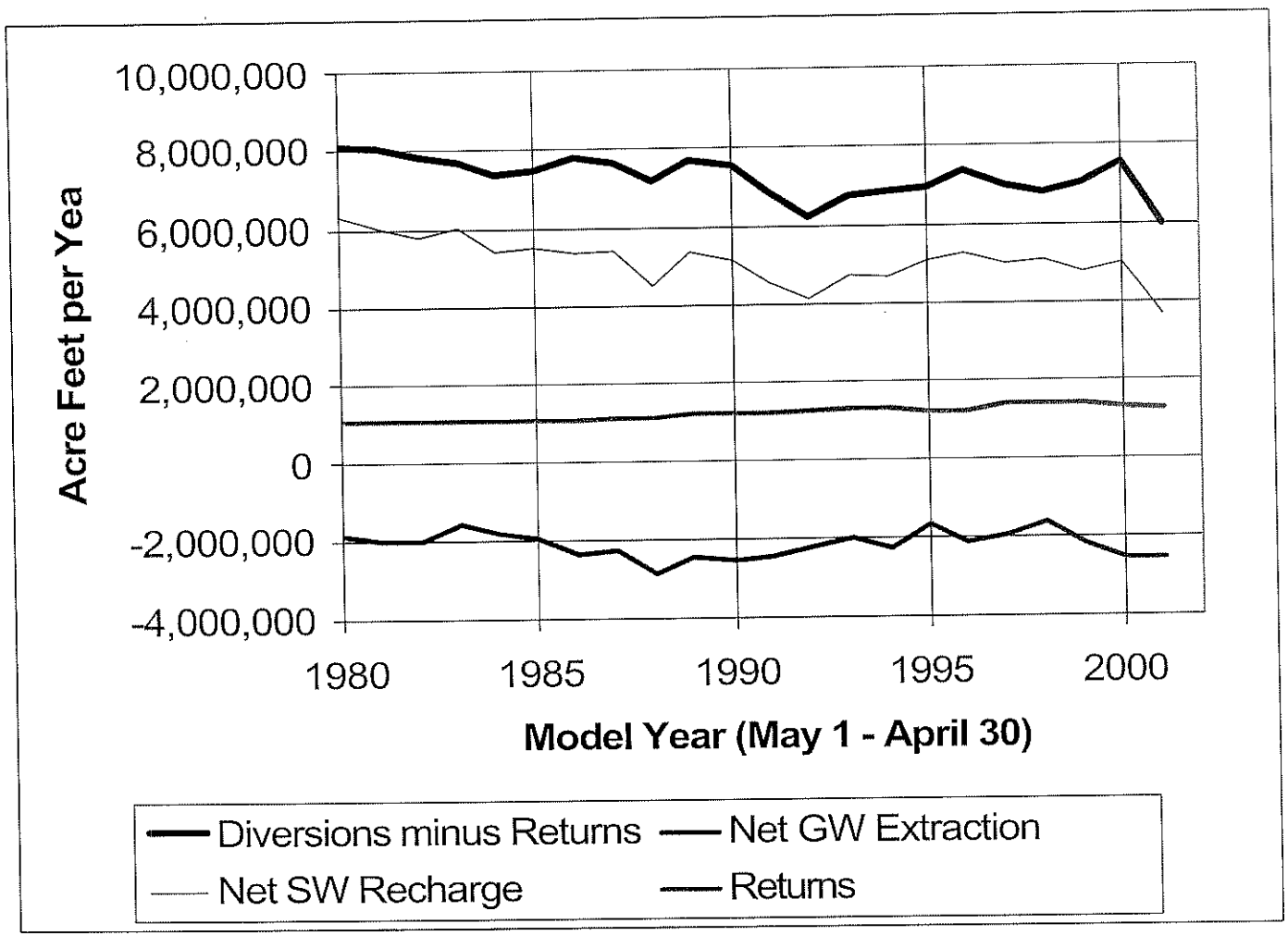

Figure 35. Diversion volume, return flow volume, net ground-water extraction and net recharge due to surface water irrigation.

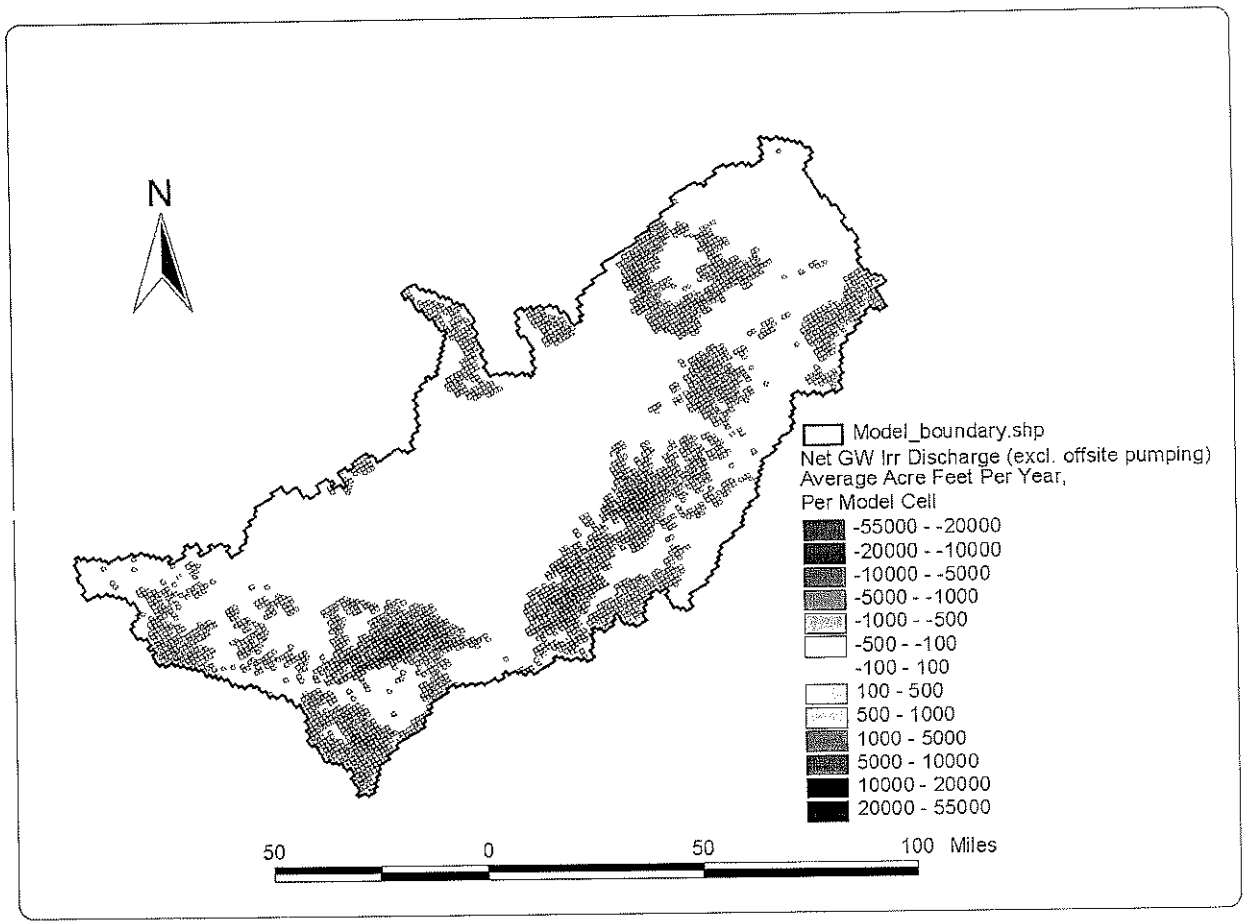

Figure 36. Areal distribution of net ground-water extraction averaged for the 22-year model calibration period.

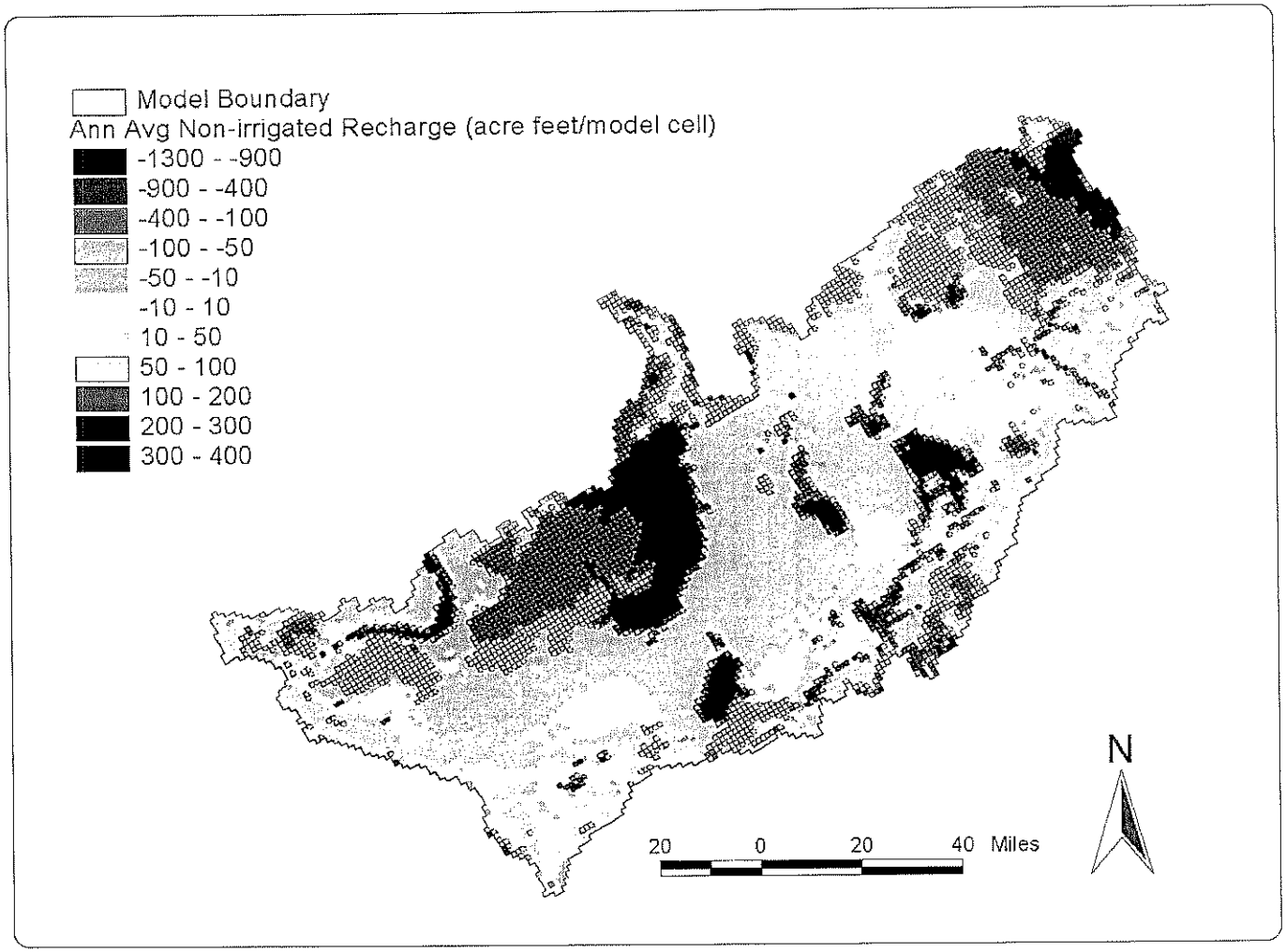

Figure 37. Spatial distribution of non-irrigated recharge averaged for the 22-year calibration period.

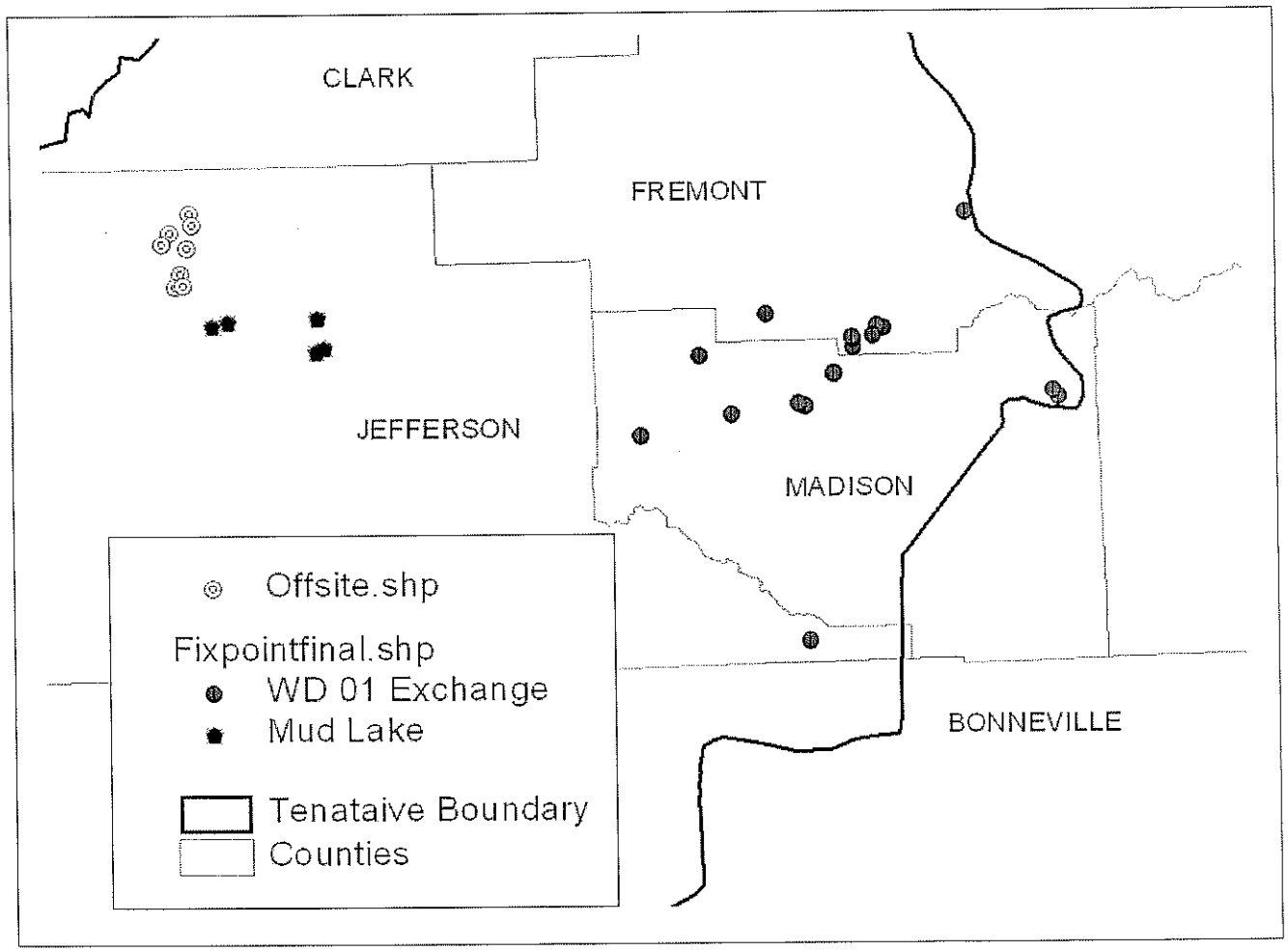

Figure 38. Exchange wells represented as fixed point pumping.

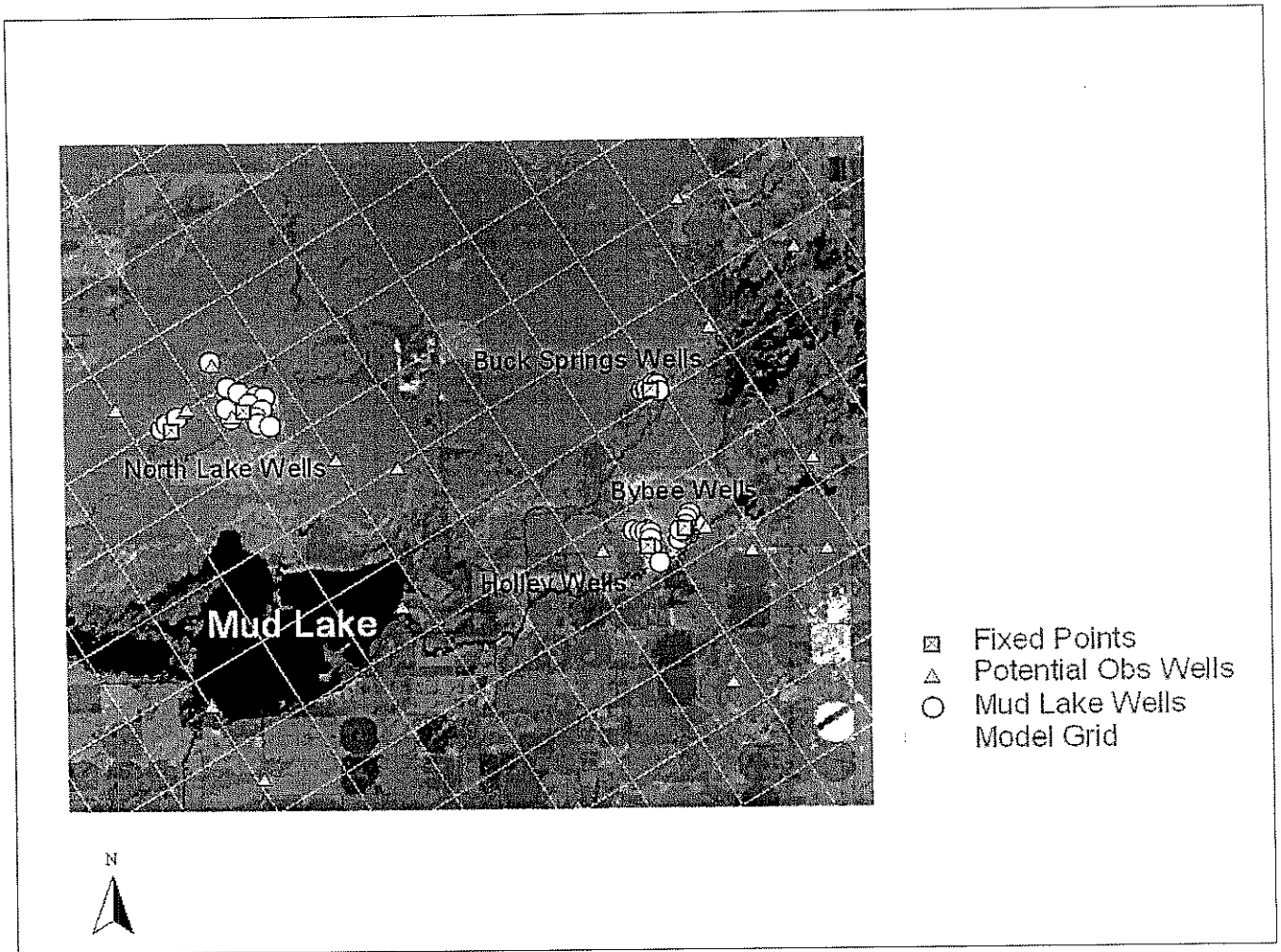

Figure 38. Fixed point wells in the Mud Lake area.

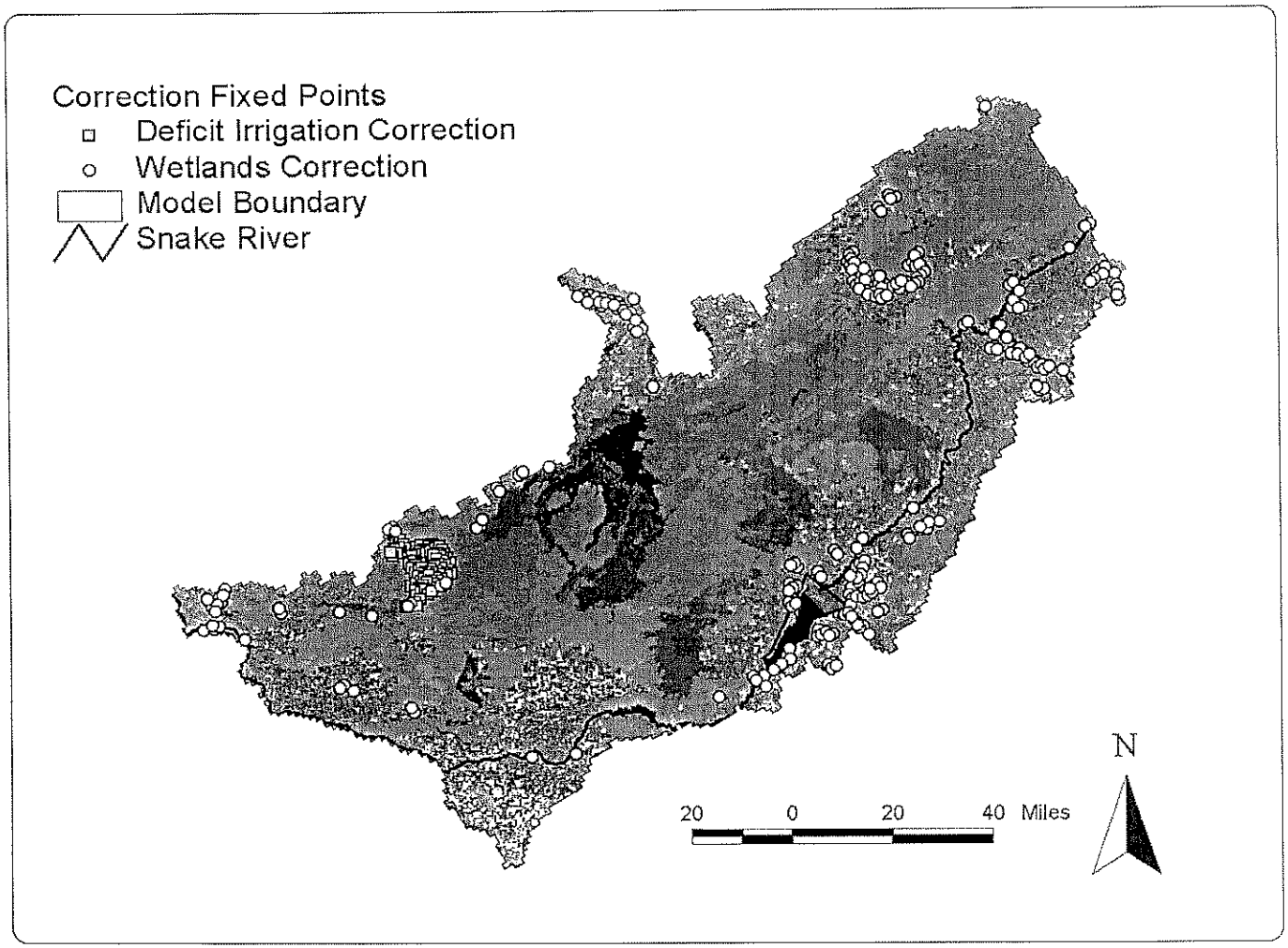

Figure 40. Location of wetlands and deficit irrigation correction fixed point wells.

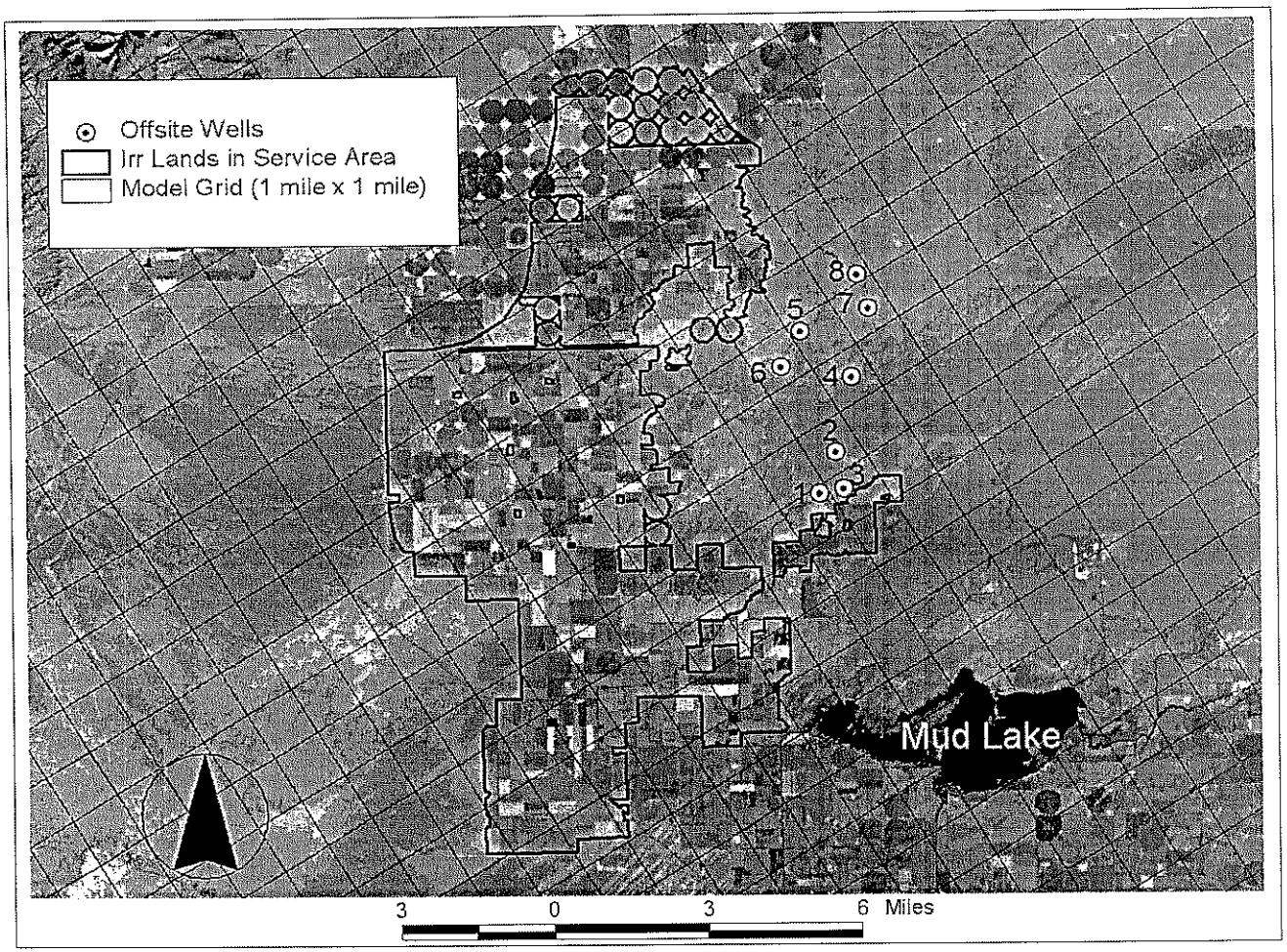

Figure 41. Location of off-site wells and destination irrigated areas.

Figure 42. Bar graph of the components of recharge for steady state model.

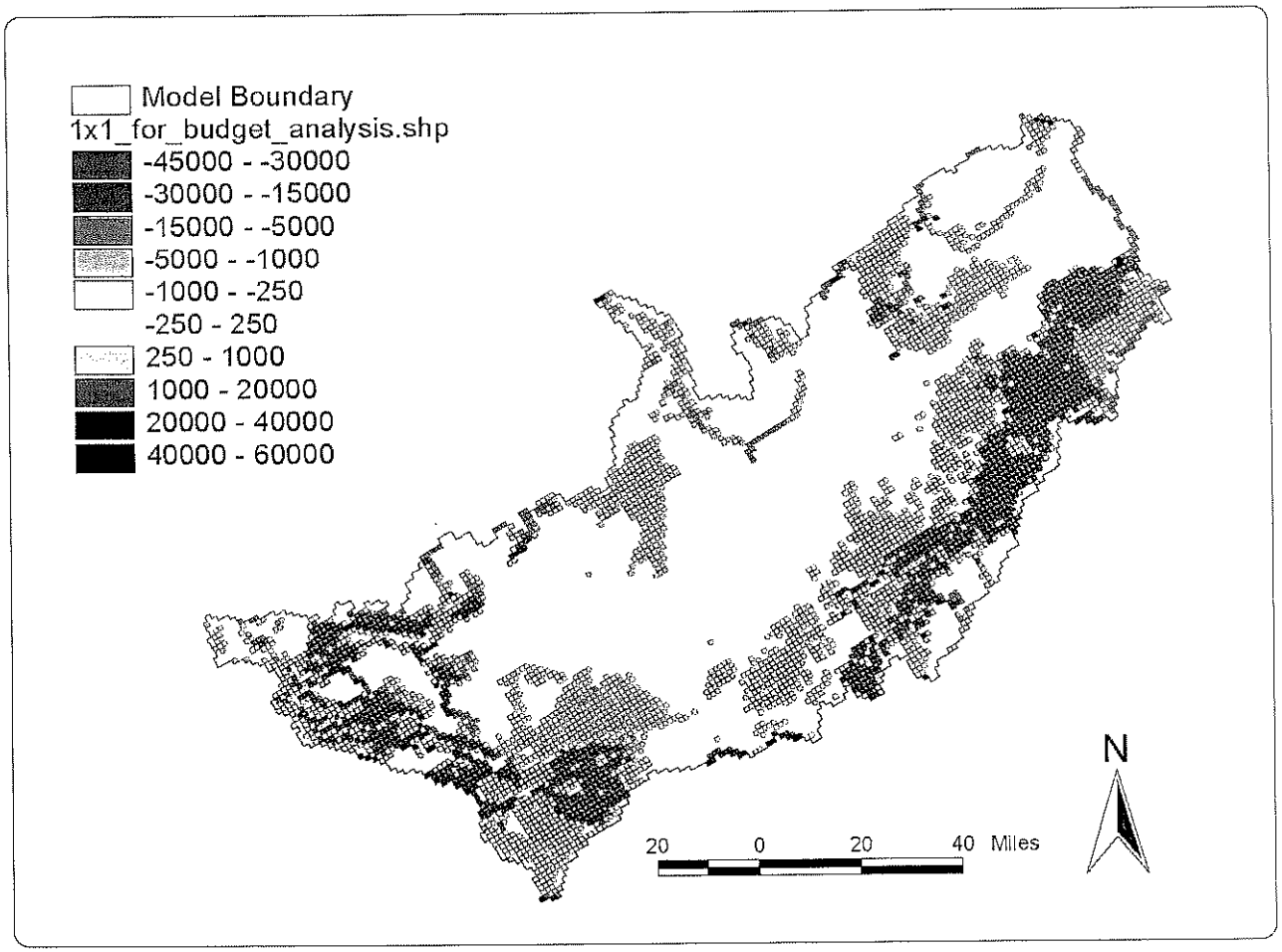

Figure 43. Areal distribution of recharge for steady state model.

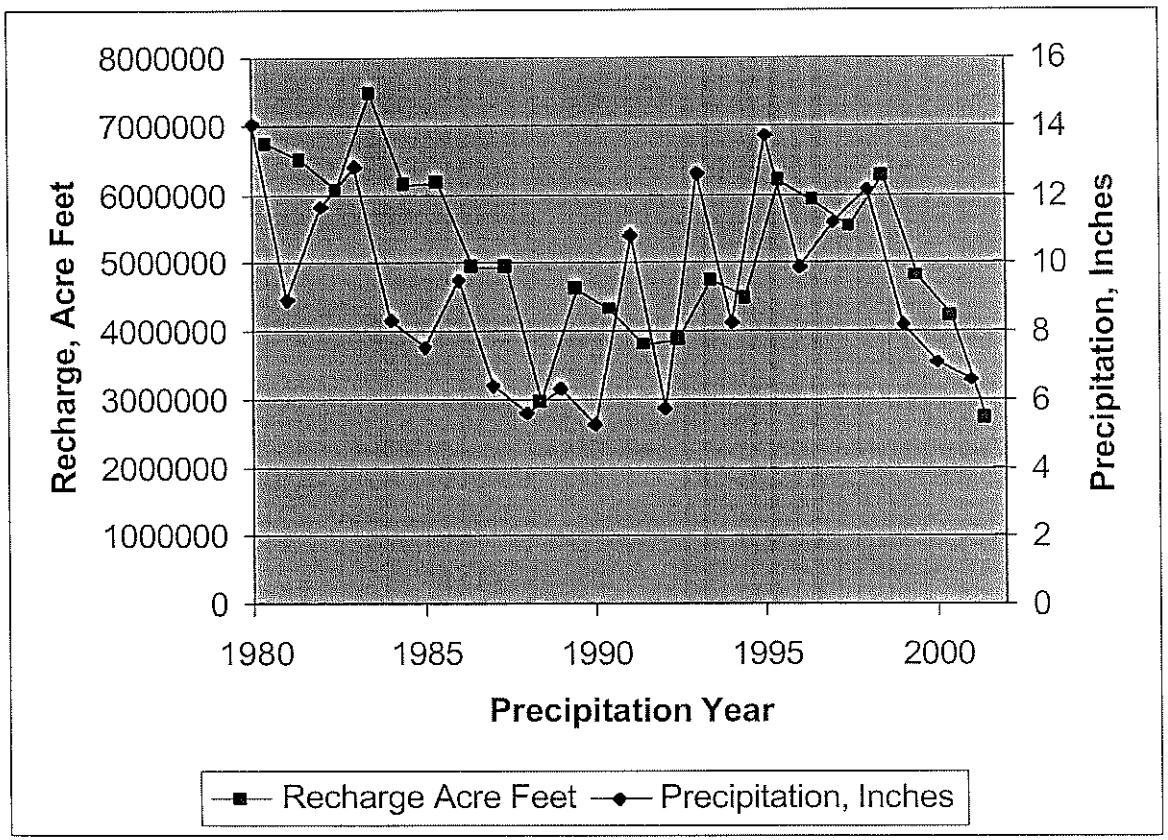

Figure 44. Recharge variation with time for the transient ESPAM model.

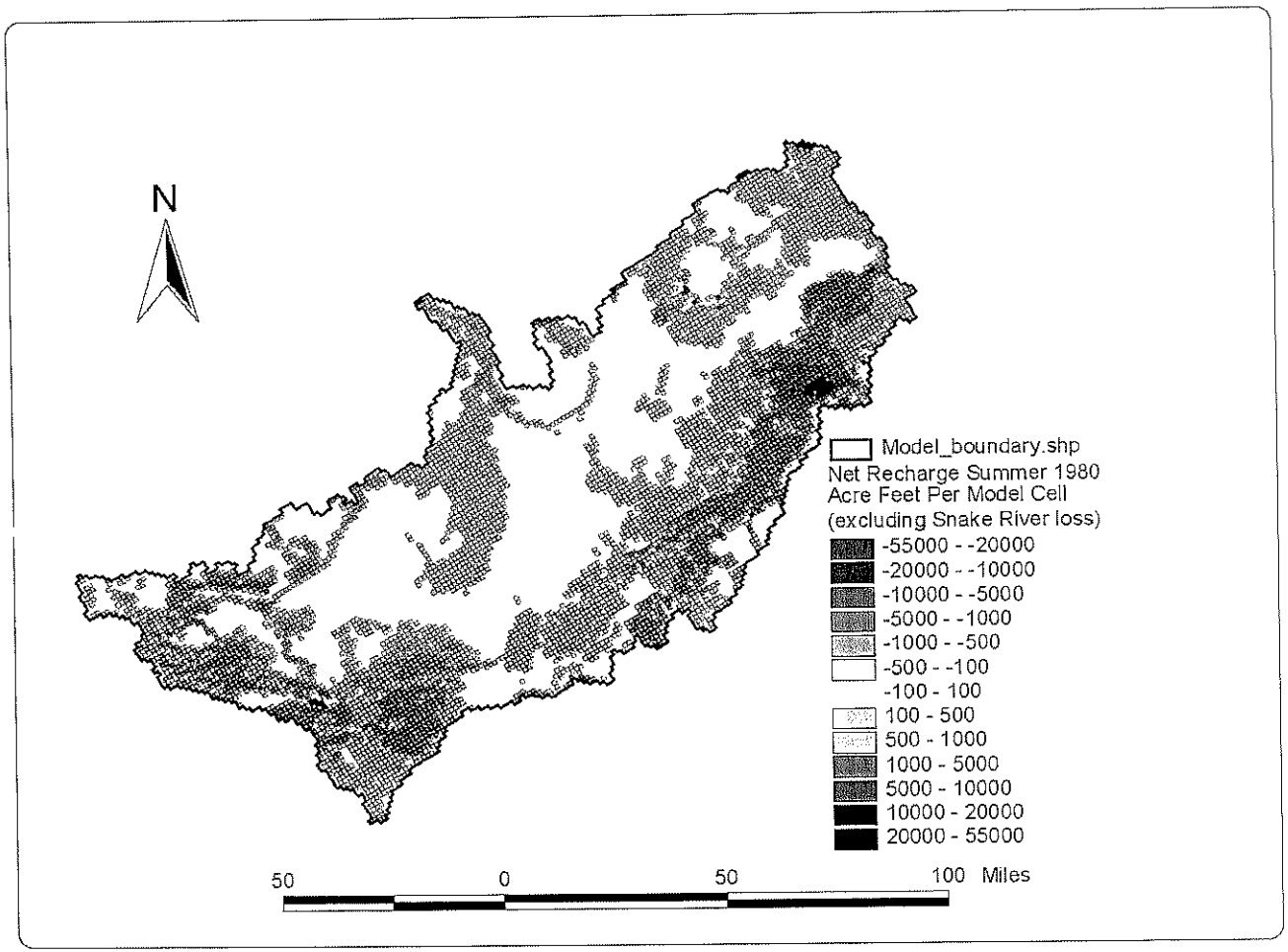

Figure 45. Areal distribution of transient recharge for 1980-1981 irrigation season.

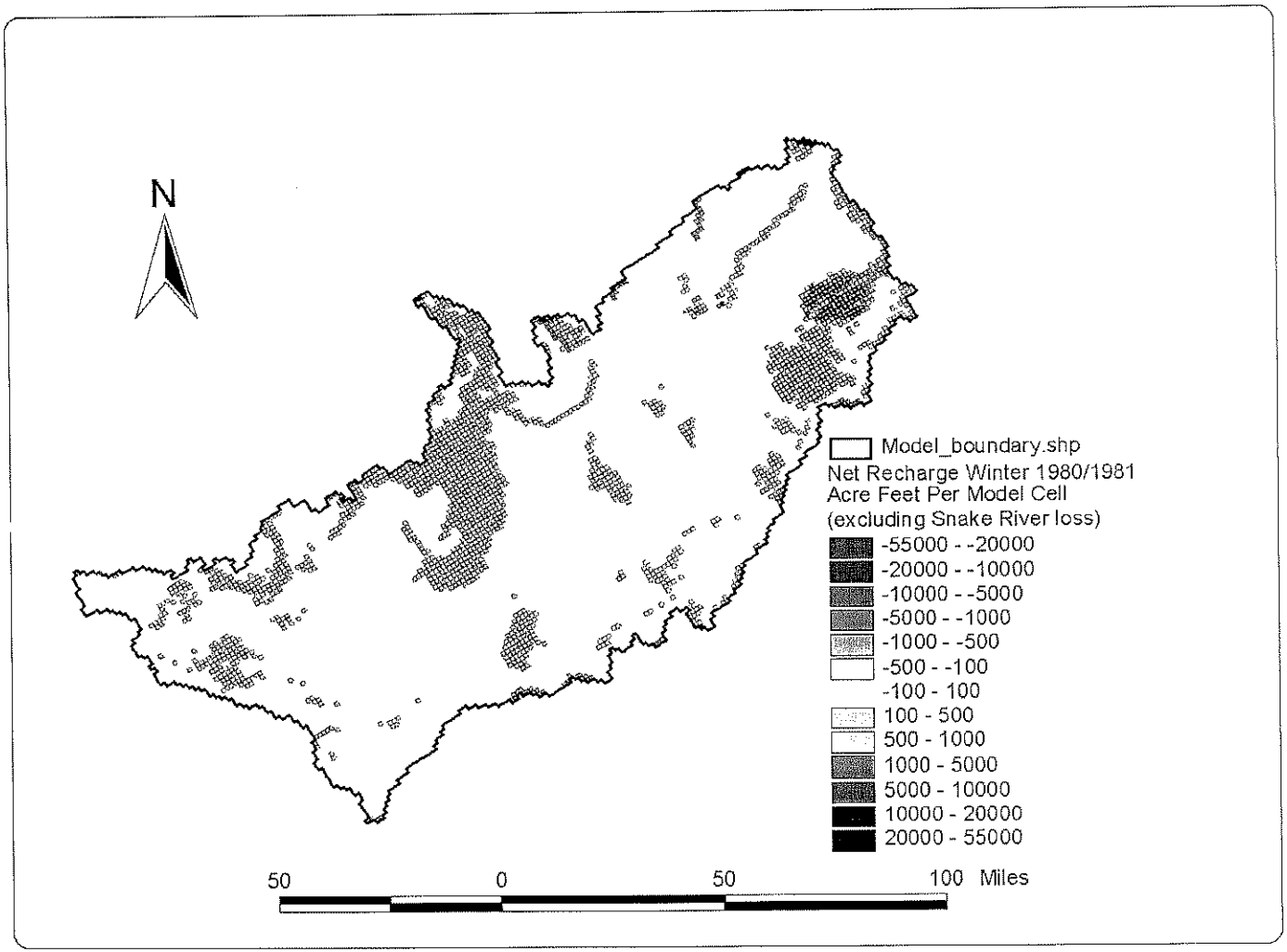

Figure 46. Areal distribution of transient recharge for 1980-1981non-irrigation season.

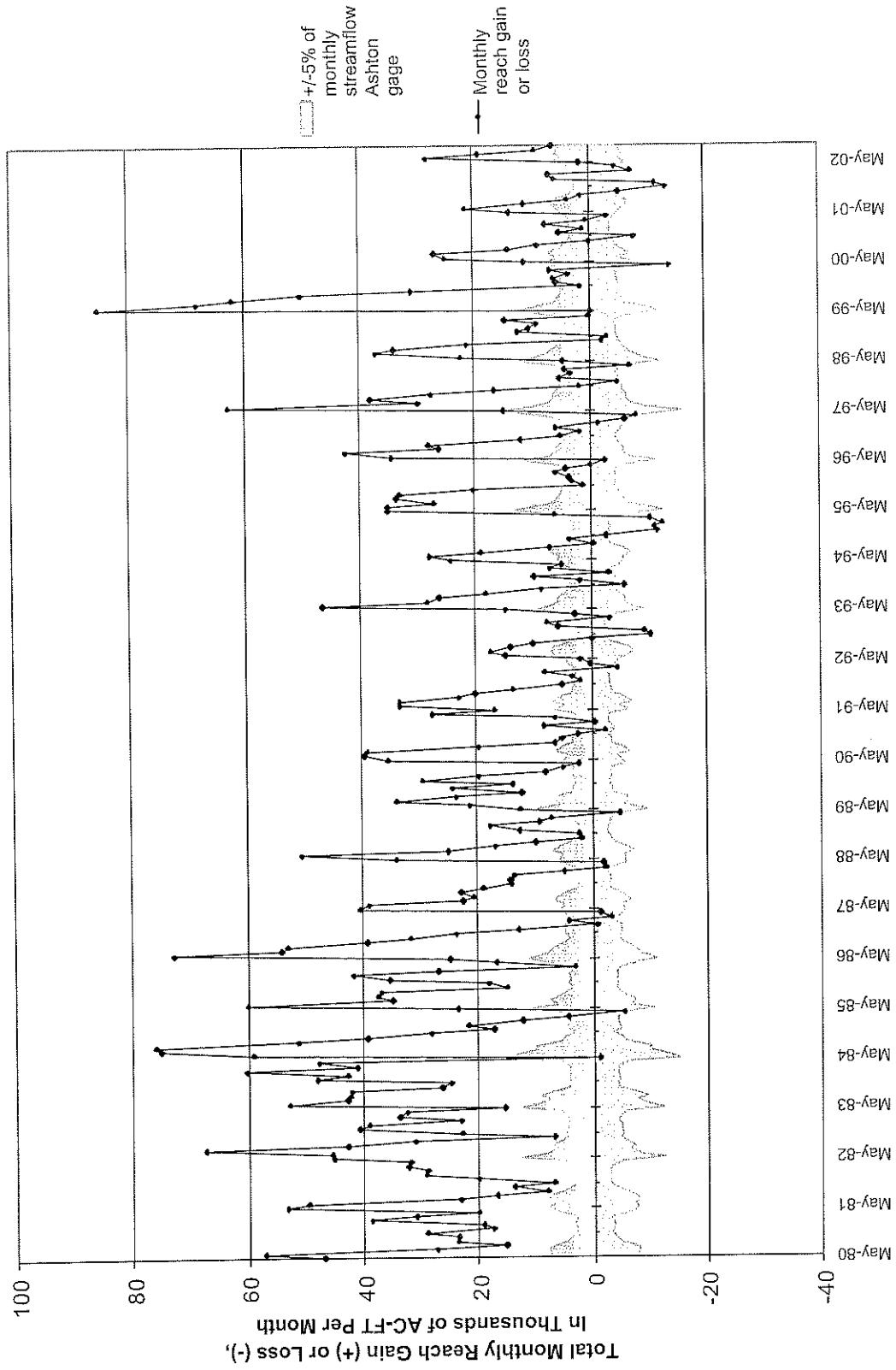

Figure 47. Monthly Snake River gains and losses: Ashton to Rexburg reach.

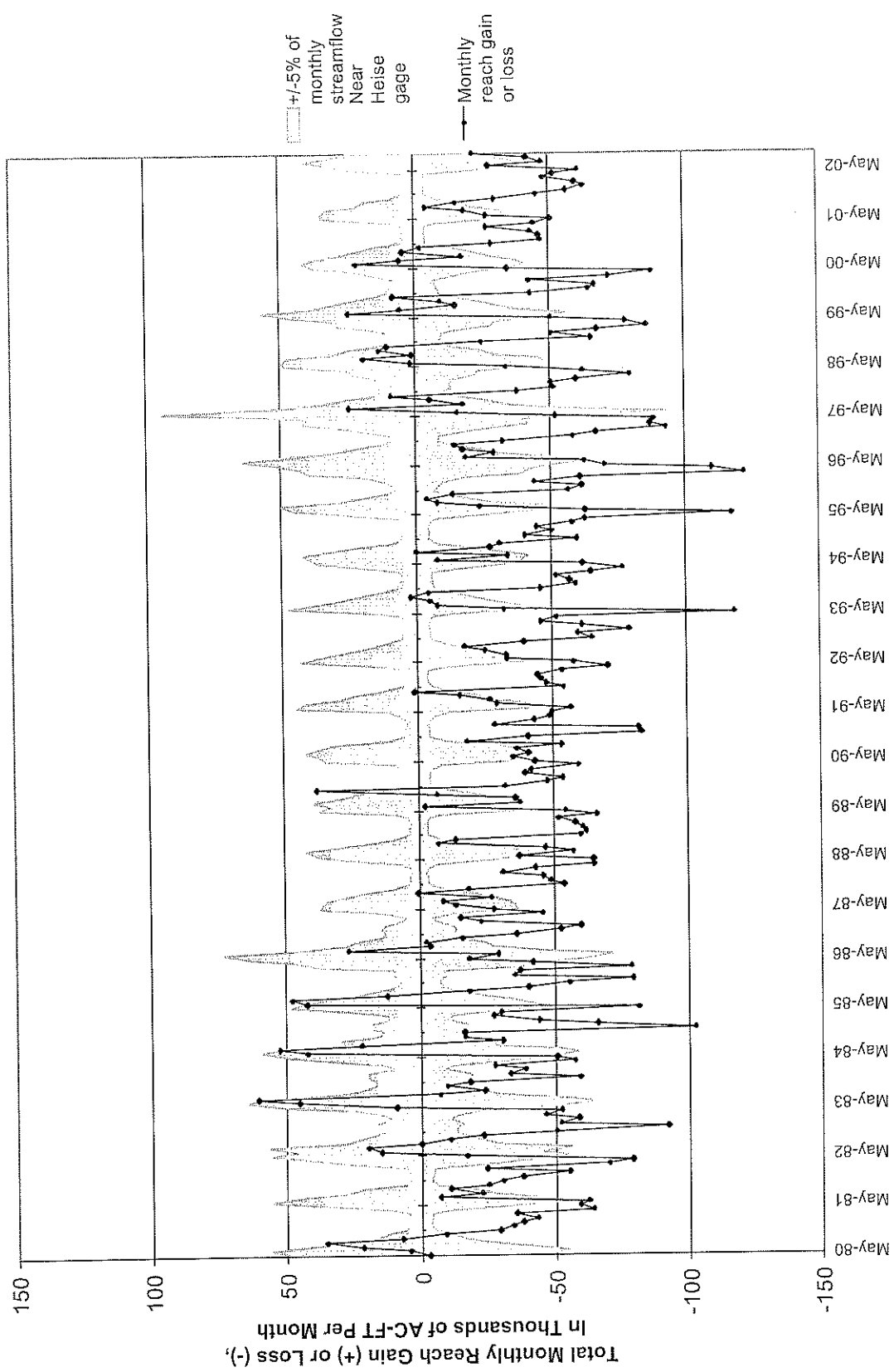

Figure 48. Monthly Snake River gains and losses: Heise to Shelley reach.

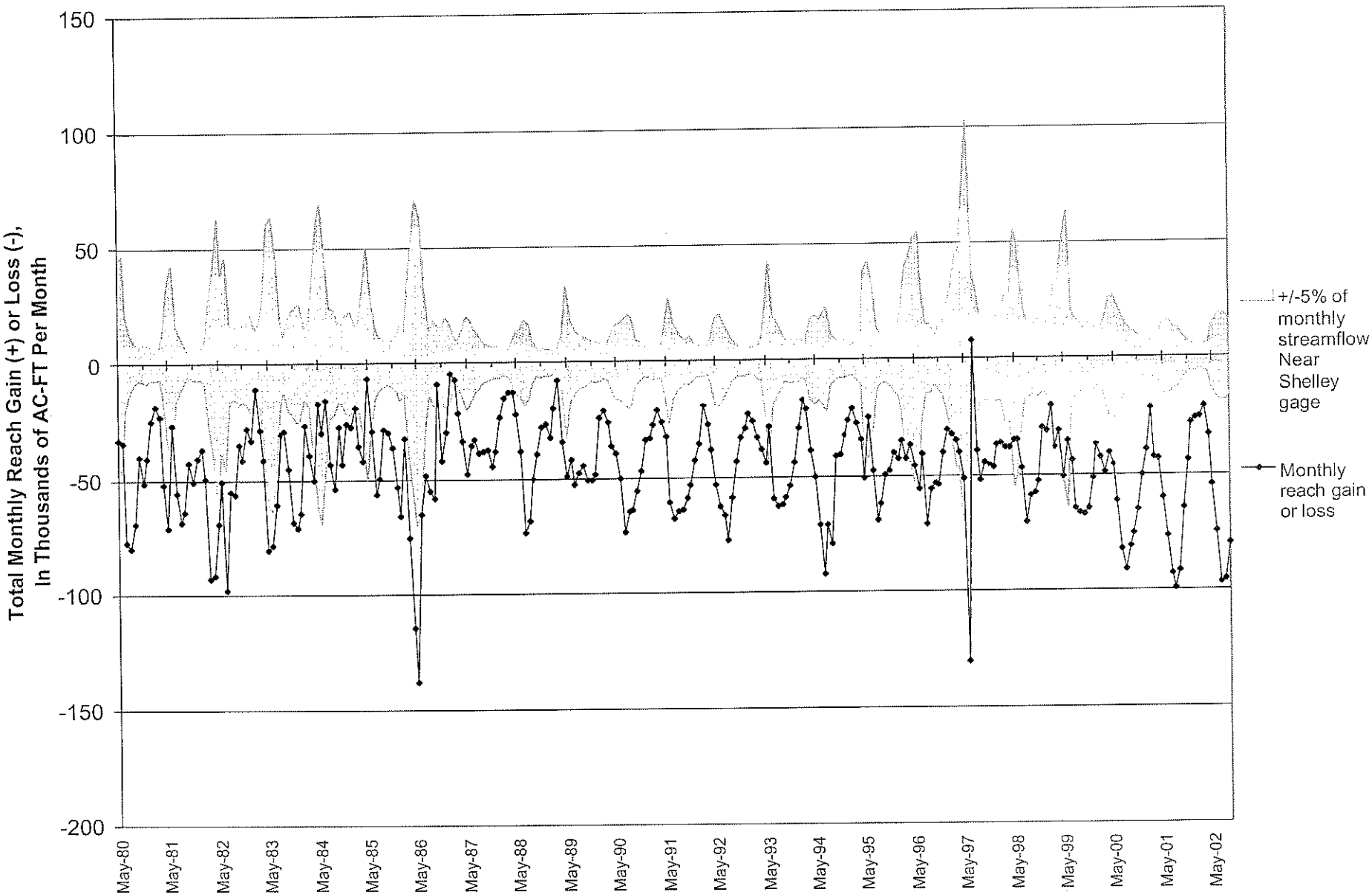

Figure 49. Monthly Snake River gains and losses: Shelley to Near Blackfoot reach.

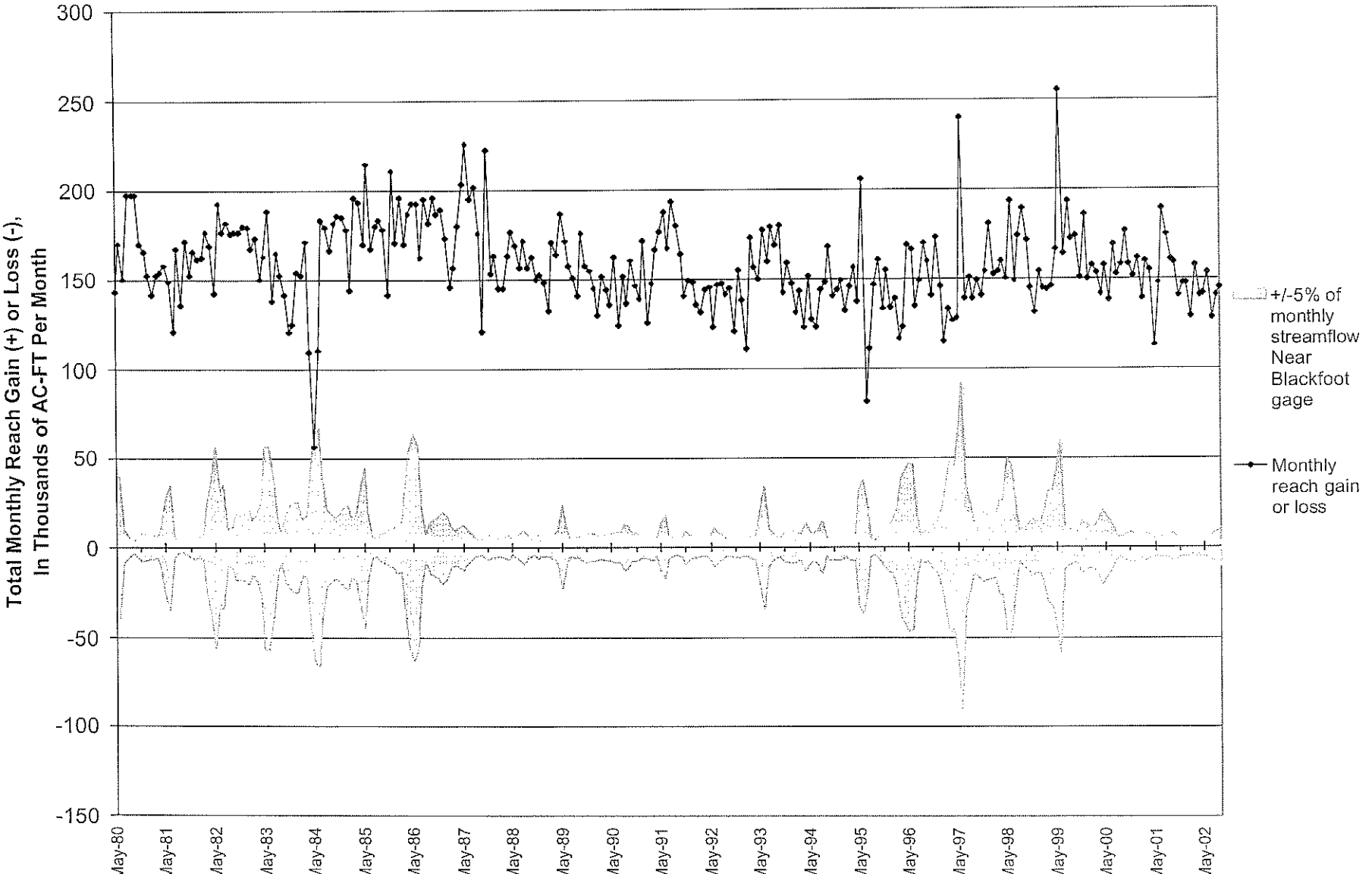

Figure 50. Monthly Snake River gains and losses: Near Blackfoot to Neeley reach.

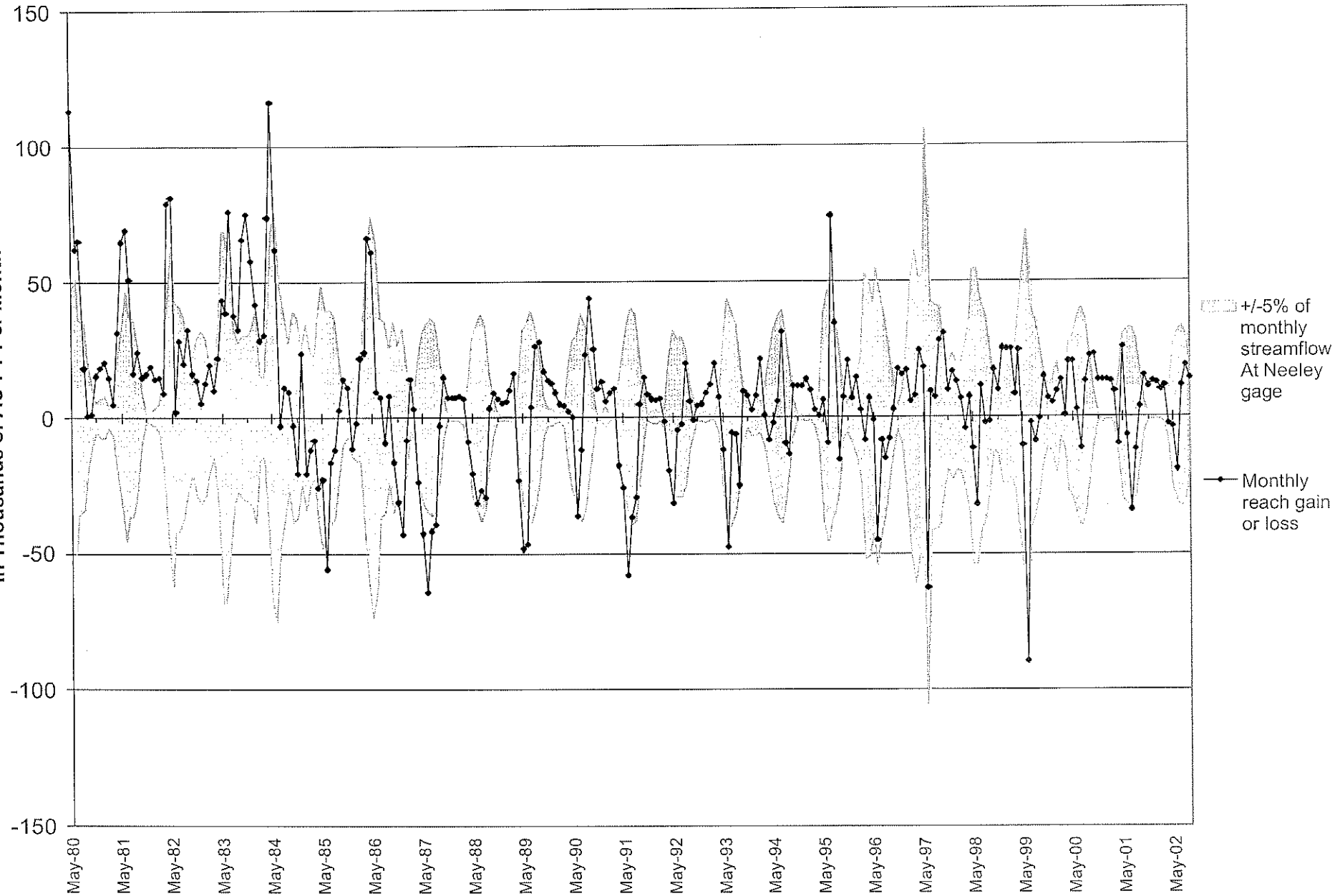

Figure 51. Monthly Snake River gains and losses: Neeley to Minidoka reach.

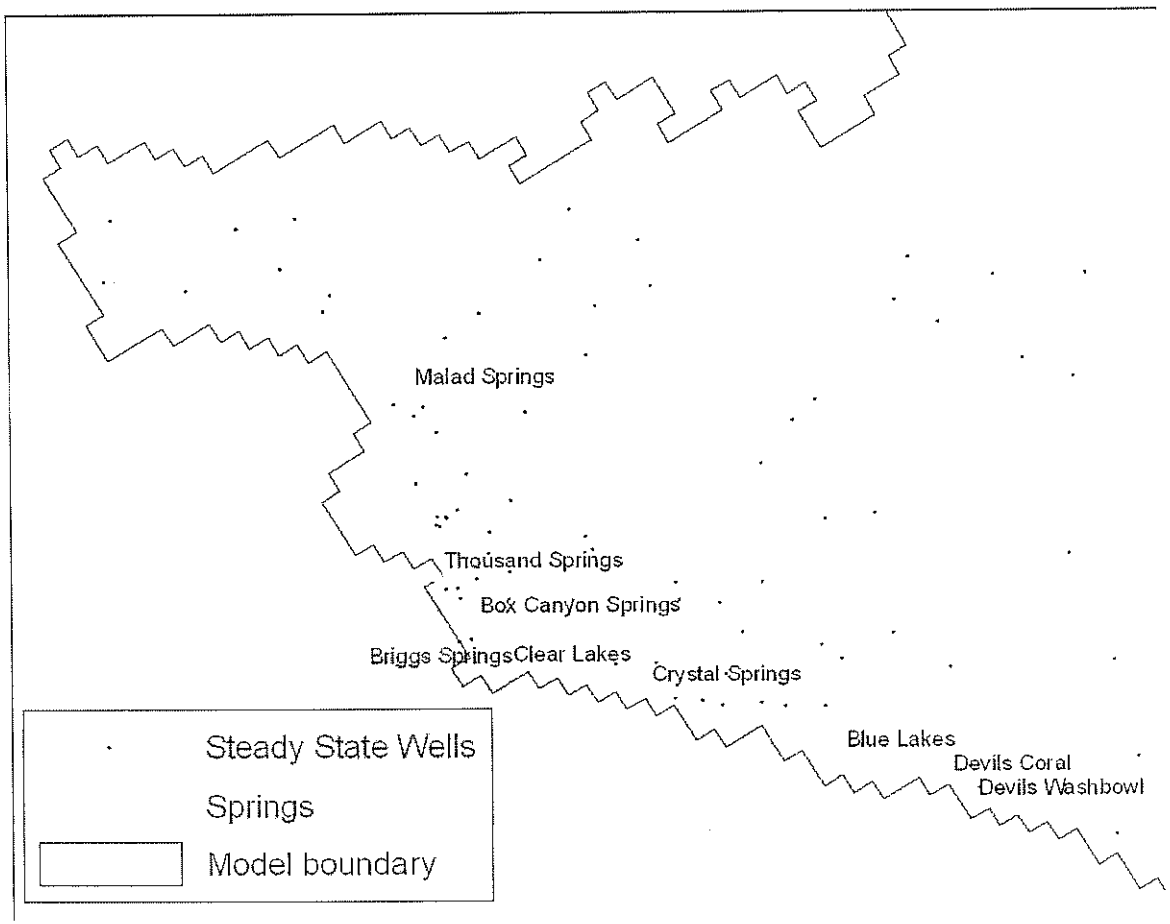

Figure 52. Location of springs used as calibration targets.

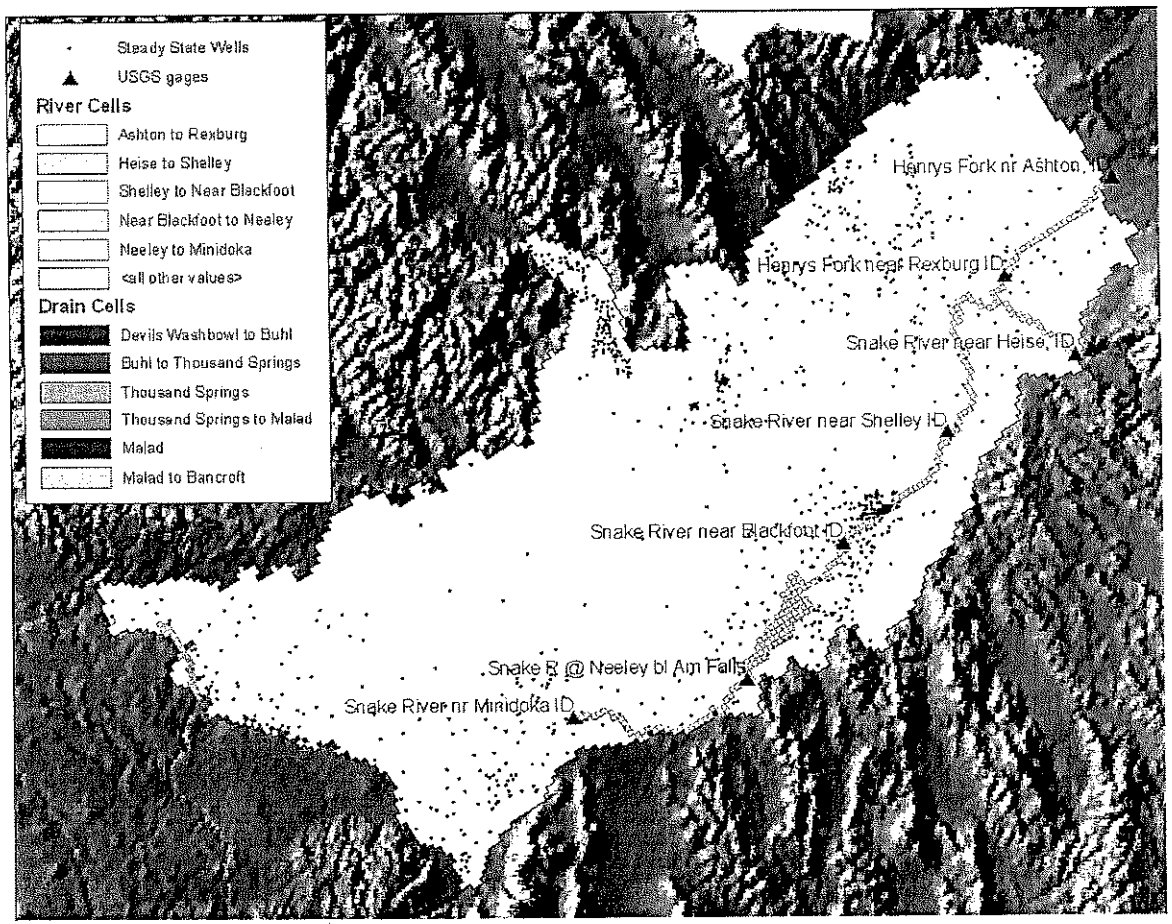

Figure 53. Location of steady state calibration water level targets.

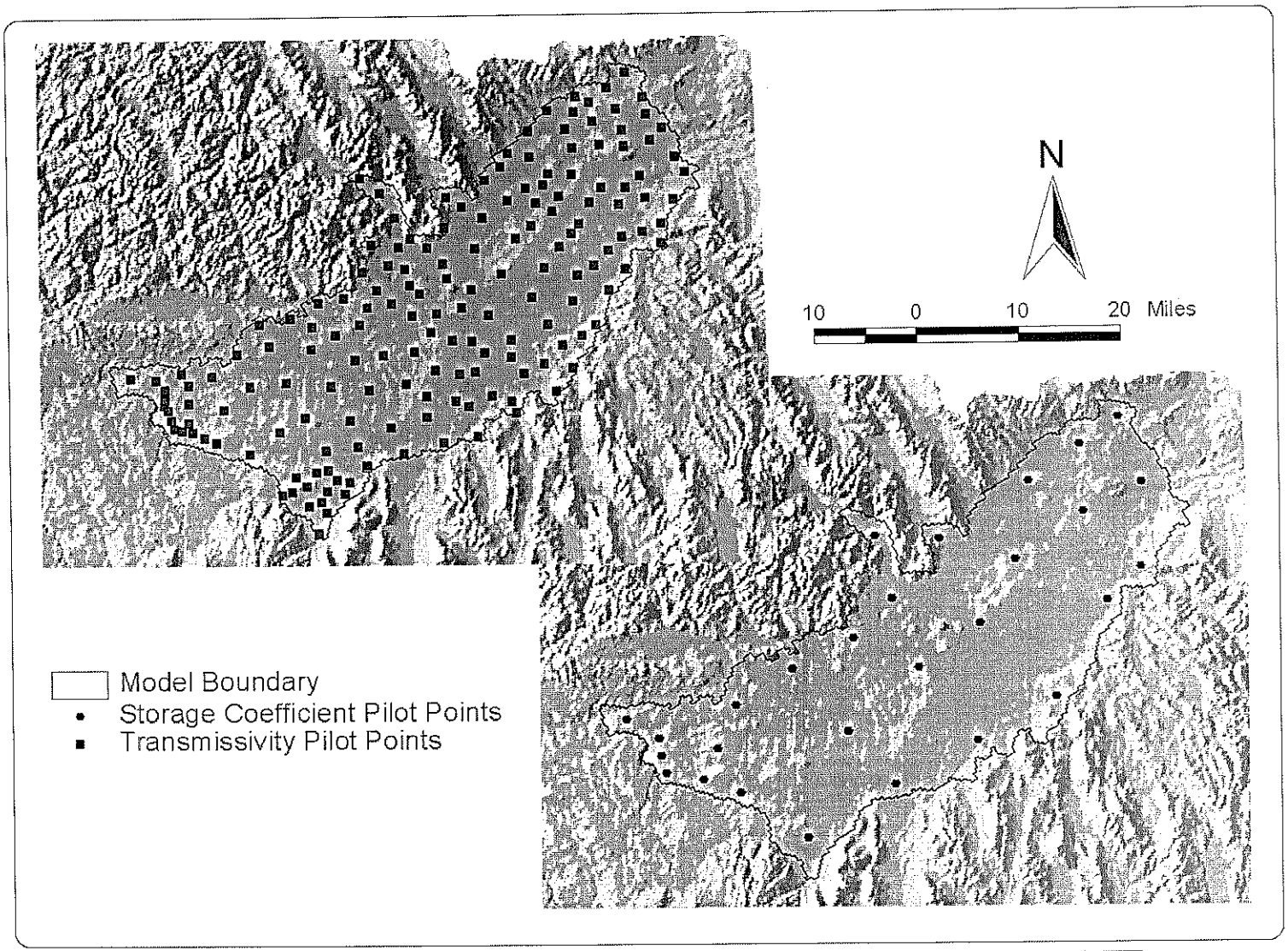

Figure 54. Location of pilot points used for calibration of transmissivity and storativity.

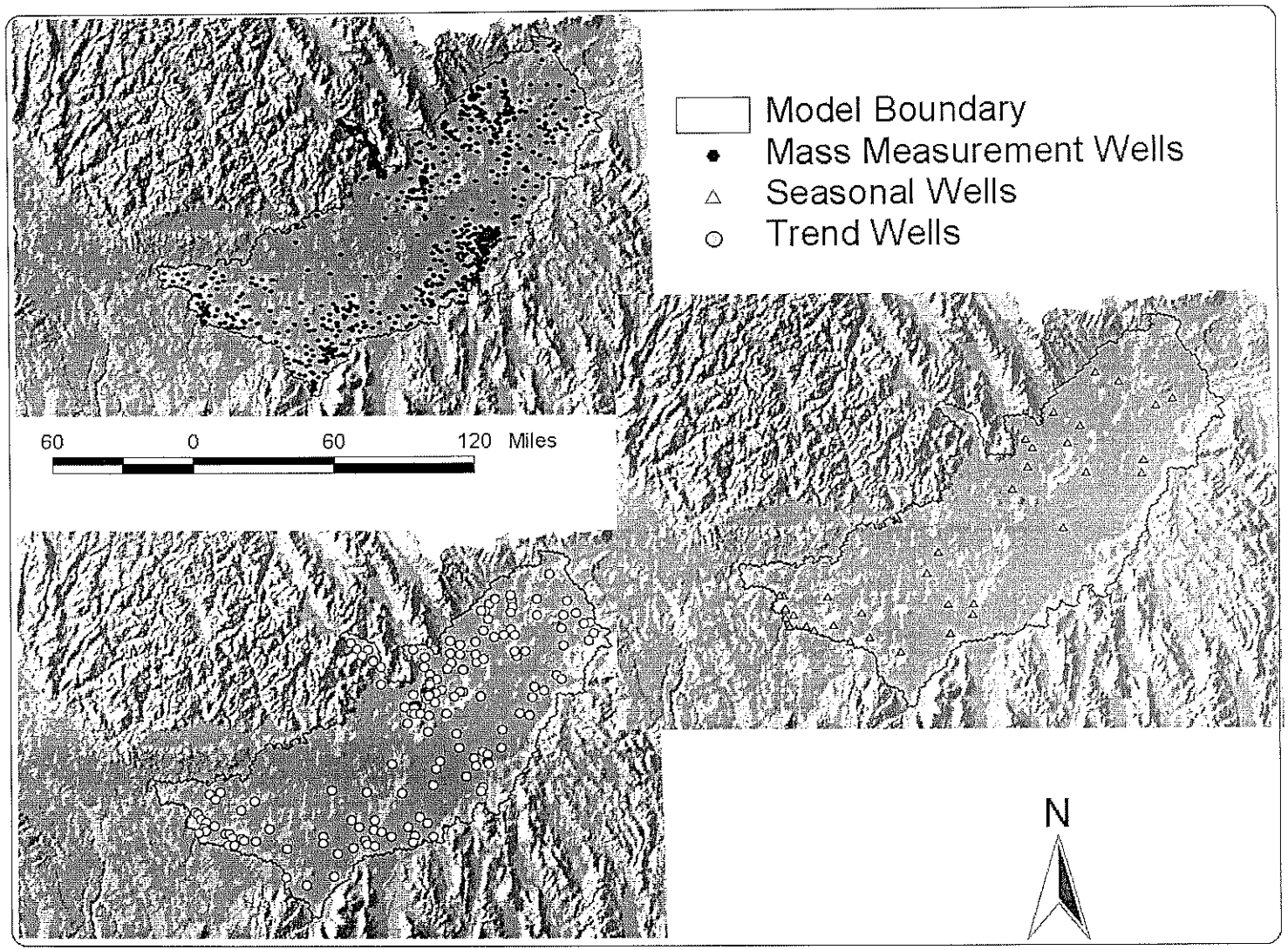

Figure 55. Location of transient aquifer water level observations.

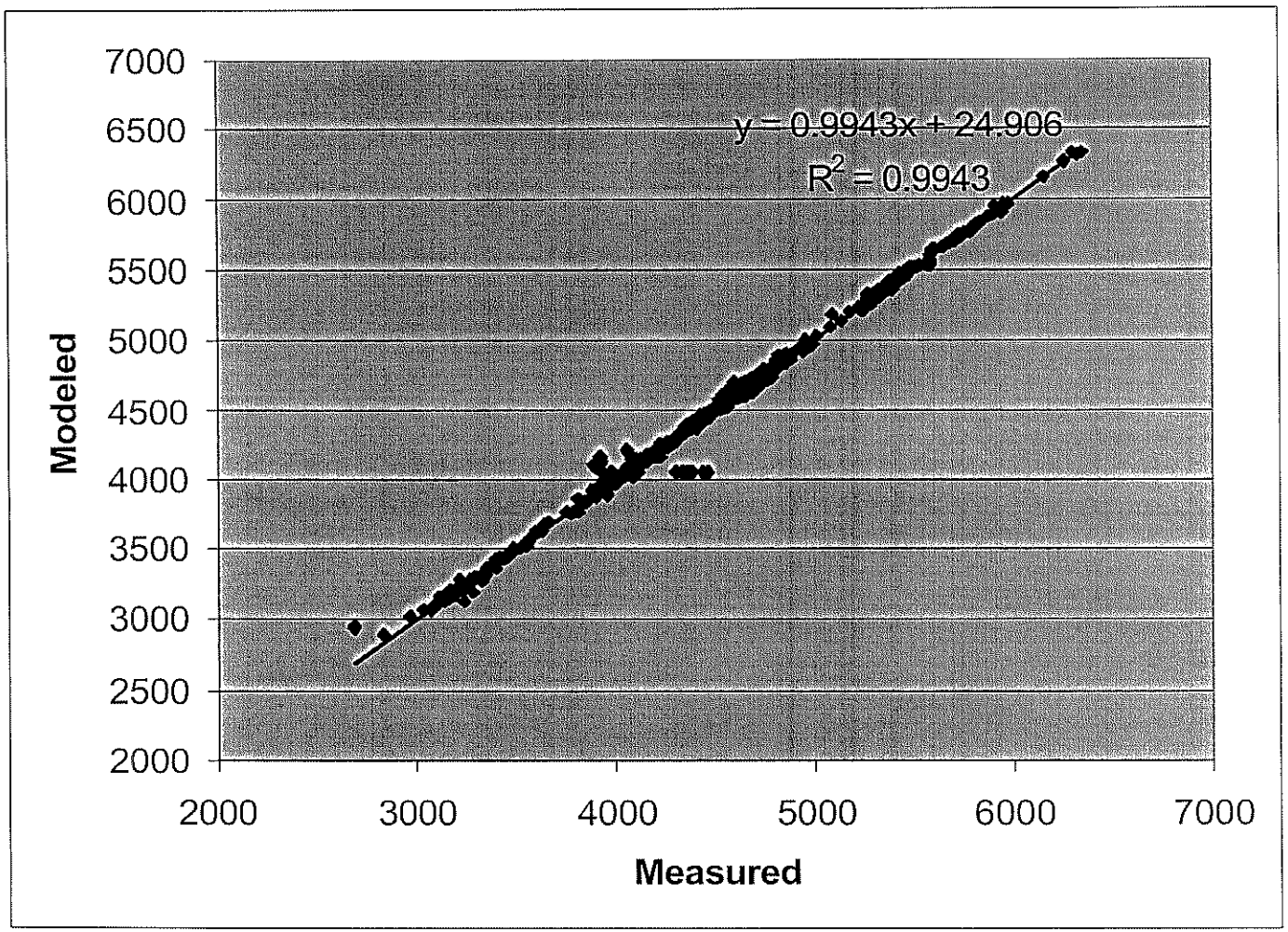

Figure 56. Scatter plot of model-predicted versus observed steady aquifer water levels (ft).

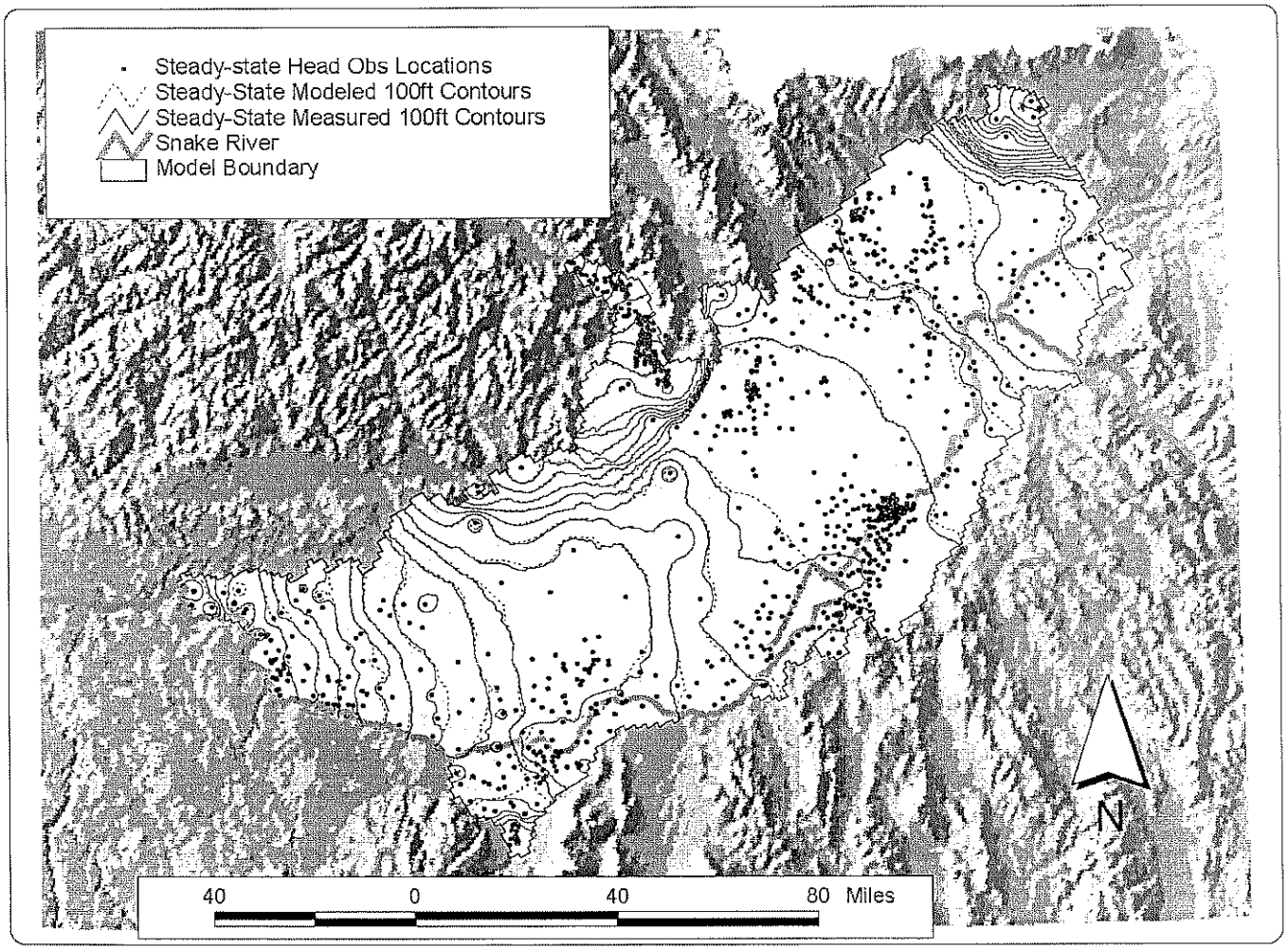

Figure 57. Steady state model-predicted versus observed aquifer potentiometric surface.

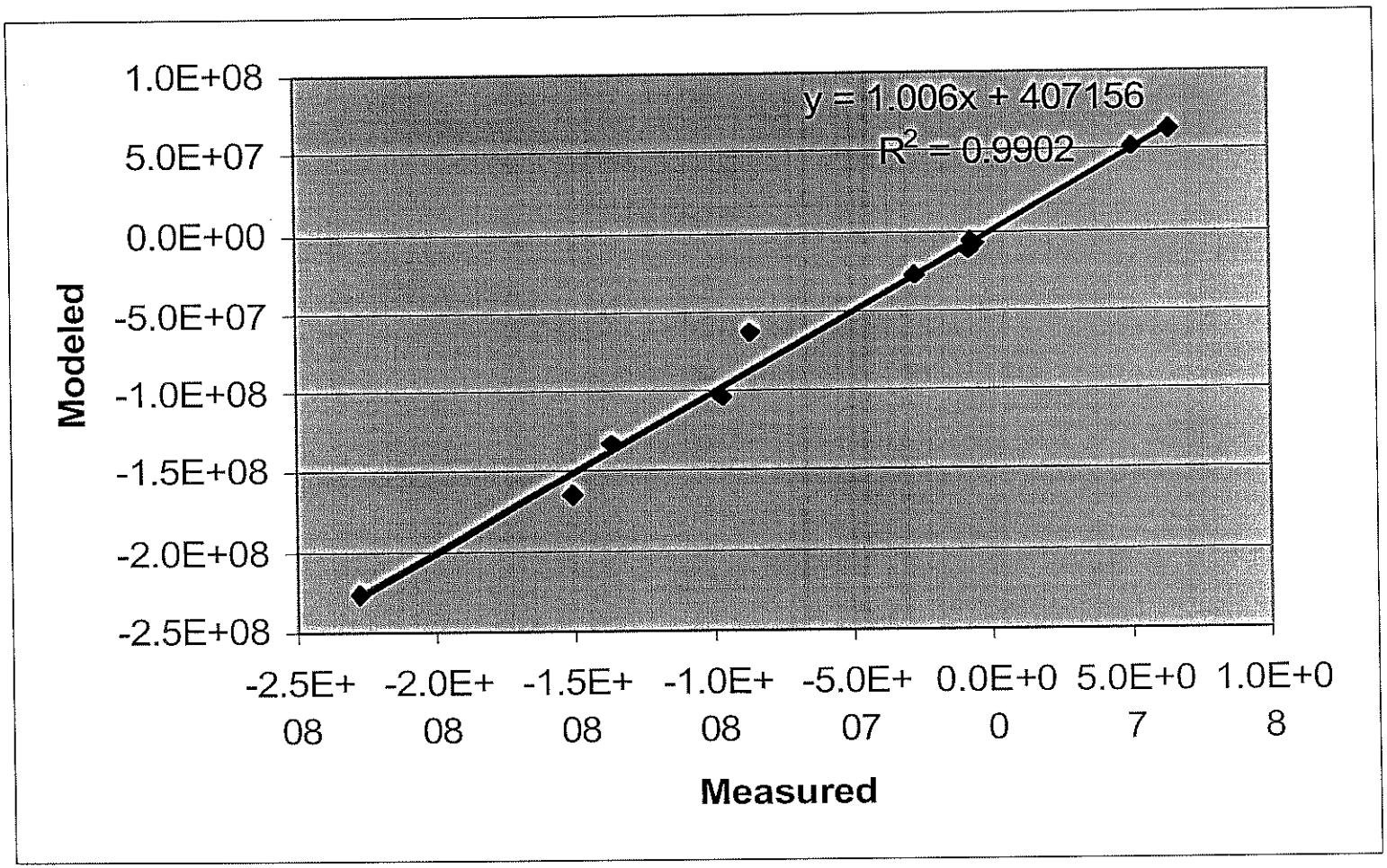

Figure 58. Scatter plot of model-predicted versus observed steady state river and spring fluxes (ft^3/d).

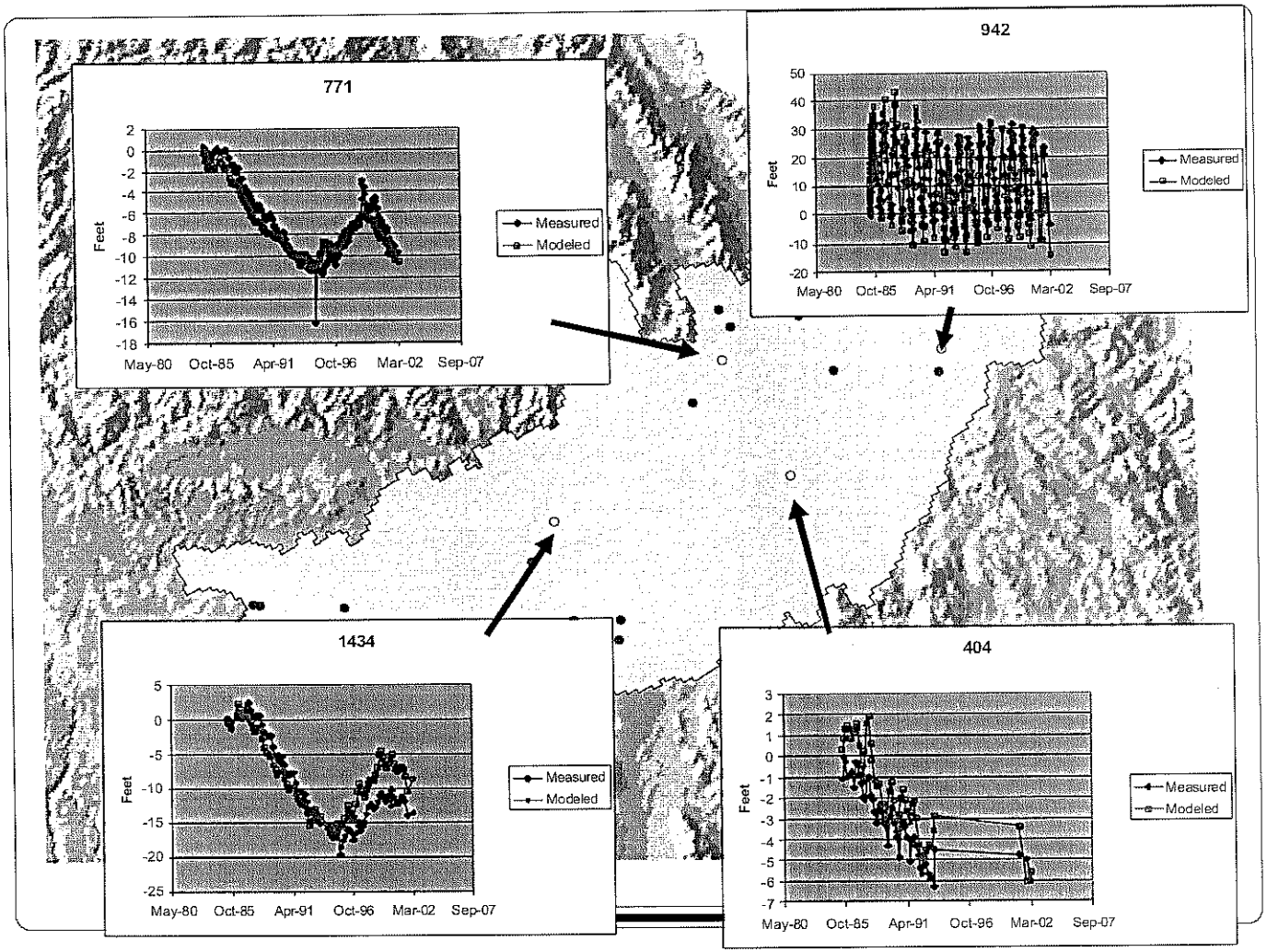

Figure 59. Selected seasonal well fits (1).

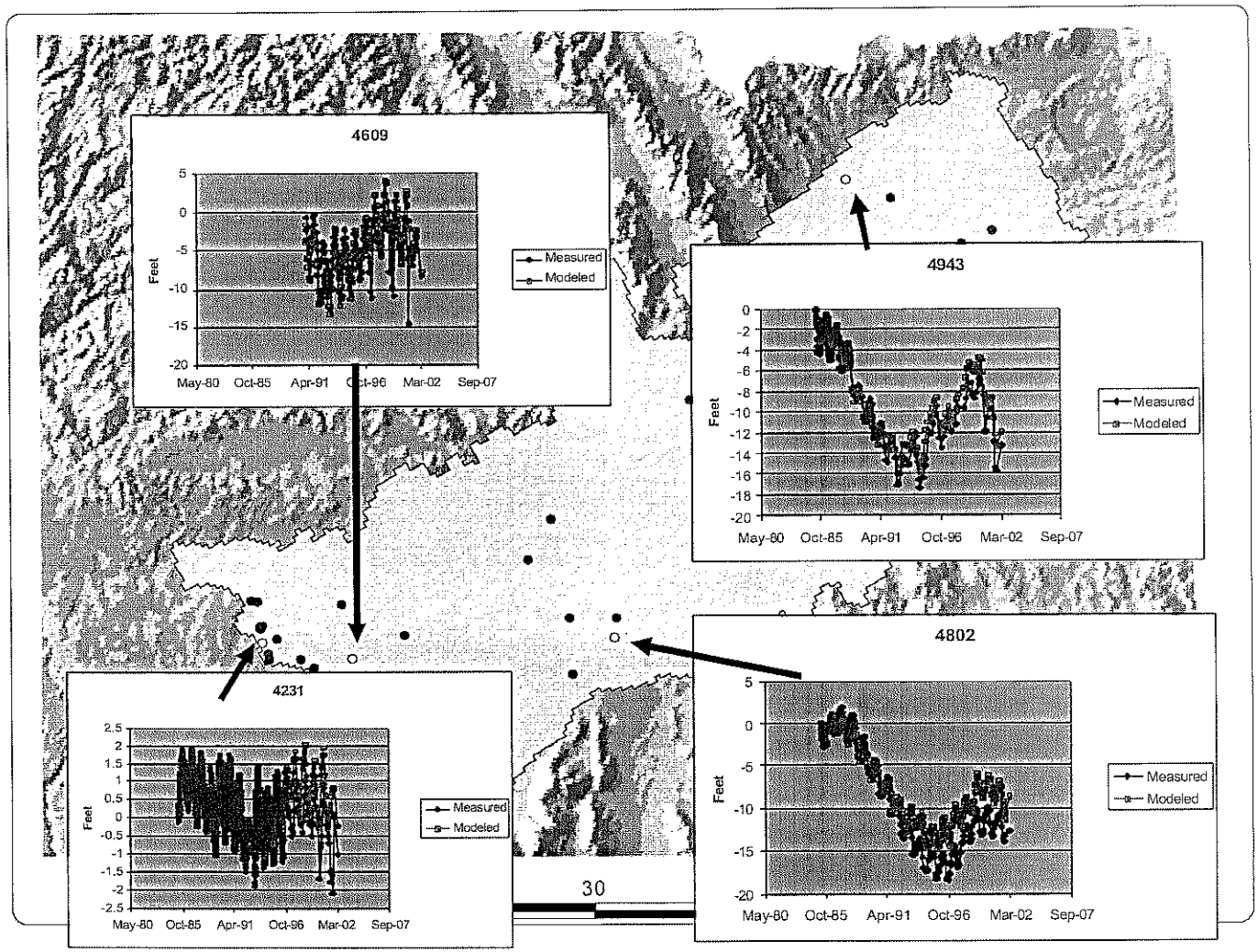

Figure 60. Selected seasonal well fits (2).

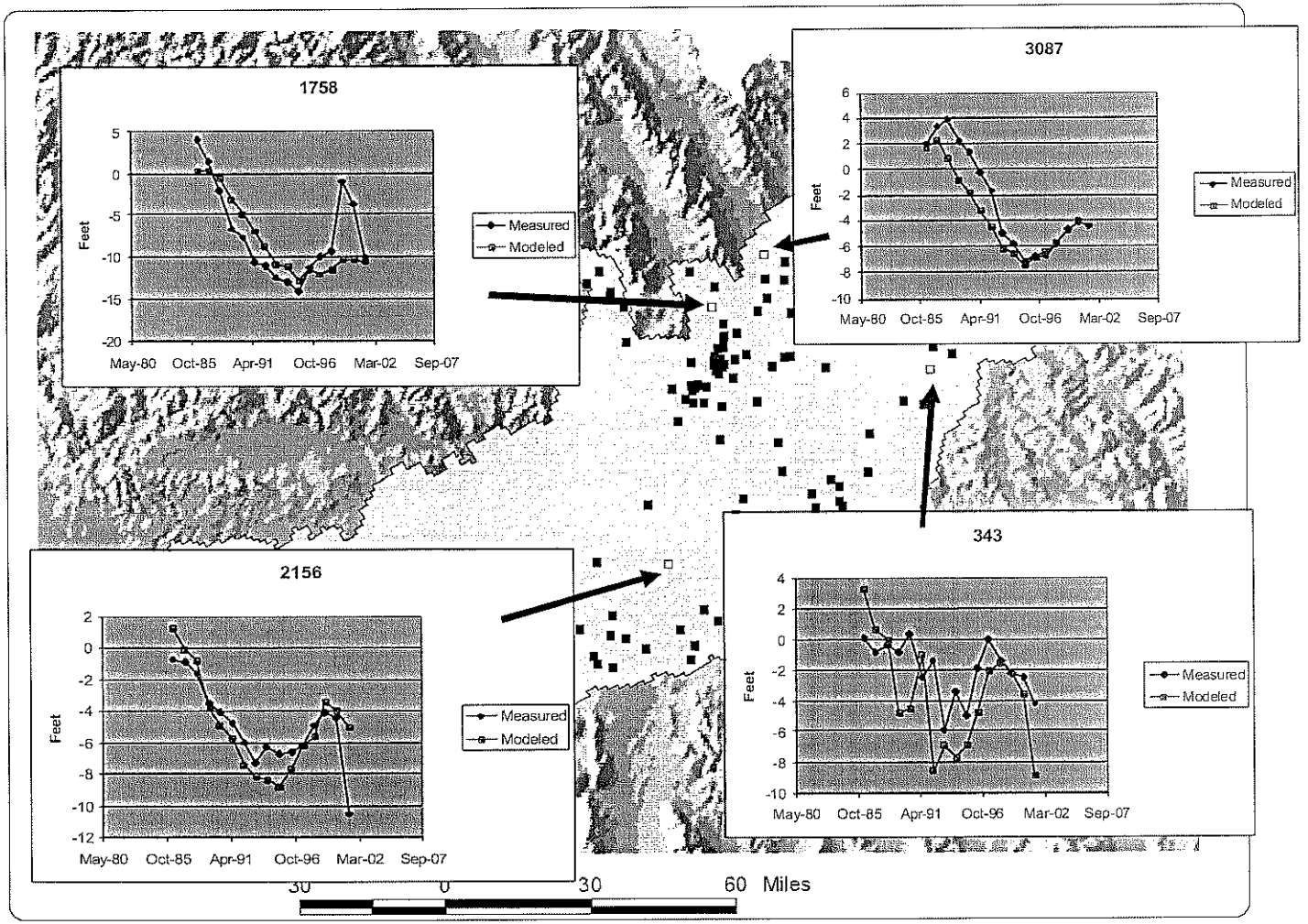

Figure 61. Selected trend well fits (1).

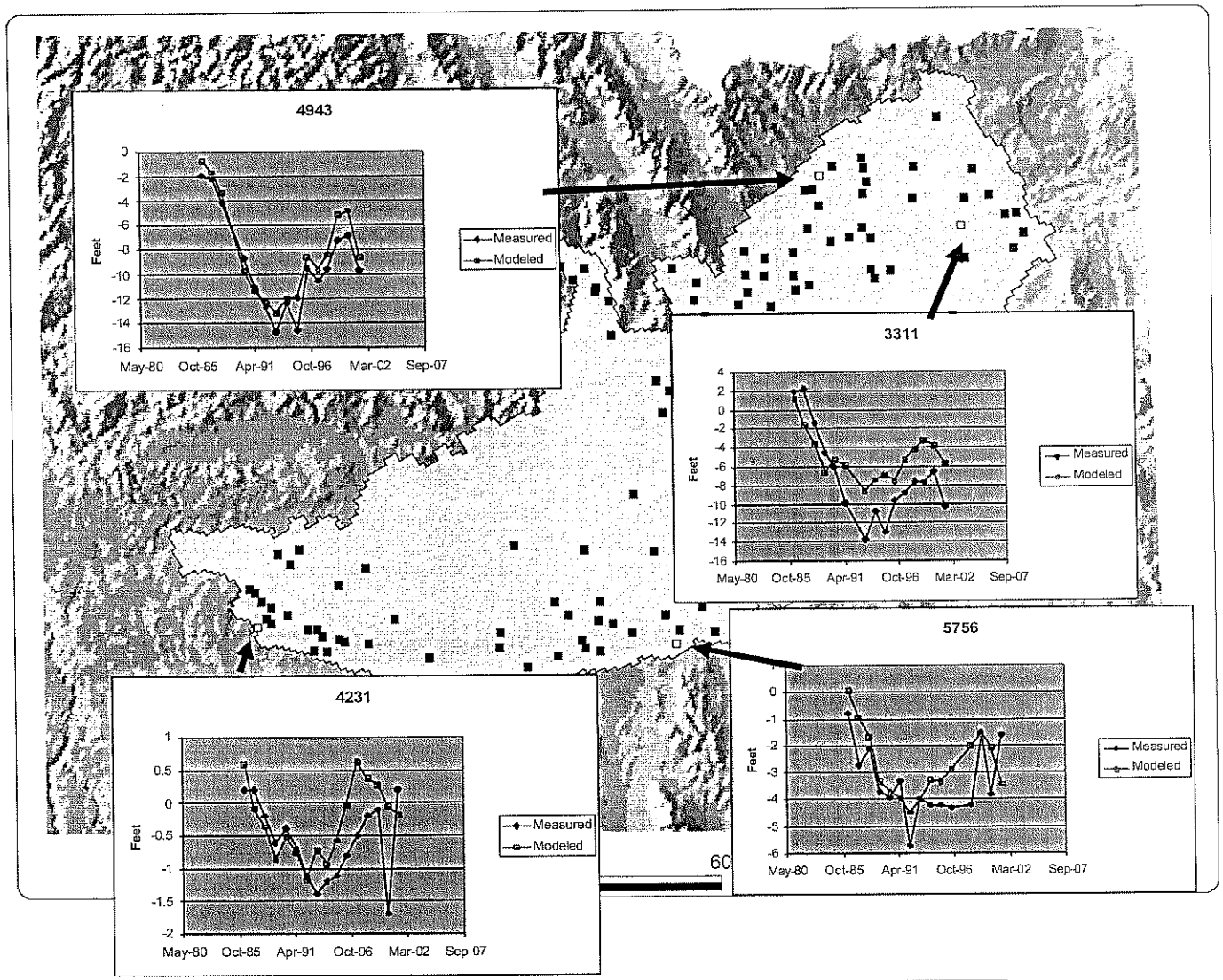

Figure 62. Selected trend well fits (2).

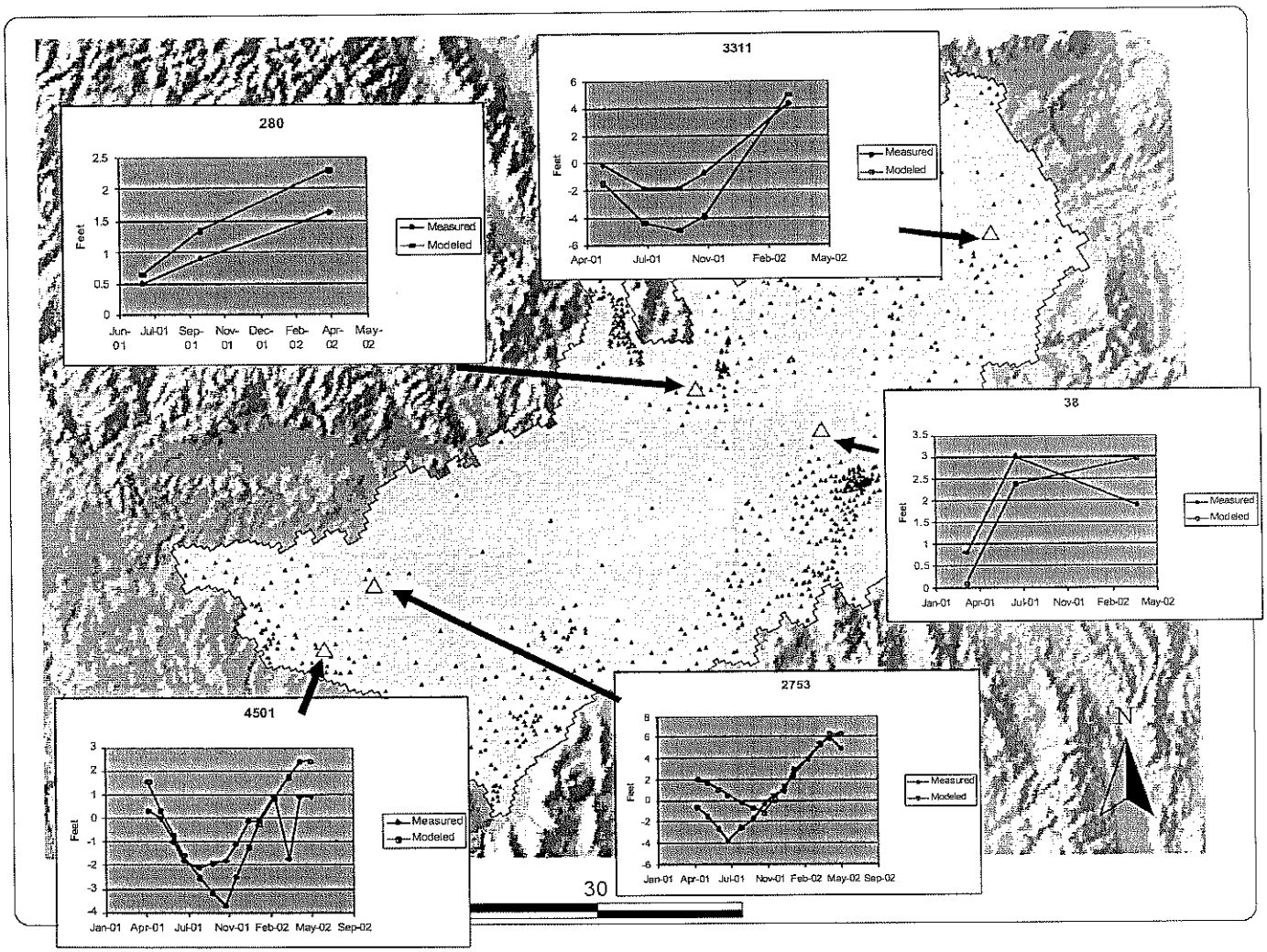

Figure 63. Selected mass measurement well fits.

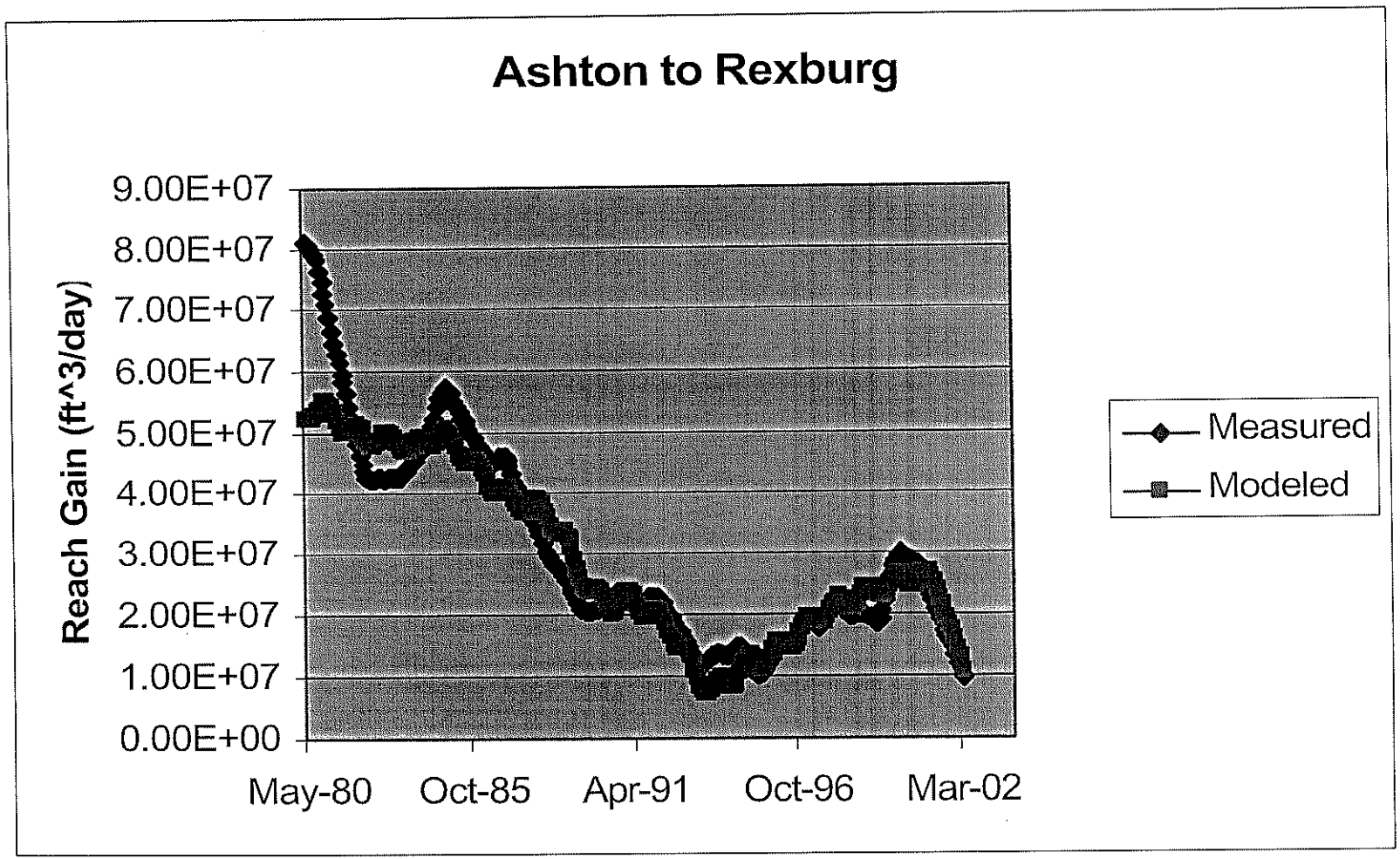

Figure 64. Modeled versus observed reach gain—Ashton to Rexburg reach, filtered data.

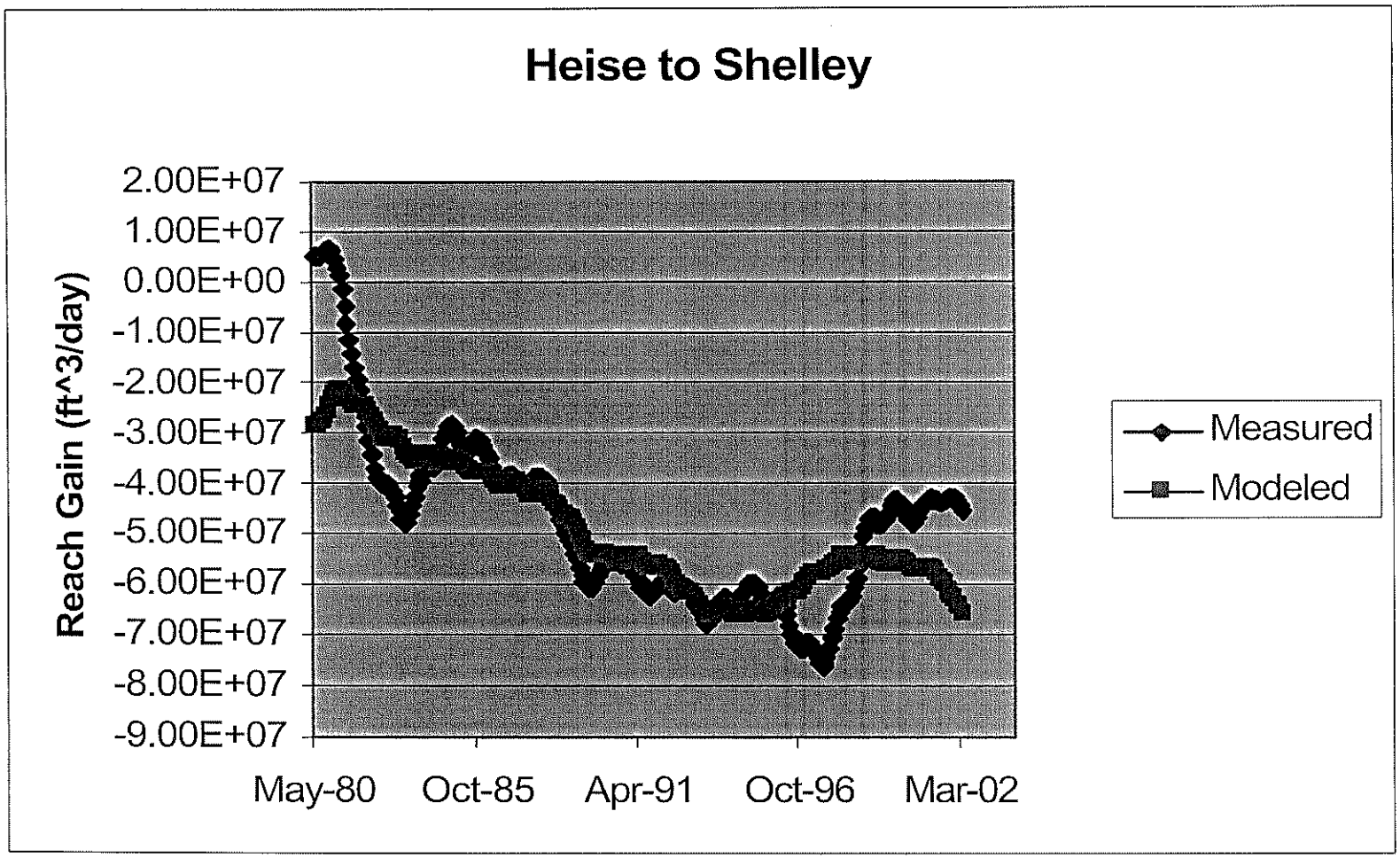

Figure 65. Modeled versus observed reach--Heise to Shelley reach, filtered data.

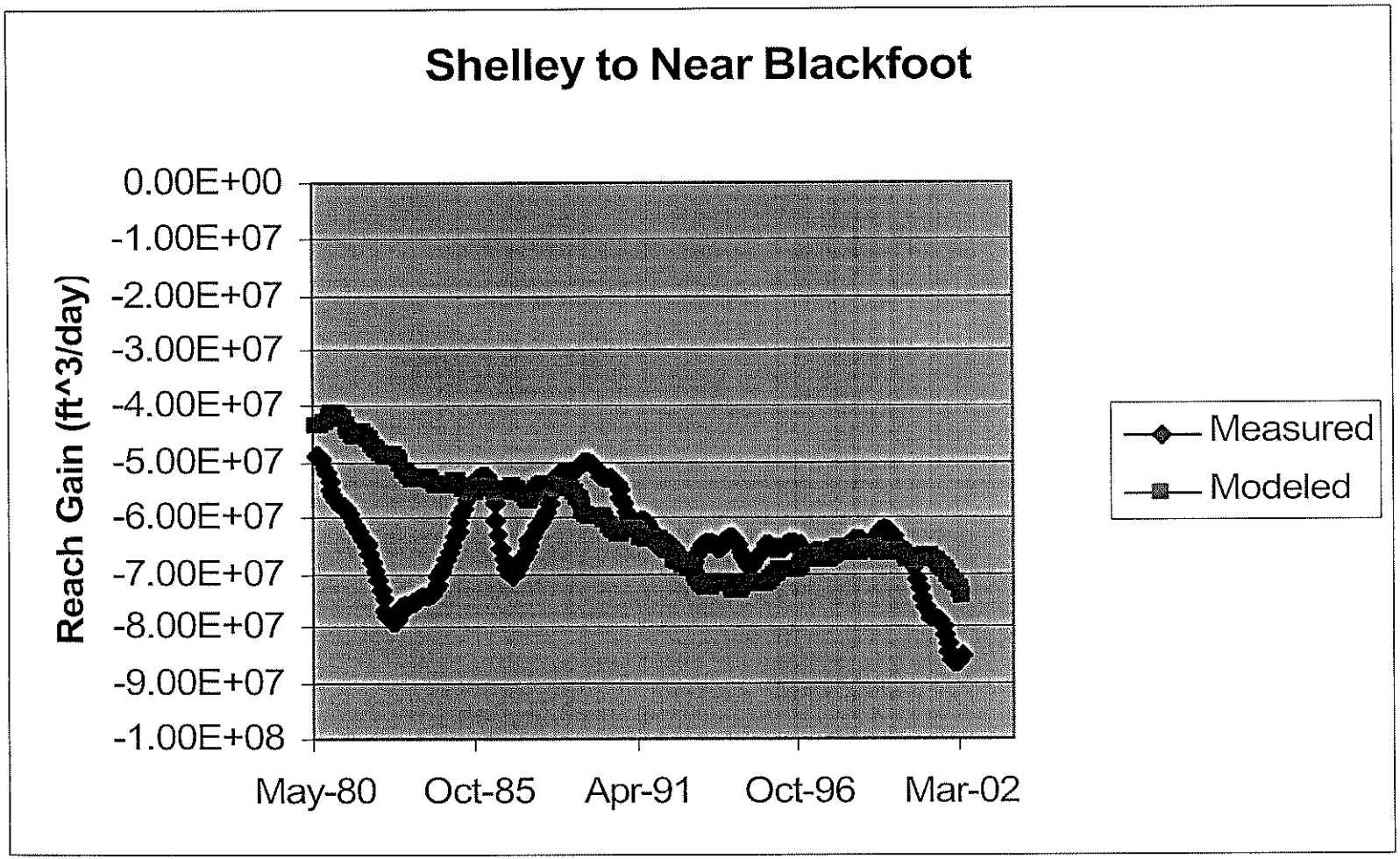

Figure 66. Modeled versus observed reach gain—Shelley to Near Blackfoot reach, filtered data.

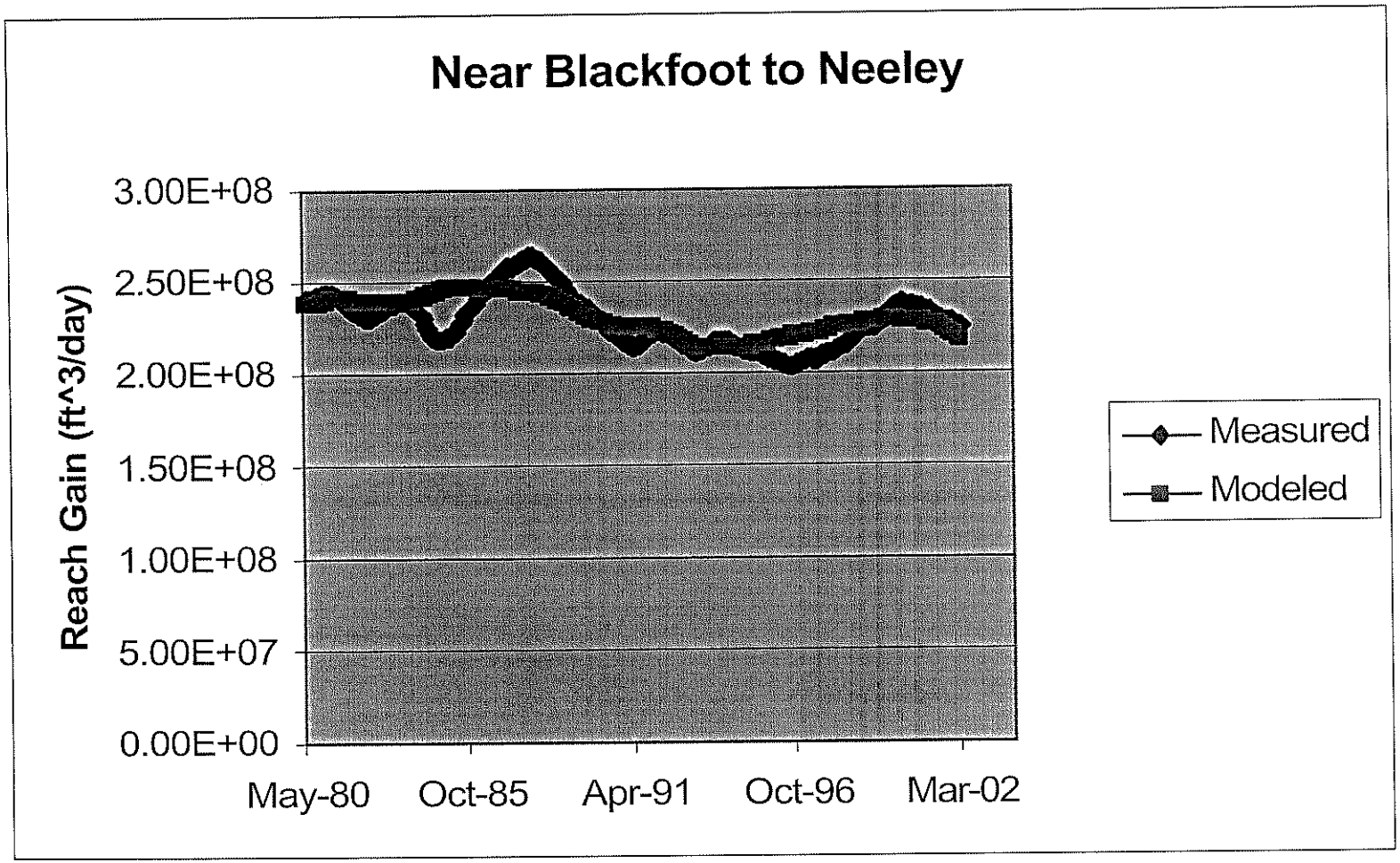

Figure 67. Modeled versus observed reach gain—Near Blackfoot to Neeley reach, filtered data.

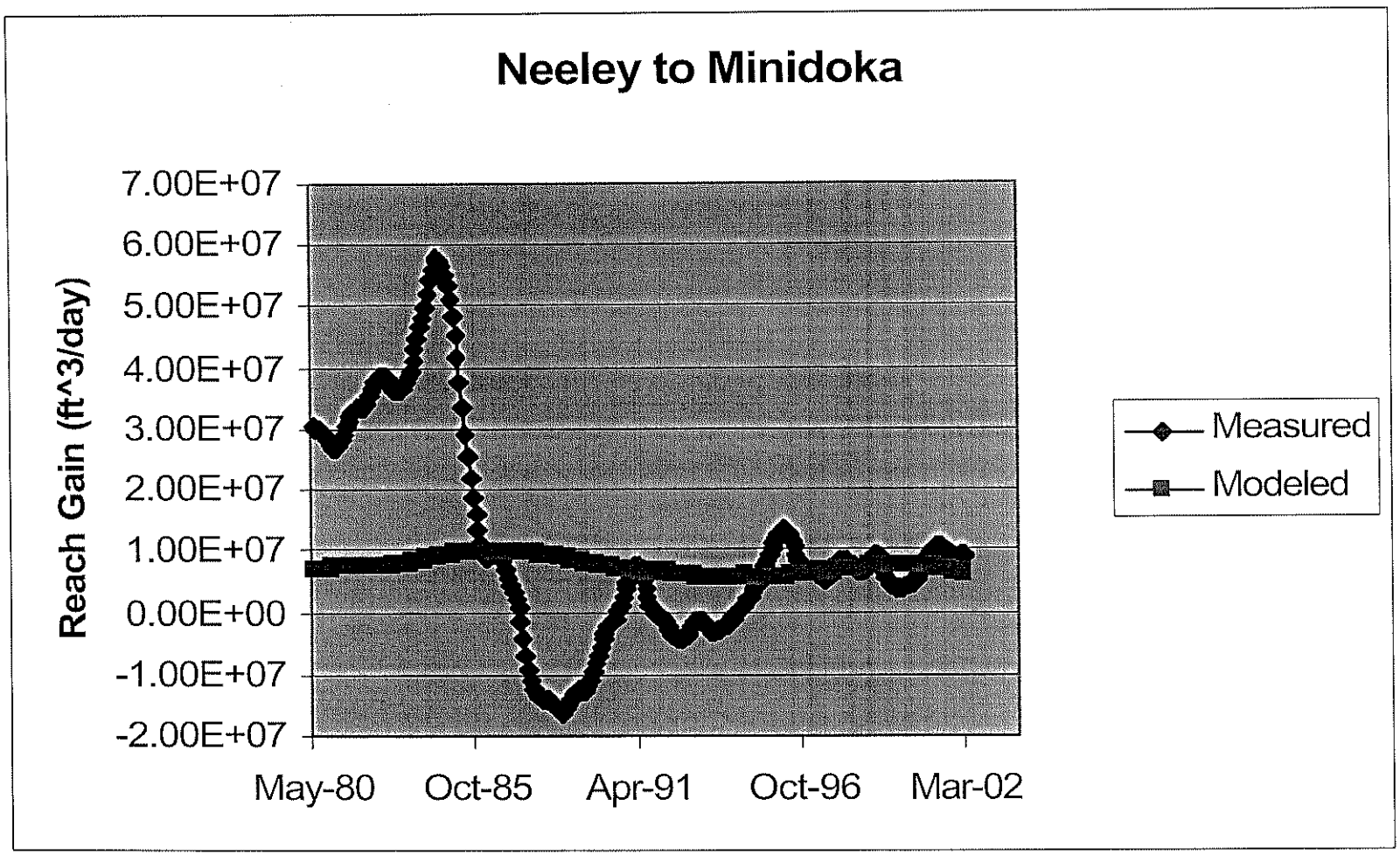

Figure 68. Modeled versus observed reach gain—Neeley to Minidoka reach, filtered data.

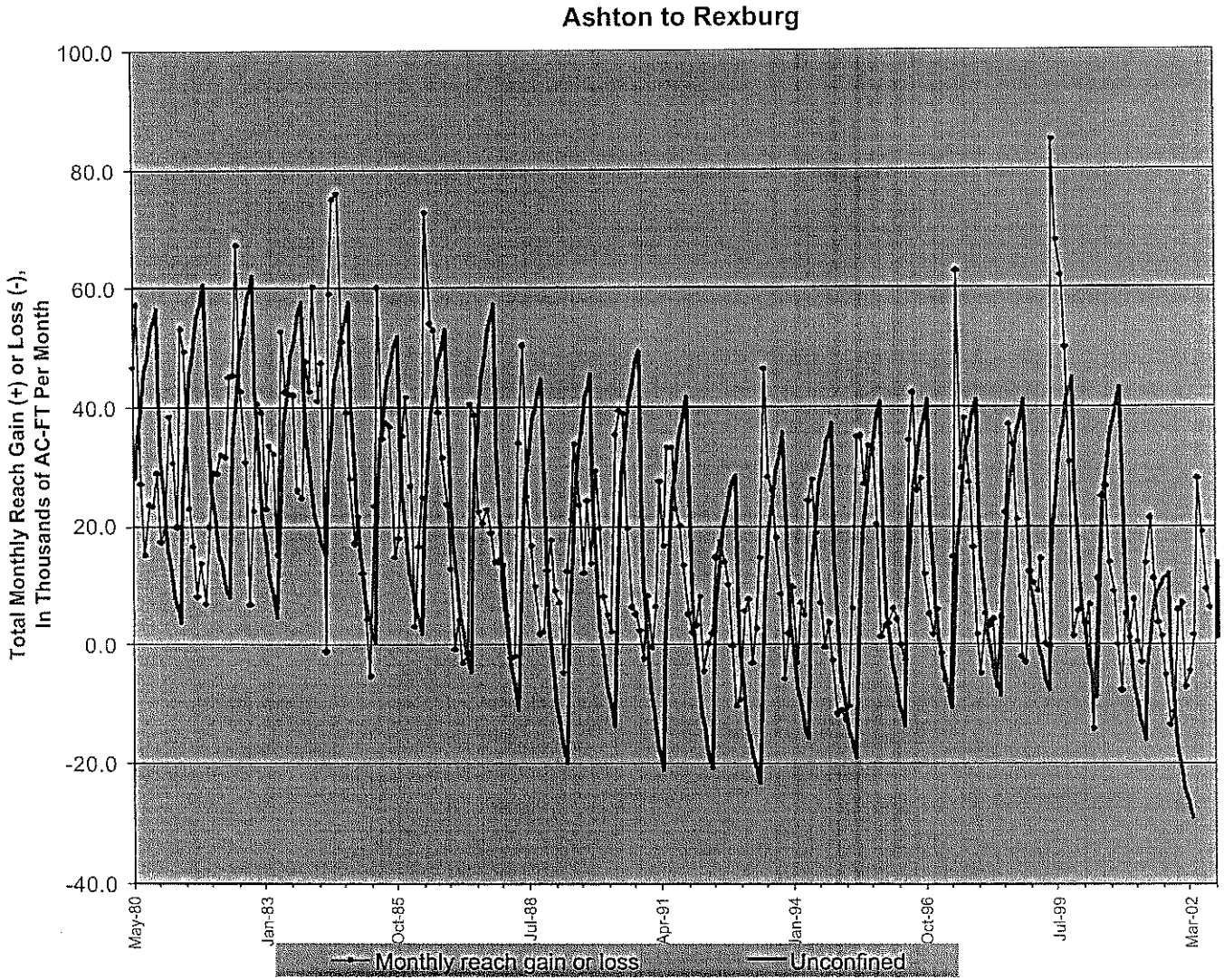

Figure 69. Modeled versus observed reach gain—Ashton to Rexburg reach, monthly unfiltered data.

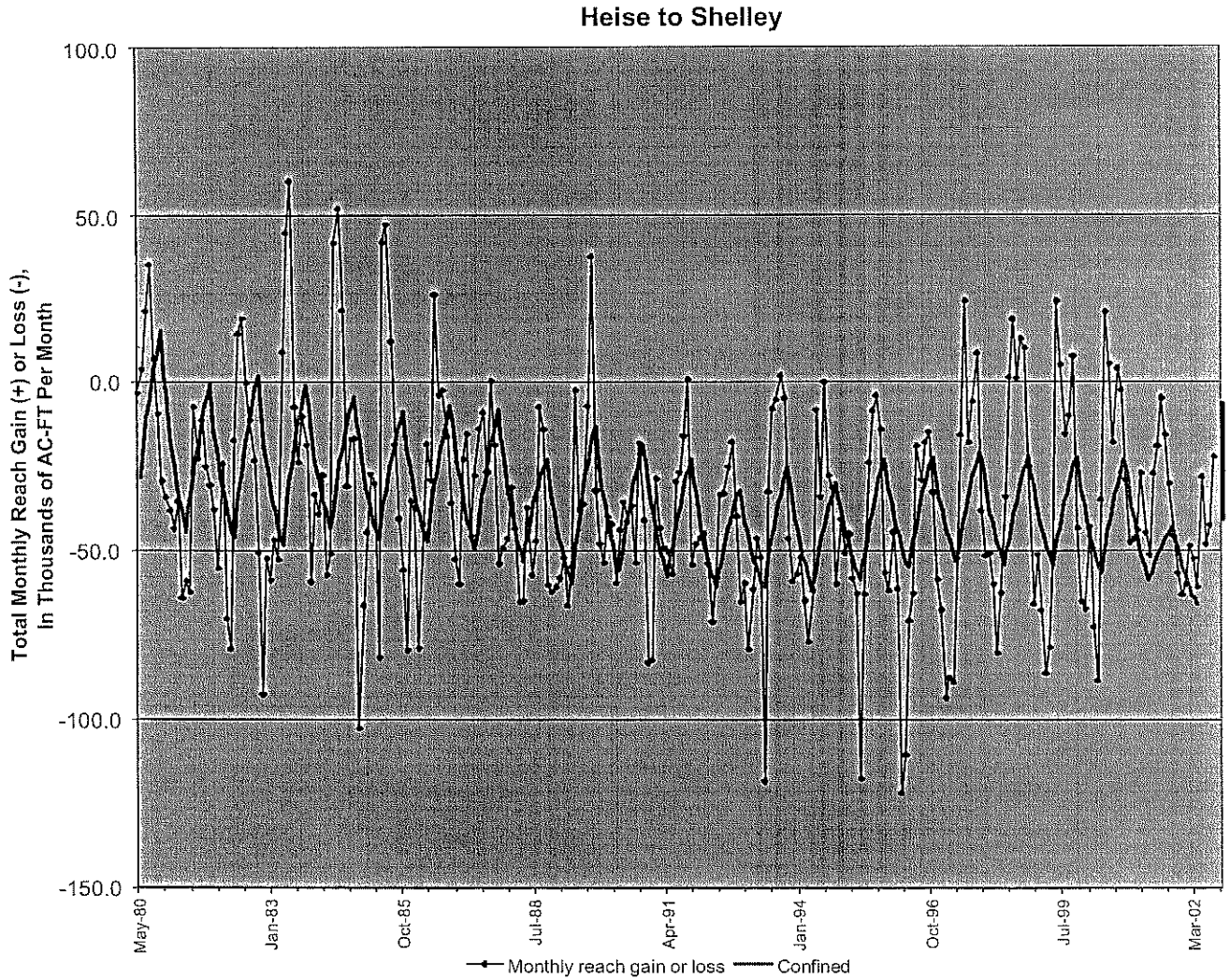

Figure 70. Modeled versus observed reach--Heise to Shelley reach, monthly unfiltered data.

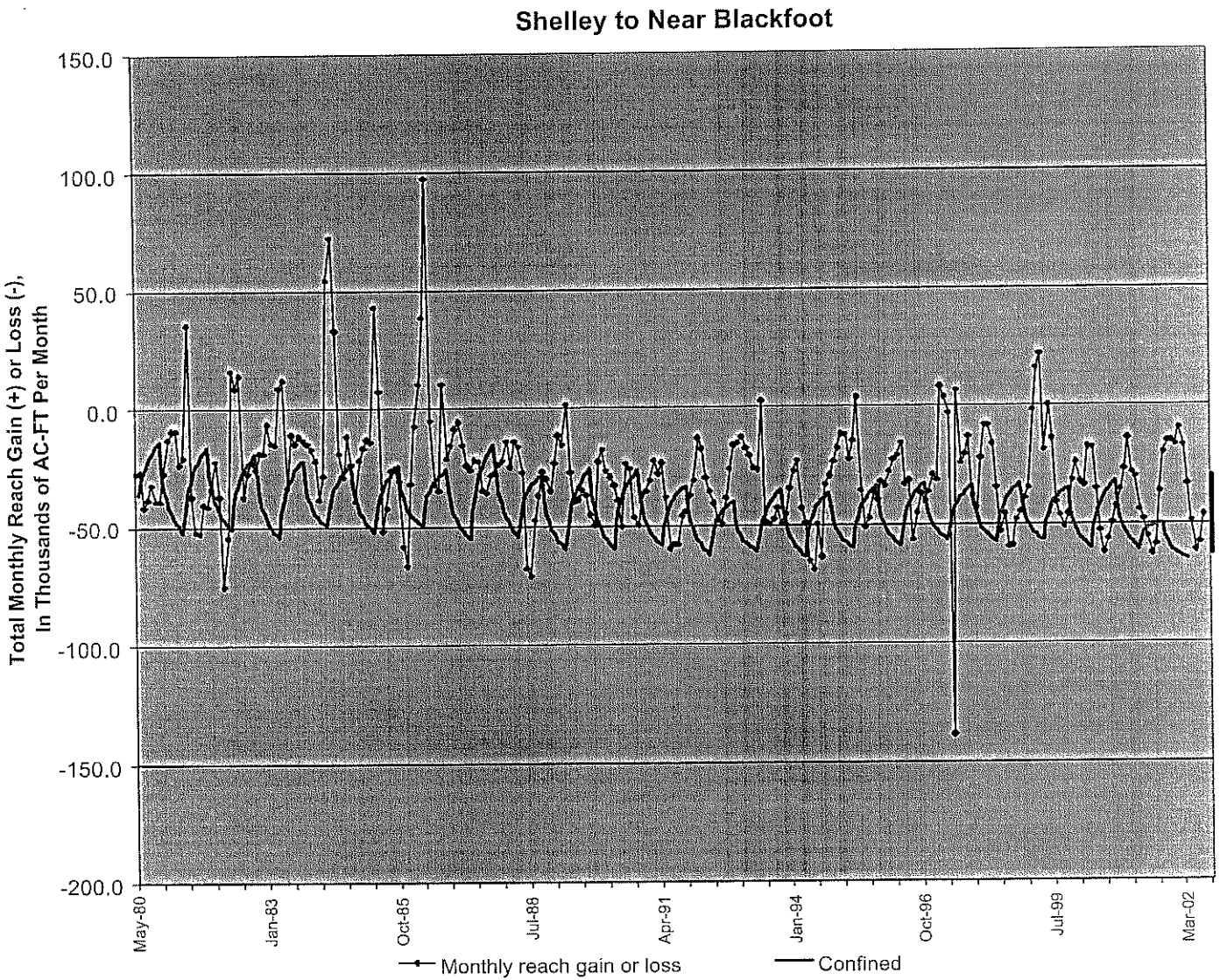

Figure 71. Modeled versus observed reach gain—Shelley to Near Blackfoot reach, monthly unfiltered data.

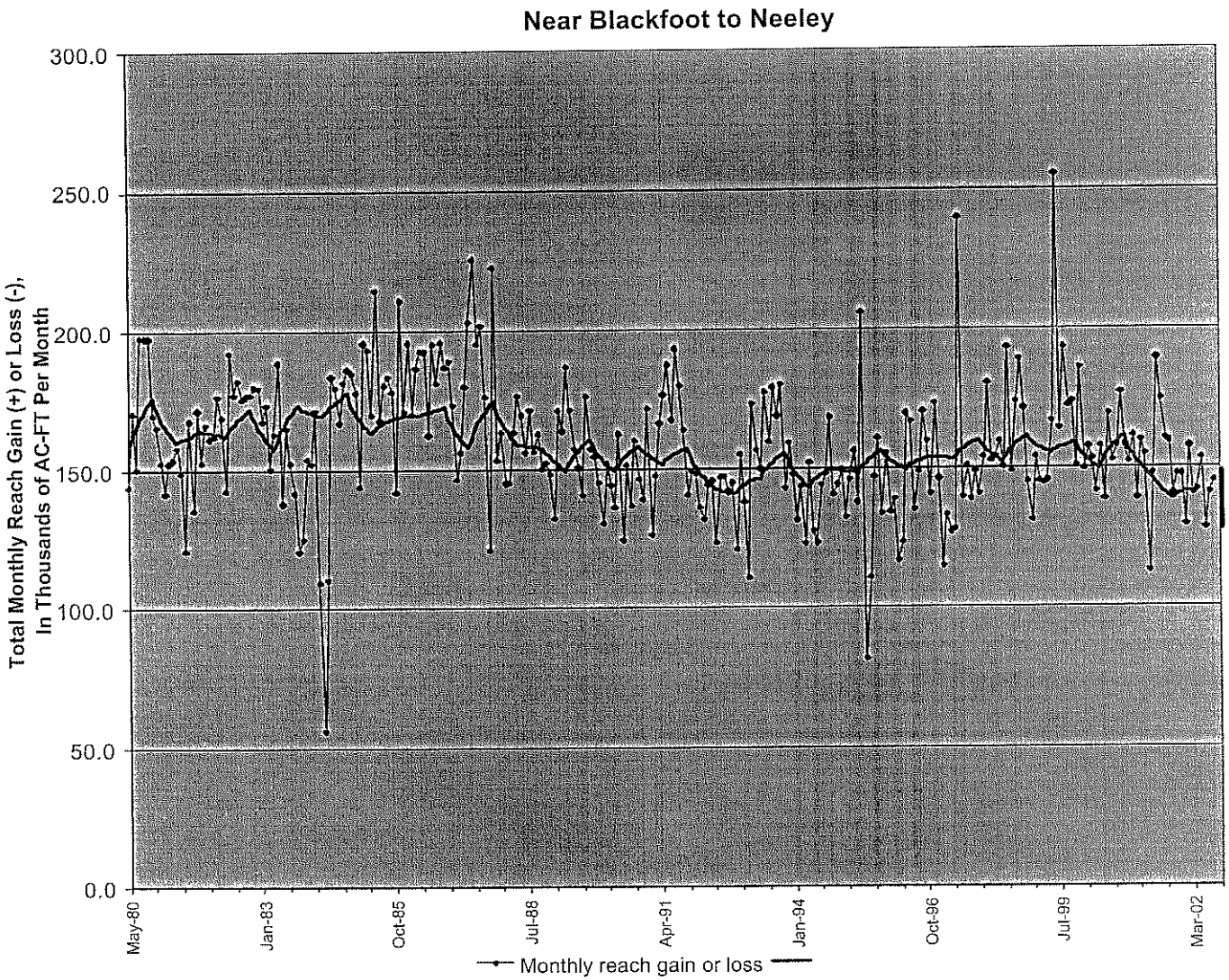

Figure 72. Modeled versus observed reach gain—Near Blackfoot to Neeley reach, monthly unfiltered data.

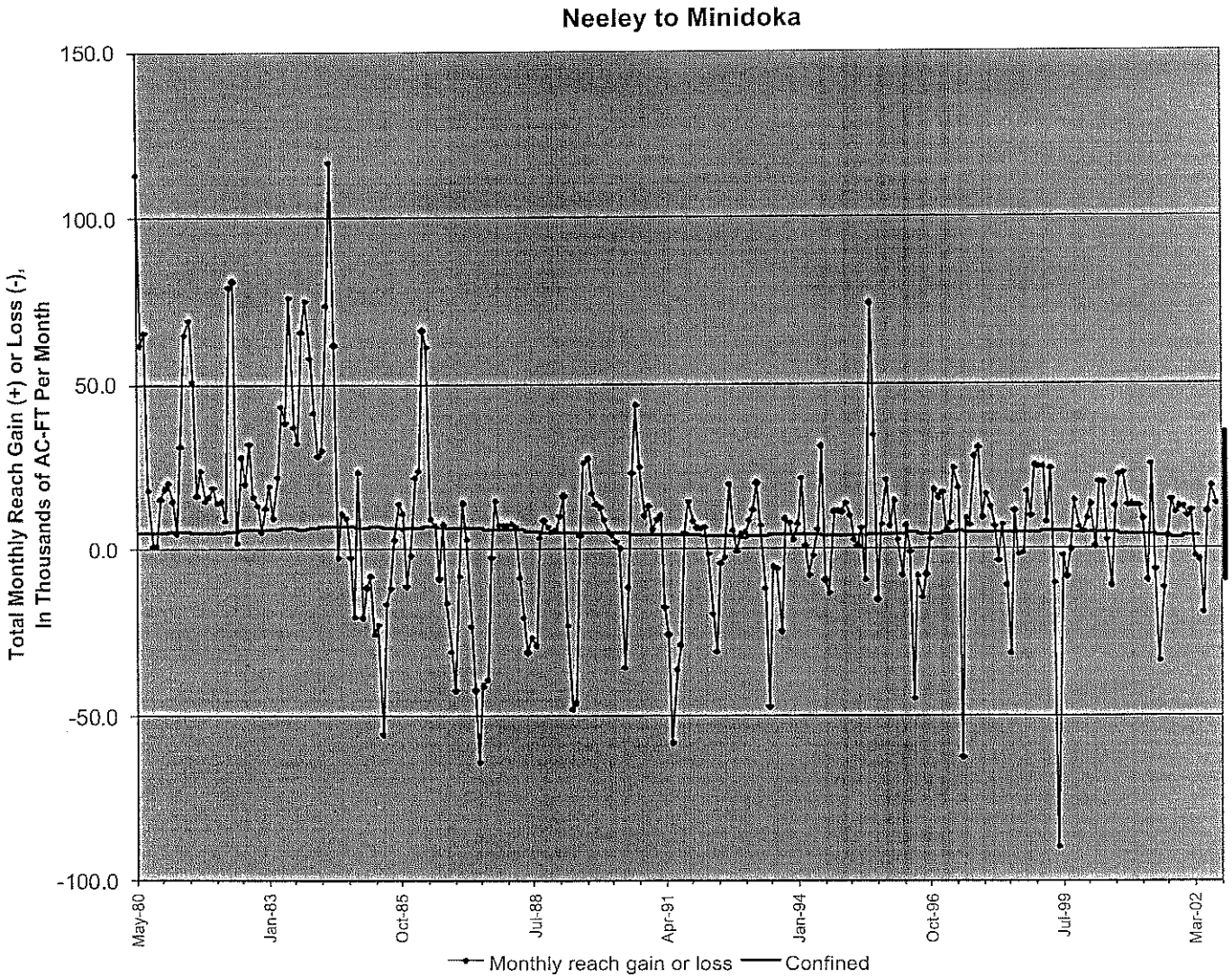

Figure 73. Modeled versus observed reach gain—Neeley to Minidoka reach, monthly unfiltered data.

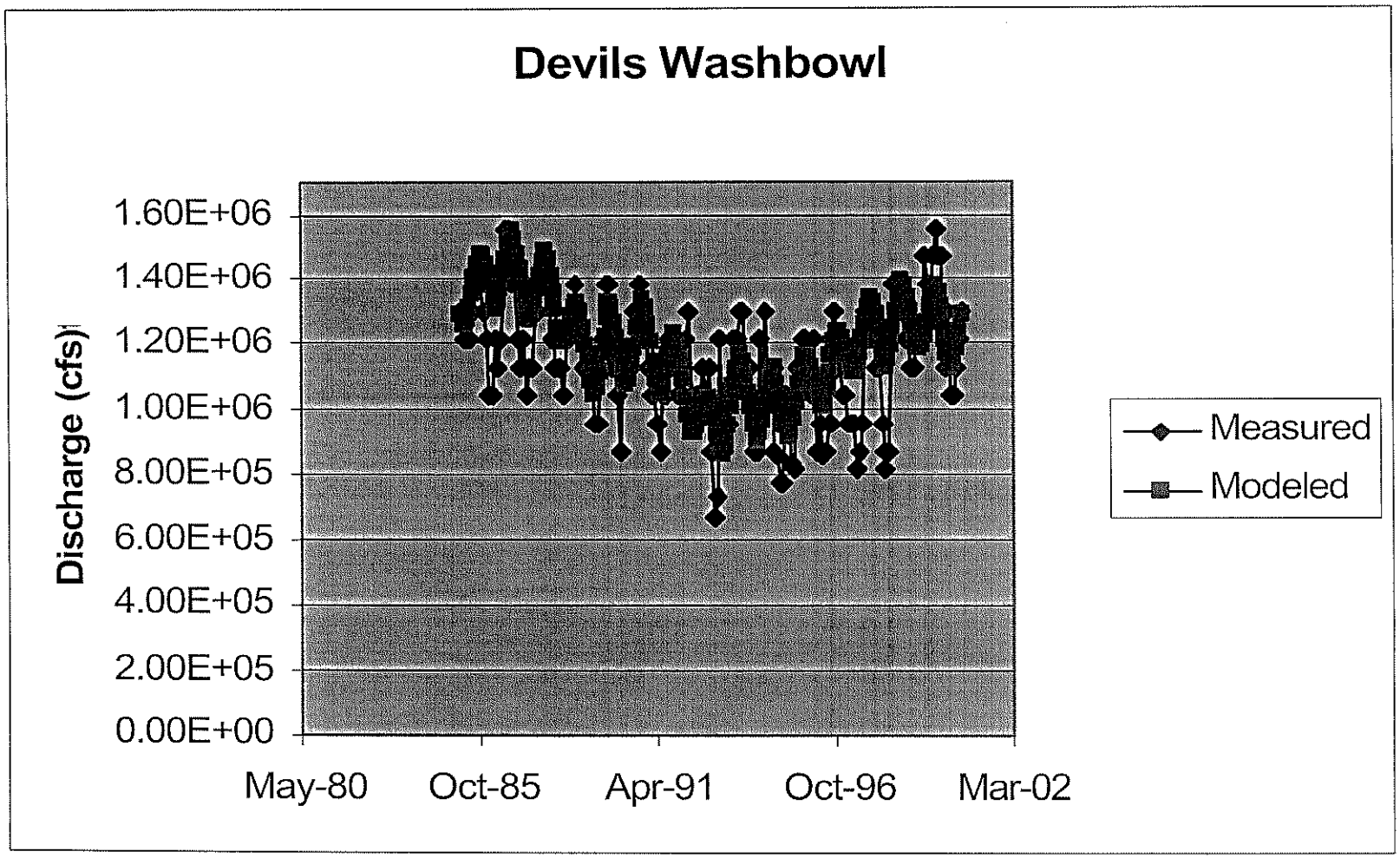

Figure 74. Modeled versus observed spring discharge—Devils Washbowl (cfs).

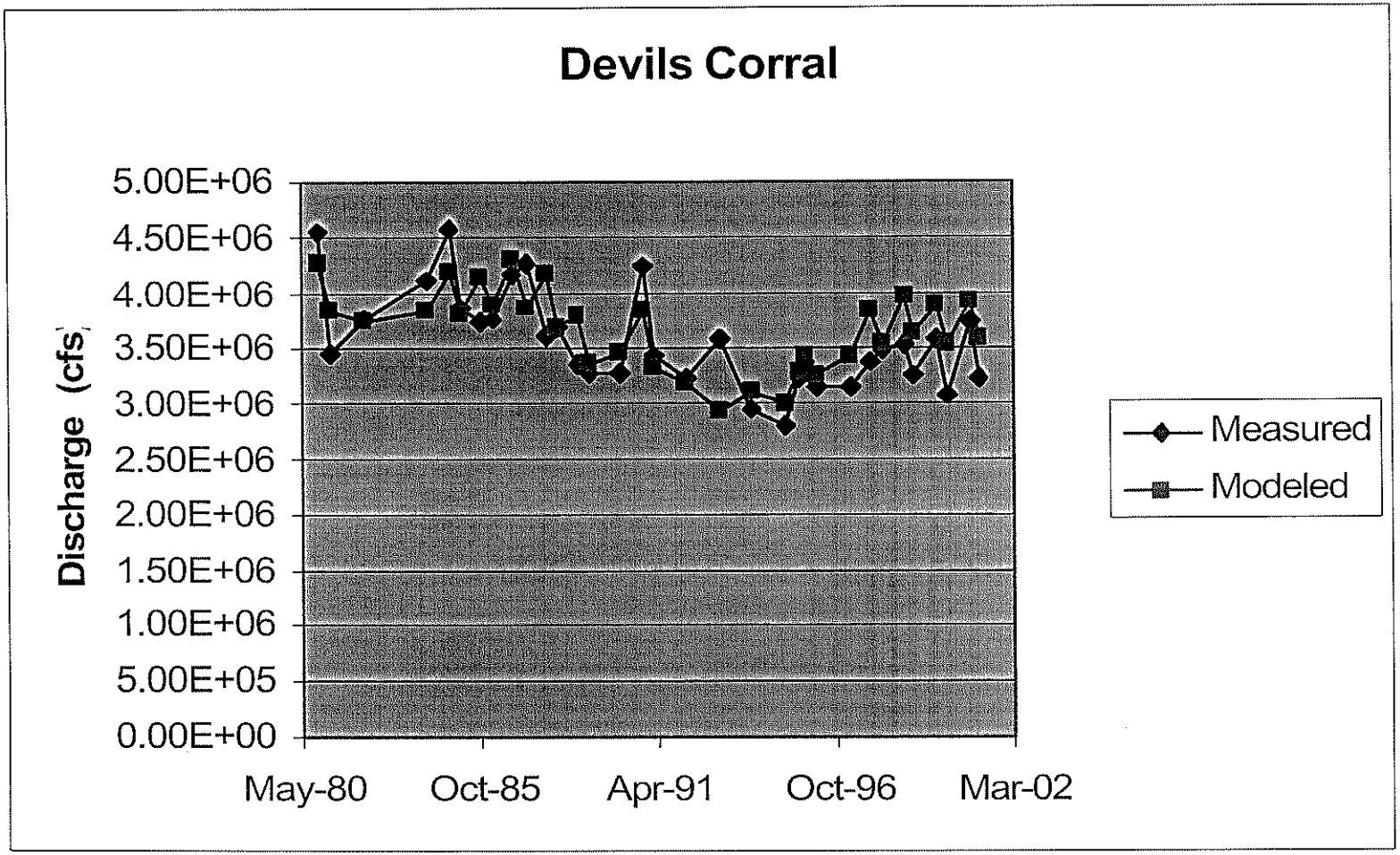

Figure 75. Modeled versus observed spring discharge—Devils Corral (cfs).

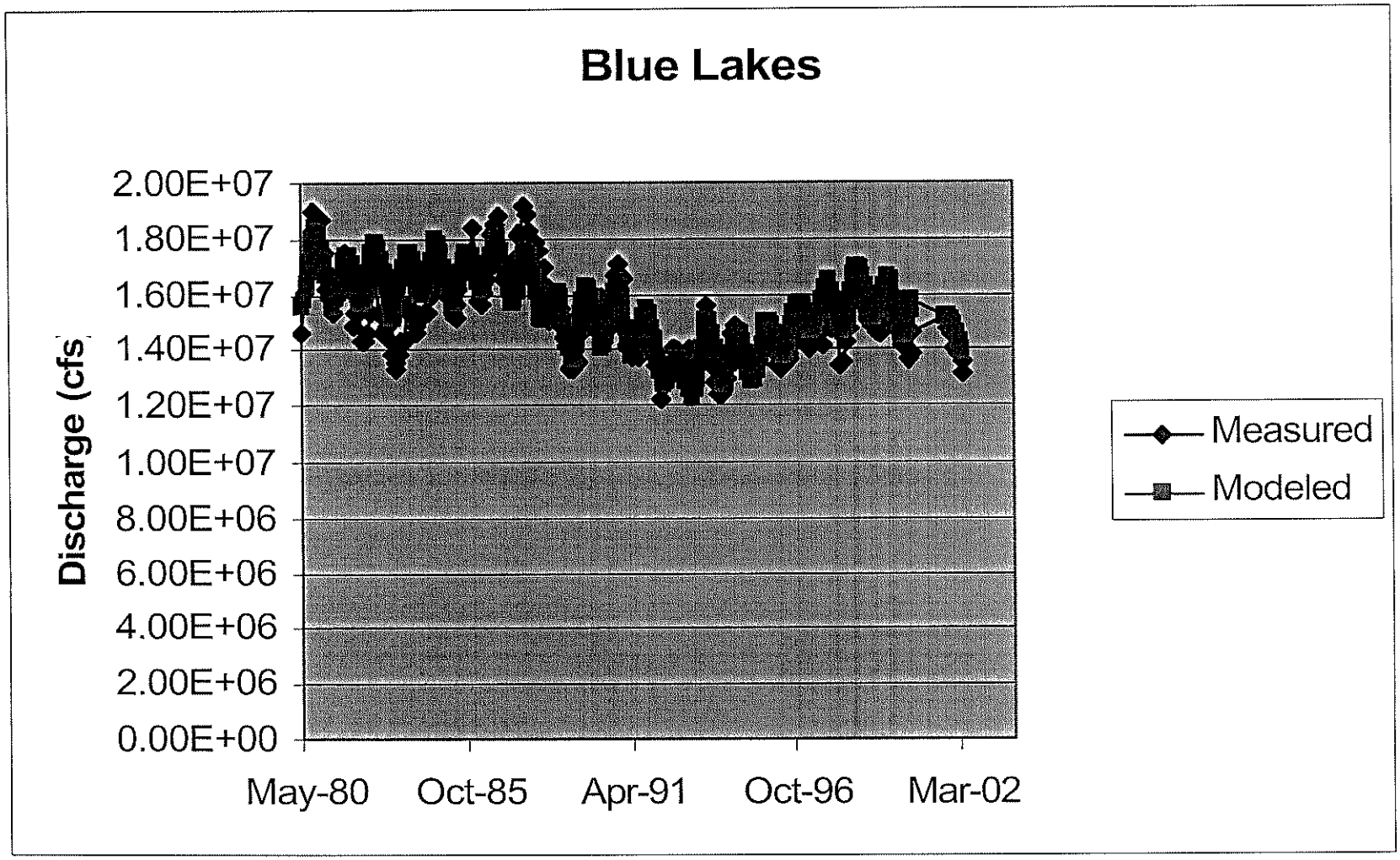

Figure 76. Modeled versus observed spring discharge—Blue Lakes (cfs).

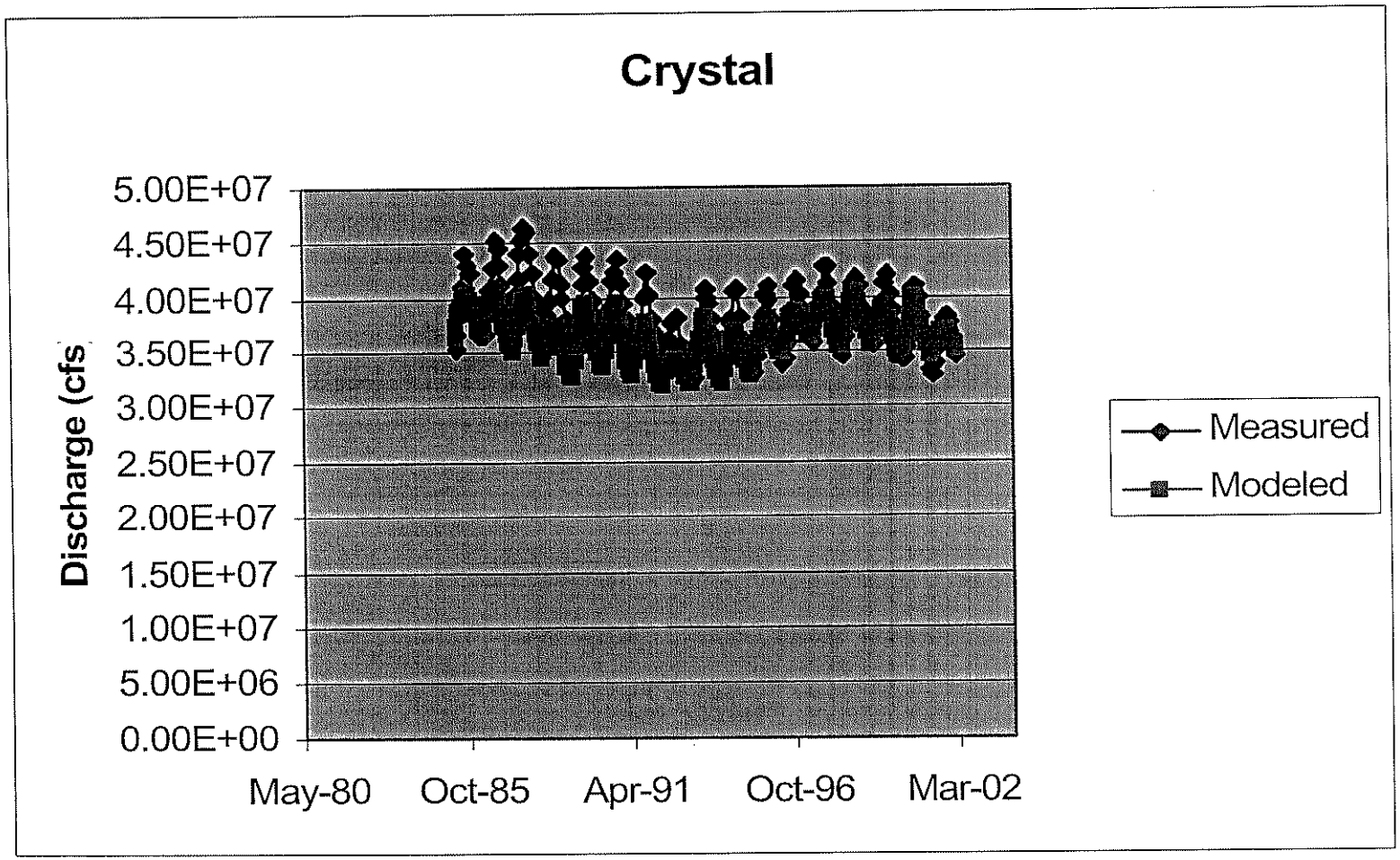

Figure 77. Modeled versus observed spring discharge—Crystal (cfs).

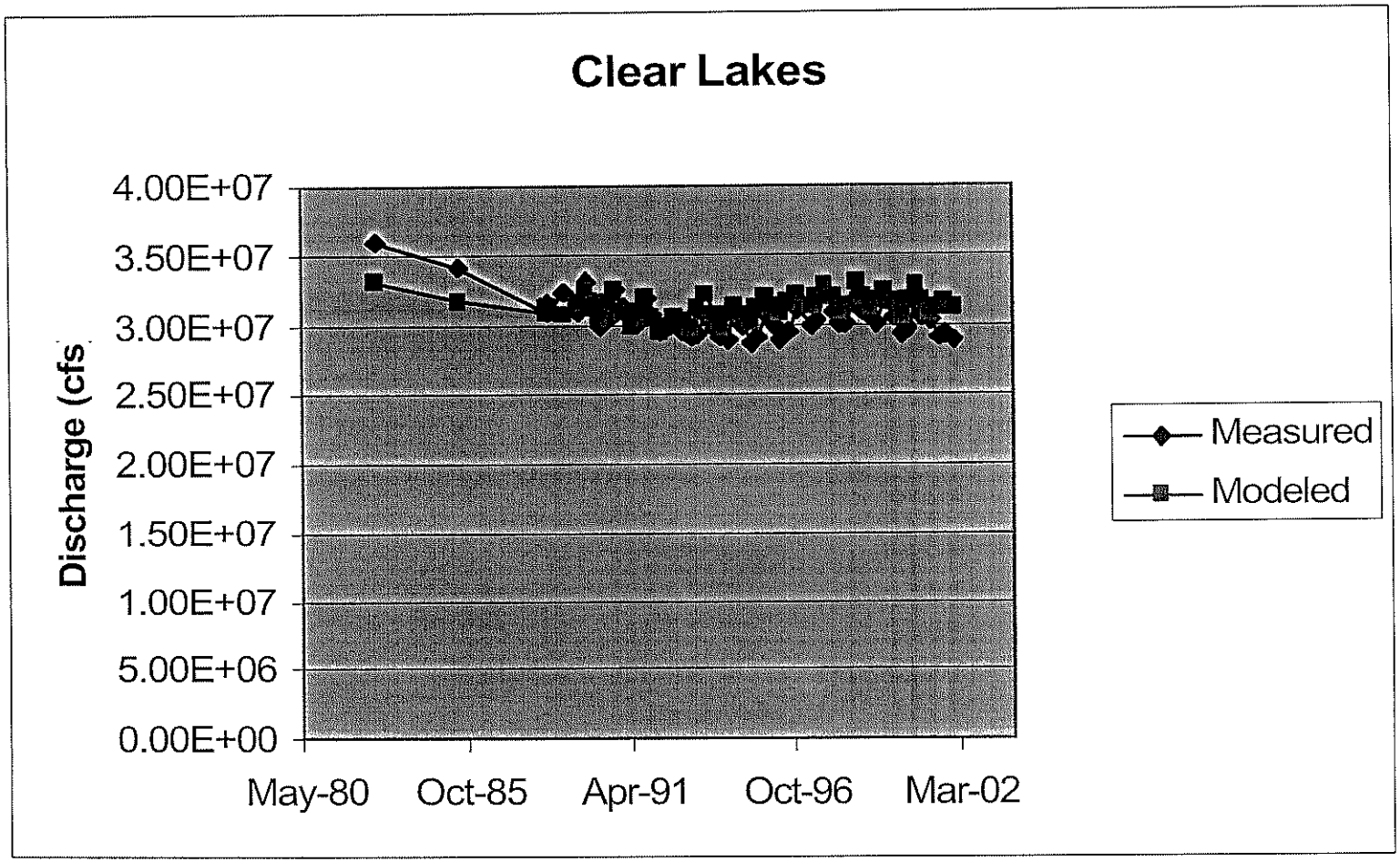

Figure 78. Modeled versus observed spring discharge—Clear Lakes (cfs).

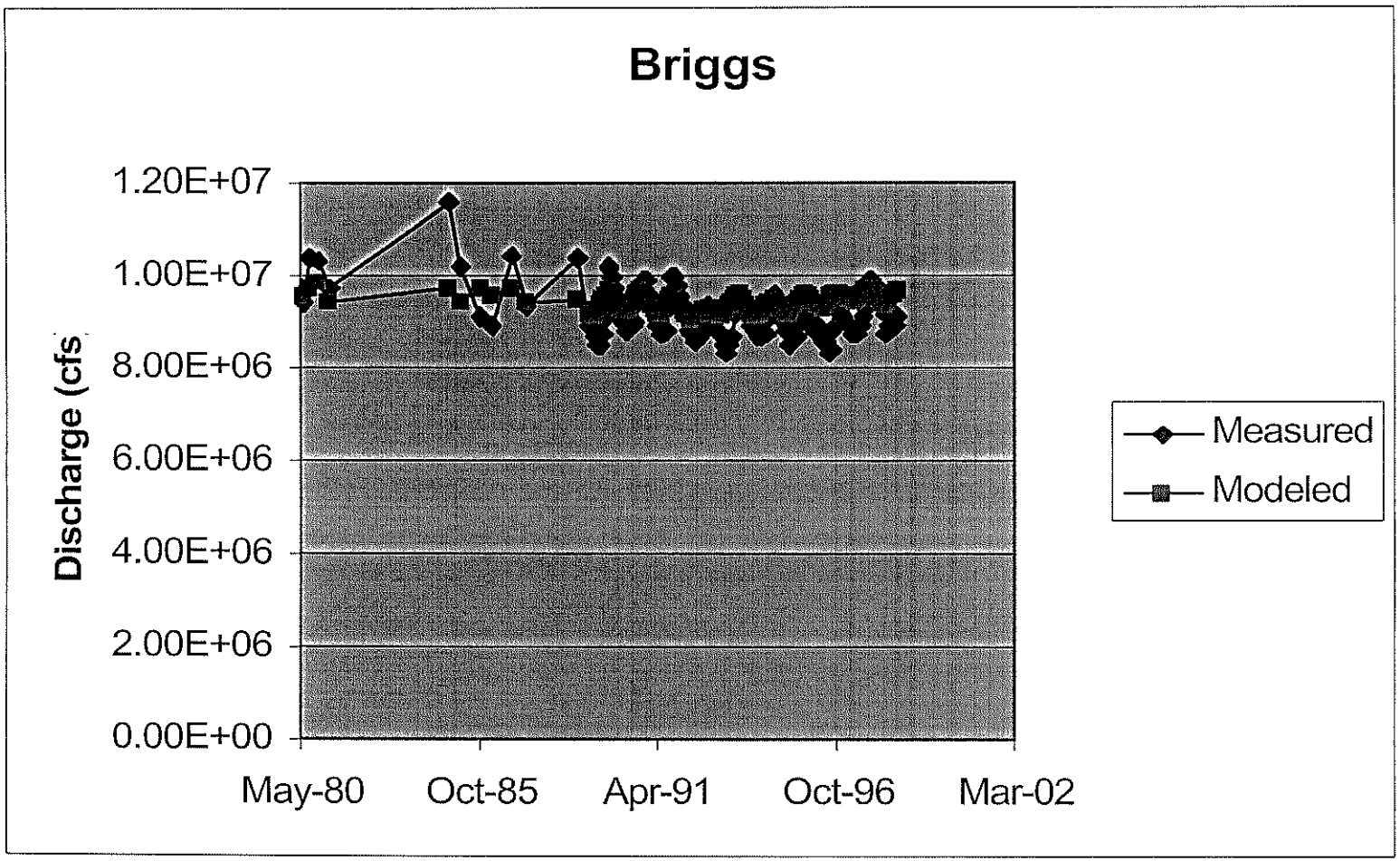

Figure 79. Modeled versus observed spring discharge—Briggs (cfs).

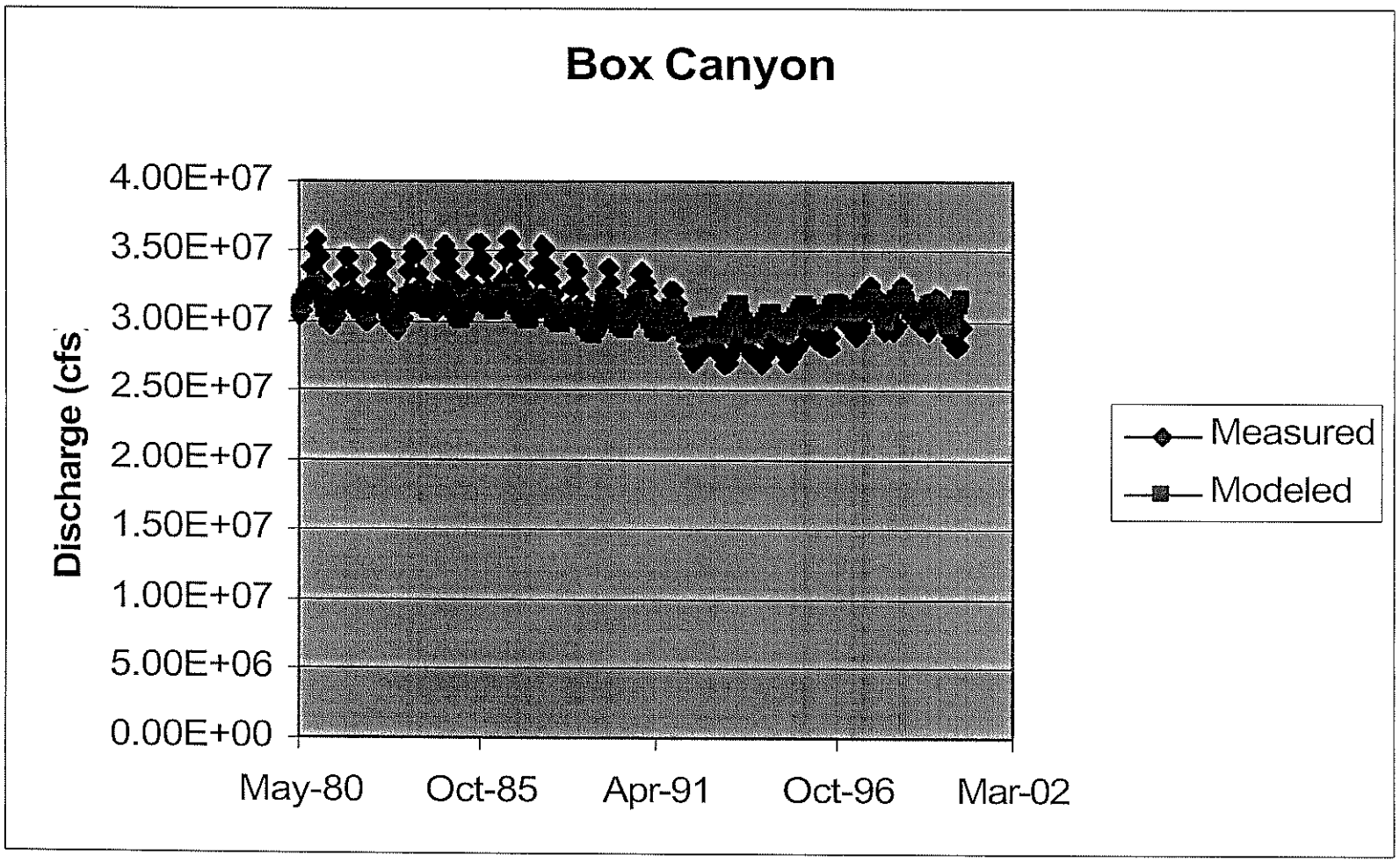

Figure 80. Modeled versus observed spring discharge—Box Canyon (cfs).

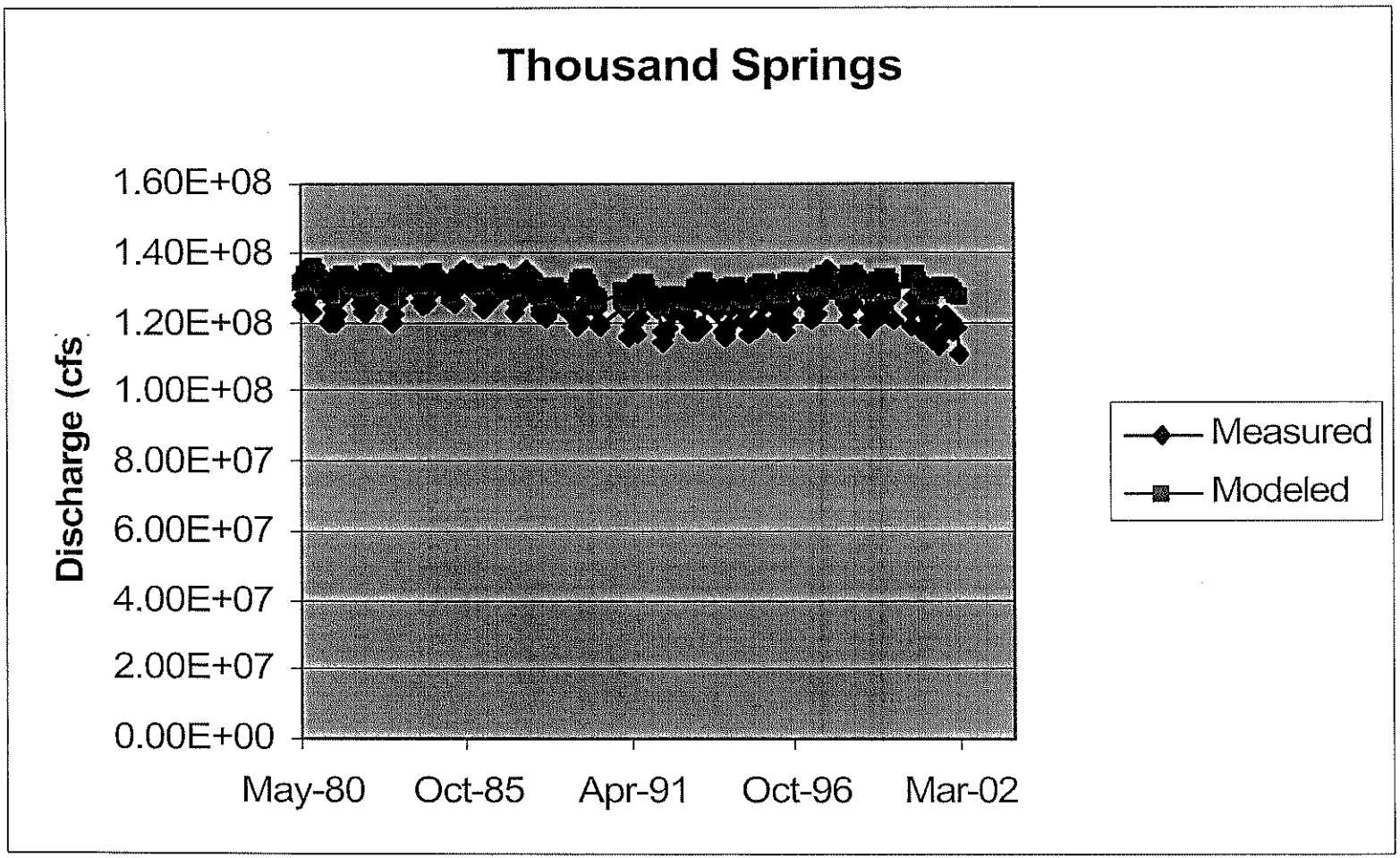

Figure 81. Modeled versus observed spring discharge—Thousand Springs (cfs).

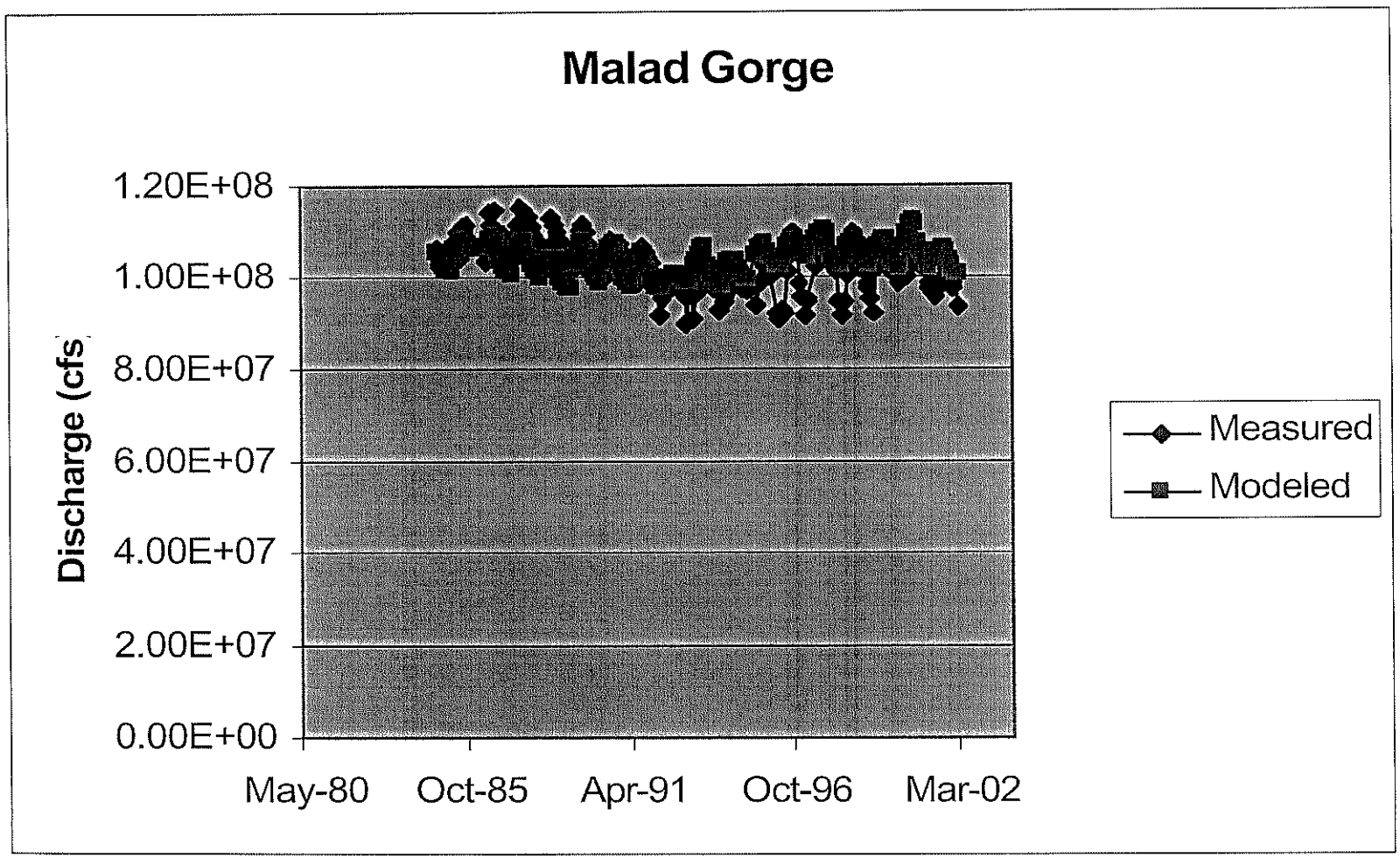

Figure 82. Modeled versus observed spring discharge—Malad (cfs).

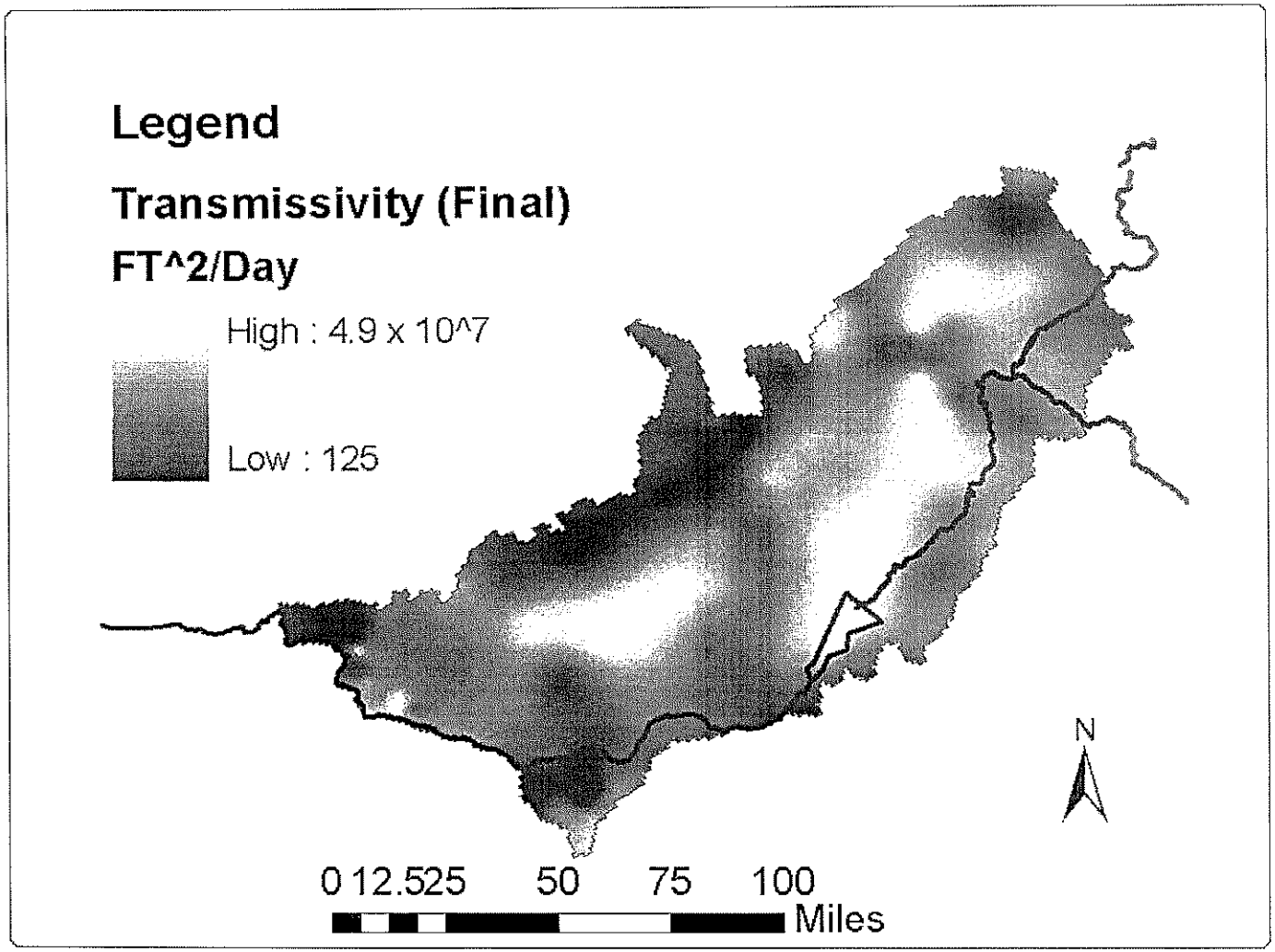

Figure 83. Transmissivity map from coupled steady state/transient calibration.

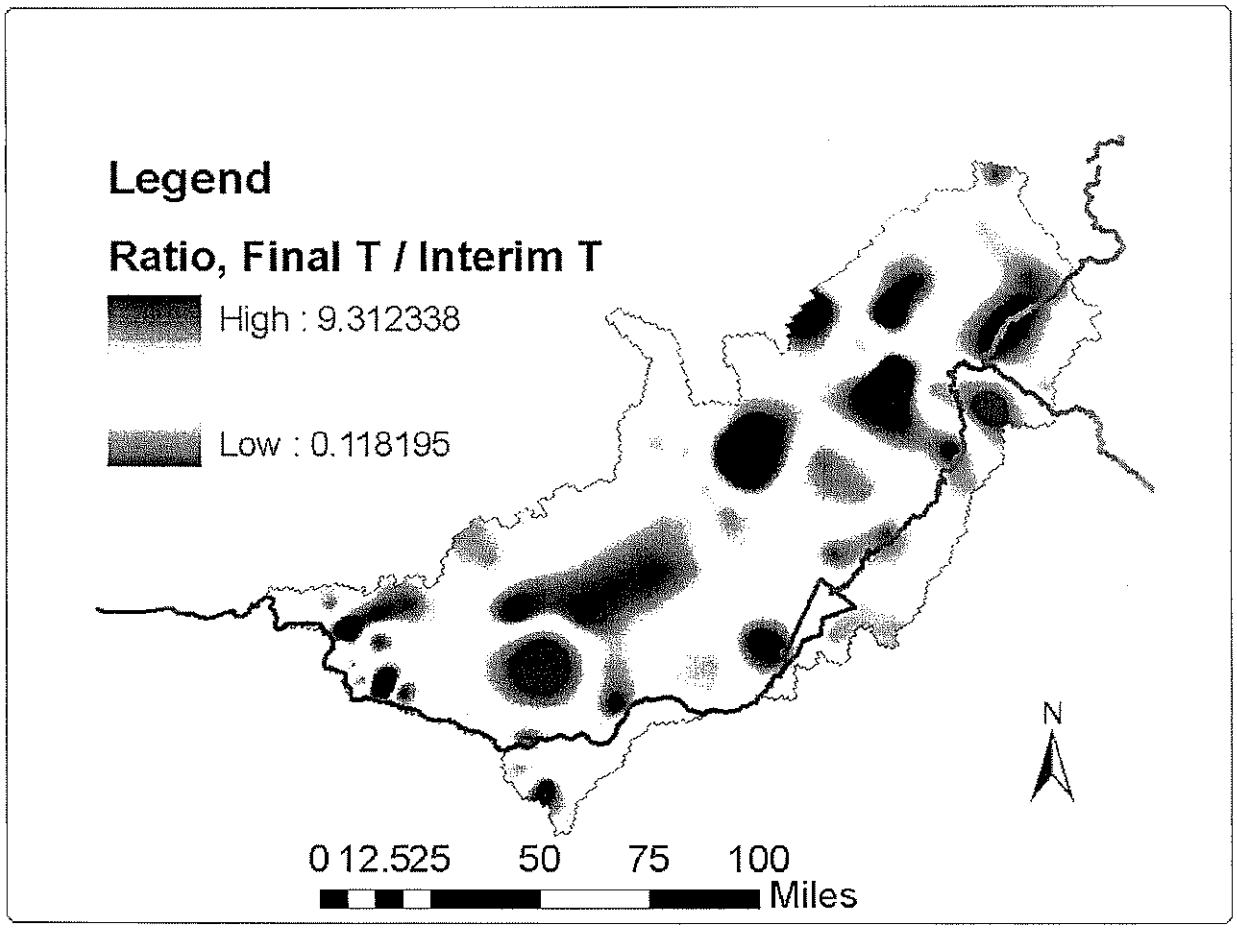

Figure 84. Ratio of final transmissivity to preliminary transmissivity.

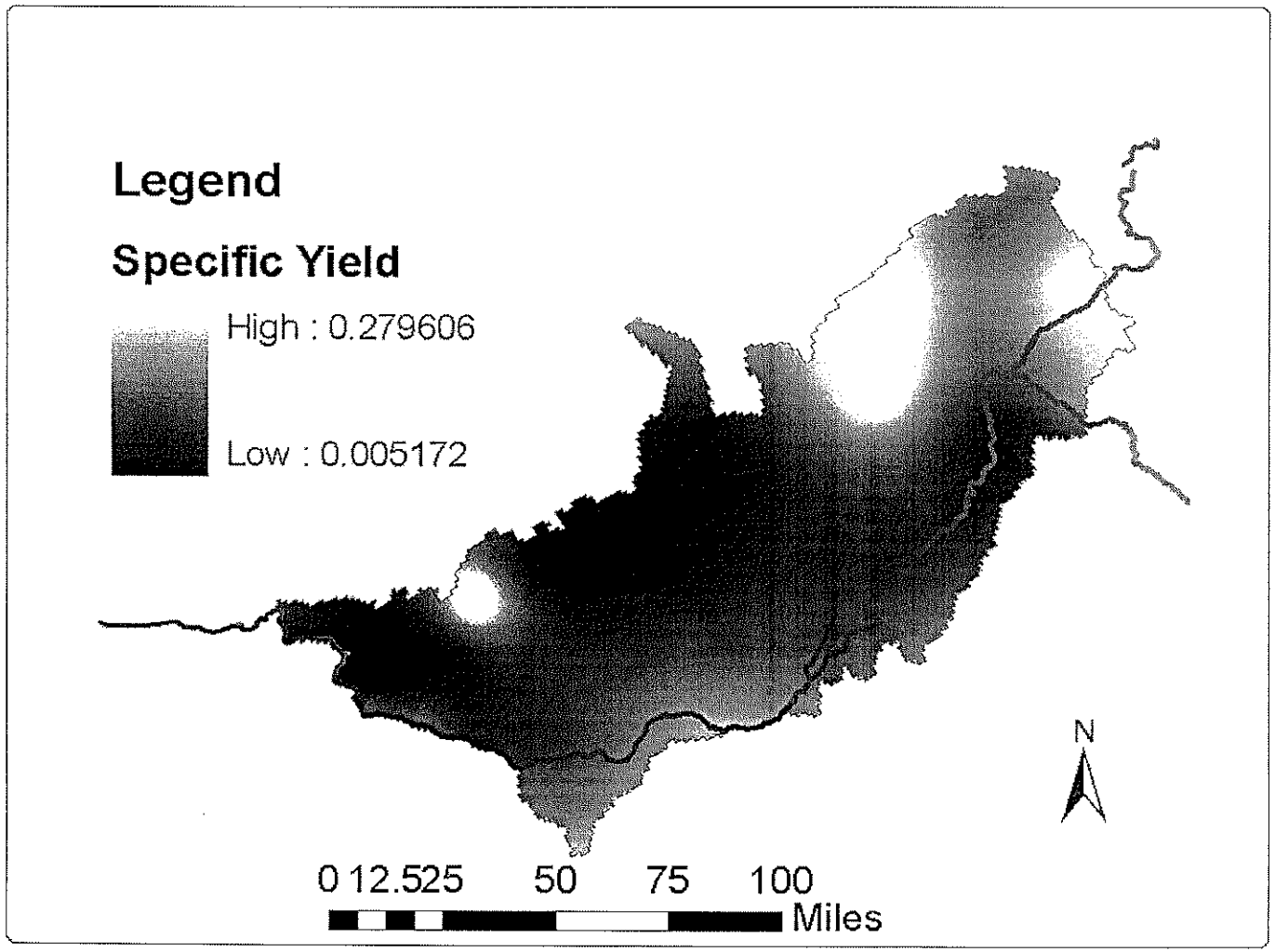

Figure 85. Map of aquifer specific yield.